Foam injection molding with physical blowing agents

Valentina Volpe

Department of Industrial Engineering

Ph.D. Course in "Scienza e tecnologie per l'industria chimica, farmaceutica e alimentare" (XI Cycle-New Series)

Foam Injection molding with physical blowing agents

Supervisor   **Ph.D. student**
Prof. Giuseppe Titomanlio   *Valentina Volpe*
Prof. Roberto Pantani

Scientific Referees
Prof. Lih-Sheng (Tom) Turng
Prof. Volker Altstädt

Ph.D. Course Coordinator
Prof. Paolo Ciambelli

Acknowledgments

Publication list

- *"Shear-Induced Nucleation and Growth in Isotactic Polypropylene",* R. Pantani, I. Coccorullo, V. Volpe, G. Titomanlio, Macromolecules 2010, 43, 9030–9038

- *"Mutual effect of flow and crystallization: investigations in flow-induced crystallization and crystallization induced solidification",* R. Pantani, I. Coccorullo, V.Speranza, V. Volpe, S. Di Domenico, G.Titomanlio, Polymer Processing Society 26th Annual Meeting, July 4-8, 2010 Banff (Canada)

- *"Injection molding of microcellular polymers",* V. Volpe*, A. Sorrentino, R. Pantani, G. Titomanlio, XVI Scuola Nazionale di Scienza dei Materiali – INSTM, 27 settembre-2 ottobre 2010 Bressanone (BZ)

- *"Injection molding of microcellular polymers",* V. Volpe*, A. Sorrentino, R. Pantani, G. Titomanlio, proceedings EPF 5th Summer School - "Fundamental and developments in polymer processing science and technology", 15-20 Maggio 2011, Gargnano (BS)

- *"Injection molding of microcellular PLA",* V. Volpe*, A. Sorrentino, R. Pantani, G. Titomanlio, proceedings Third International Conference on Biofoams, Capri (Na) 21-23 settembre 2011

- *"Foam injection molding of poly(lactic acid) with physical blowing agents",* R. Pantani, A. Sorrentino, V. Volpe, G.Titomanlio, Polymer Processing Society 29th Annual Meeting, Nuremberg (Germany) 15-19 Luglio 2013.

Index

Figures index

viii

ix

Tables index

Abstract

Foam injection molding uses environmental friendly blowing agents under high pressure and temperature to produce parts having a cellular core and a compact solid skin (the so-called "structural foam"). The addition of a supercritical gas reduces the part weight and at the same time improves some physical properties of the material through the promotion of a faster crystallization; it also leads to the reduction of both the viscosity and the glass transition temperature of the polymer melt, which therefore can be injection molded adopting lower temperatures and pressures.

In this work, the effect of the addition of a blowing agent within a polymeric matrix and the influence of the process conditions on the rheology of the melt, on the physical and mechanical properties and on the morphology of the final product was analyzed.

Several polymeric materials were adopted in this work: two thermoplastic polymers commonly used for conventional injection molding and previously well characterized, namely a semi-crystalline polypropylene and an amorphous polystyrene, and two grades of a biodegradable polymer, polylactic acid (PLA). With particular reference to biodegradable polymers, the utilization of the foam injection molding process with physical blowing agents seems the ideal solution to problems of moldability caused by the high viscosity and operative condition very close to those of degradation for this class of materials.

Before the foam injection molding, the PLA was foamed by means of a batch foaming system. In particular, the effect of foaming temperature, solubilization time and cooling rate on the morphology of the samples and on their density was analyzed.

Several foam injection molding experiments were carried out by using cavities with two different thicknesses and under different experimental conditions. Rheological measurements of the polymer/gas solutions were also obtained by means of a modified nozzle with a slit rheometer with pressure transducers which allow to obtain on-line viscosity measurements.

Rheological measurements conducted on the polymer-gas mixtures, showed a significant reduction in viscosity. Furthermore, reduction in density of the foamed samples compared to the unfoamed ones varies with increasing amount of gas injected and increases with increasing injection flow rate, reaching values higher than 40% for polystyrene and of almost 50% in the case of PLA. The analysis of the mechanical properties for both materials showed that the values of Young's modulus were lower than that of the molded part without gas. However, the reduction in Young's modulus of the foamed parts compared to the Young's modulus of the unfoamed ones is almost entirely compensated by the reduction in density. On increasing the amount of gas, the morphology of the samples becomes more homogeneous,

with an increasing void percentage and smaller bubbles radius. However, there seems to be an optimal physical blowing agent content that leads to the best microcellular structure and the maximum density reduction and mechanical properties.

Finally, a study of the effect of gas on the crystallinity of the PLA was carried out by Differential Scanning Calorimetry (DSC) and Wide Angle X-ray Scattering. Results shown a higher cristallinity of the foamed core with respect to the compact skin and the unfoamed part. This is an aspect of considerable importance for biodegradable polymers, for which the crystallinity has a marked effect on properties.

Chapter 1
State of the art

1.1 Injection molding

Injection moulding is one of the most versatile and important manufacturing processes, capable of mass-producing complicated plastic parts in net shape with excellent dimensional tolerance.

Injection molding was patented in 1872 by the brothers Hyatt (USA) and in spite of passing of the century XX this process suffered an enormous evolution, and nowadays it is possible to observe technology and sophisticated equipment associated to injection molding.

Injection molding is a cyclic process. The number of operations that take place in an injection molding machine between two consecutive moldings is called "molding cycle". The optimization of this cycle is fundamental to ensure an economical and competitive process.

The raw material (resin), placed in the form of pellets inside the hopper, is fed into the barrel by the screw rotation. The solid resin is heat-melted by means of band heaters and by the frictional heat generated on the inside of the barrel. The injection molding cycle starts when the mould closes. This step should be as quick as possible to reduce cycle time. Following is the sequence of the steps which take place during injection molding

Injection: after the nozzle of the cylinder takes contact with the mold, the piston (or the screw) is pushed forward obliging the molten polymer to flow into the mold. The injection speed (or ideally the profile of speeds) results from a compromise between speed (to secure the global filling of impression) and the quality of the final product (very high speeds can produce marks on the surface and levels of orientation exaggerated). Flows injections of 100 to 500 g/s are a common practice.

Pressurization/holding: after the filling of the mold, it is necessary to continue to pressurize the melt inside the impression, in order to reduce the shrinkage due to cooling and to prevent the melt reflux. However, the pressurization must not be excessive, in order to avoid damages which can result a difficult ejection. This phase ends as soon as the channel of entry in the mold (named "gate"), or the part itself, are solidified.

Cooling Time: as soon as the consolidation of the gate has occurred, the piston returns to back position (in case of screw machines this starts to swirl initiating the plasticating of more material, being force to retracted due of generated pressure), and the molding continues to cool inside of a mold. The cooling phase ends as soon as the part reaches a temperature that allows the extraction without distortion. This part of the cycle is merely an operation of heat loss by the material, depending on the thickness of molding and the project of the mold (namely of its cooling system). The slower the cooling will be, the lower will result the intensity of the internal tensions due to cooling.

Opening/ Ejection: the time for this operation depends on the characteristics of the closing unit and on the movements of the mould for opening. It is a critical operation from the productive point of view, and takes place simultaneously, by means of appropriate mechanisms, with the separation of sprue and feed channels.

Pause Time: it is the period of time that passes from the moment at which the part it is ready to be moved of the mold and the beginning of a new cycle. It can be reducer to nearly zero for automatic systems.

1.2 Cellular materials

Cellular materials, otherwise known as *foams*, are biphasic materials, usually made of a solid matrix in which a fluid phase is dispersed. In general, the fluid phase is dispersed in the matrix in the form of three dimensional polyhedra, known as cells.

The first cellular synthetic plastic was an unwanted cellular phenol–formaldehyde resin produced by early workers in this field. The elimination of cell formation in these resins, as given by Baekeland in his 1909 patent, is generally considered the birth of the plastics industry. The first commercial cellular polymer was sponge rubber, introduced between 1910 and 1920. Cellular polymers have been commercially accepted in a wide variety of applications since the 1940s [1]. The development of various technologies for polymer synthesis and more recently, of newly designed polymer processing equipment, was the key factor that propelled the development of polymeric foams between the 1950s and the 1970s. Dedicated efforts from scientists and engineers around the world resulted in an increased understanding of foaming mechanisms and in enhanced techniques for efficient foam production. After the 1980s, increasing insight in environmental issues of both polymeric materials and blowing agent contributed further to the reinforcement of the foam industry(Lee S. T. 2007) [2].

The use of polymer foams in today's world has constantly increased. Polymer foams are found virtually everywhere in our modern world and are used in a wide variety of applications. The selection of a polymer for

application in the form of foam requires the analysis of the desired properties, degree of difficulty or facility of material processing and production costs.

The foam of polymeric materials can be carried out either by mechanical, chemical or physical means. Some of the most commonly used methods are the following [3]:

- Thermal decomposition of chemical blowing agents, generating either nitrogen or carbon dioxide or both, by application of heat or as a result of exothermic heat of reaction during polymerization.
- Mechanical whipping of gases into a polymer system, which hardens either by catalytic action or heat or both, thus entrapping the gas bubbles in the matrix.
- Volatilization of low boiling liquids within the polymer mass as a result of the exothermic heat of reaction or by application of heat.
- Volatilization by exothermic heat of reaction of gases produced during polymerization, such as occurs in the reaction of isocyanate with water to form carbon dioxide.
- Expansion of gas dissolved in a polymer mass upon reduction of pressure in the system.
- Incorporation of micro-sphere in a polymer mass. The hollow micro-sphere may consist of either glass or plastic beads.
- Expansion of gas filled beads by application of heat, or expansion of these beads in a polymer mass by heat of reaction.
- Physical expansion of gas in solution with a polymer matrix due to a pressure reduction.

Polymeric foams can be classified in *open-cell*s and *closed-cells*. The gas phase in a cellular polymer is distributed in voids, pores, or pockets called cells. If these cells are interconnected in such a manner that gas can pass from one to another, the material is termed *open-celled*. If the cells are discrete and the gas phase of each is independent of that of the other cells, the material is termed *closed-celled* (Figure 1).

(a)   *(b)*
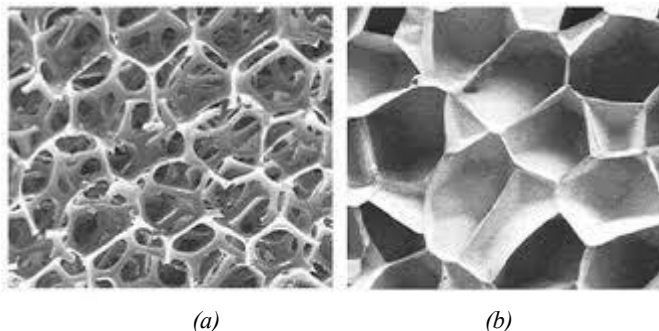
Figure 1. *Polymeric foams: open-cells* (a) *and closed-cells* (b).

Chapter 1

Foams may be *flexible* or *rigid* depending on whether their glass transition temperature is below or above the room temperature, which in turn depends on their chemical composition, the degree of cristallinity, the degree of cross-linking. Intermediate from flexible and rigid foams are semi-rigid or semi-flexible.

The main applications for plastic foamed can be found in the building, automobile, packaging and sport industries. In Table 1 advantages and disadvantages of polymeric foams are reported.

Table 1. *Advantages and disadvantages of polymeric foams.*

Advantages	Disadvantages
Low density	Complexity of processing
Economy of the material	Relatively high levels of combustibility
Excellent thermal and acoustic insulation	Levels of toxic fumes produced by combustion of relatively high
Design freedom	Difficulties reprocessing
Comfort	Environmental problems associated with some expanding agents

1.2.1 Foaming process

Foams with thermoplastic matrix are generally produced by a process based on the phase separation that occurs within a polymer/gas solution. The phase separation is induced by compelling the system to a condition of thermodynamic instability. The basic foaming process consists in three main steps: bubble formation or nucleation, growth of the bubble and stabilization of the structure. In Figure 2 it is possible to see the evolution of temperature and pressure during the steps of a foaming process.
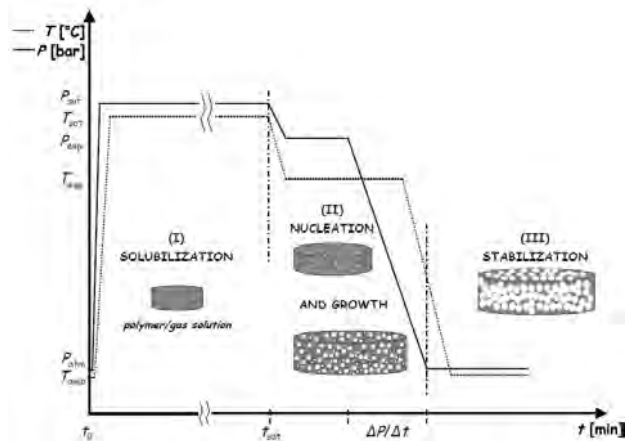
Figure 2. *Evolution of temperature and pressure during a discontinuous process of foaming.*

4

The first step in the production of a foam is the formation of gas bubbles in the liquid phase. Thermodynamically there are two processes to generate bubbles, homogeneous and heterogeneous nucleation.

Homogeneous nucleation

In the classical theory of nucleation, the nucleation rate is governed by the rate at which invisible gas clusters are energized by effective diffusion as a result of supersaturation to exceed the critical radius. In particular, homogeneous nucleation occurs when a sufficient number of dissolved gas molecules form clusters for time a long enough to make a critical bubble radius to cross over the resistance path, as shown in Figure 3.
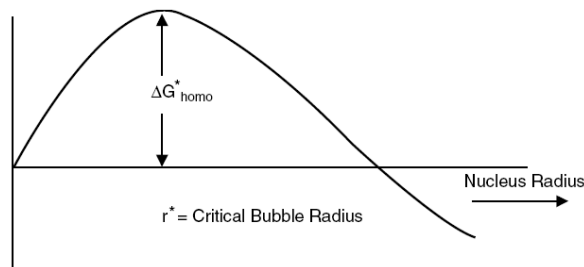
Figure 3. *Homogeneous bubble nucleation.*

Figure 4A shows a single phase containing molten polymer saturated with gas at a certain pressure. Figure 4B shows the formation of a second gas phase when the pressure is reduced from P_0 to P_S. Thermodynamic instability is the reason for nucleation of tiny bubbles. Formation of bubbles involves creation of new surfaces with certain volumes. Usually the embryos are spherical in size and therefore easier mathematical expressions can be derived based on thermodynamic principles.
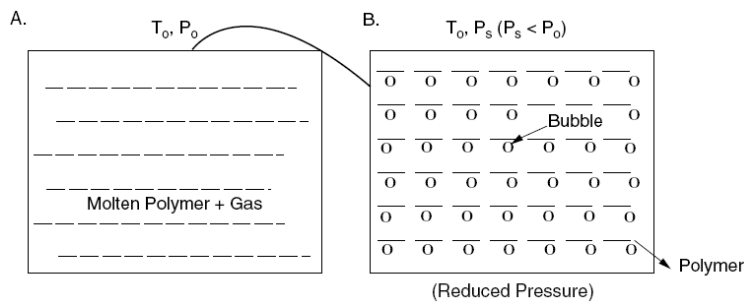
Figure 4. *Typical nucleation process. T_0 = temperature, P_0 = initial pressure and P_S = final pressure.*

Chapter 1

In the metastable region, the total work includes surface area generation, size expansion, and evaporation.

$$\Delta G = \sigma A - (P_g - P_l)V_b + n(\mu_g - \mu_l) \tag{1}$$

σ = surface tension
A = bubble surface area
P_g = gas pressure
P_l = liquid pressure
V_b = bubble volume
n = molecules number
μ_g = chemical potential
μ_l = chemical potential

At equilibrium, the chemical potentials, μ_g and μ_l, are equal, and equation 1 can be rewritten to express Gibbs free energy as:

$$\Delta G = -\frac{4}{3}\pi r^3 (P_g - P_b) + 4\pi r^4 \sigma \tag{2}$$

where r is the bubble radius. The maximum value of ΔG occurs at a critical size r^*, or when there is a critical number of gas molecules in the embryo, and represents the free energy of formation of the critical nucleus.

The spherical shape of the nucleus is assumed to represent minimum resistance for nucleation for a given volume. In general, such an assumption is reasonable. But in polymeric systems non spherical geometries might be encountered. The activation free energy for homogeneous nucleation of a critical nucleus is derived as:

$$G^*_{homo\,0} = \frac{16\pi\sigma^3}{3\ P^2} \tag{3}$$

where ΔP is the supersaturated pressure.

The nucleation rate $N_{hom\,0}$ in a gas-polymer system can be expressed as follows:

$$N_{\text{hom}\,0} = f_0 \cdot C_0 \cdot exp\left(\frac{-\Delta G^*_{\text{hom}\,0}}{kT}\right) \tag{4}$$

where $\Delta G^*_{\text{hom}\,0}$ is the minimum work to sustain a bubble, C_0 is the concentration of gas molecules per unit volume of the metastable state, and k and T are the Boltzmann constant and absolute temperature, respectively, and f_0 the frequency factor for the rate at which gas molecules join a critical nucleus.

It is possible to see that, when the degree of supersaturation is increased, the critical free energy decrease. Physically this means that a greater amount of gas in the polymer makes it easier for bubbles to form. Blander and Katz [4] obtained the following equation for the rate of nucleation:

$$N_{hom\,0} = C_0 \cdot (2\sigma/\pi m)^{1/2} \cdot exp\left(\frac{-16\pi\sigma^3}{3kT(P_b - P_l)^2}\right) \tag{5}$$

where m represents the mass of a gas molecule. In polymer processing, it is reasonable to assume P_l equal to P, representing the surrounding pressure while the gas/melt resides in the barrel. Then, the difference between P_b and P becomes superheat.

$$SH = P_b - P \tag{6}$$

In the conventional nucleation theories, the rate of nucleation is governed by the rate of diffusion (or vaporization) of gas molecules from the surrounding liquid through the interphase. For general liquids, Kagan [5], included the hydrodynamic and heat transfer effects for vaporization. Also other authors developed a similar correction to account for diffusion and viscosity-controlled nucleation rate.

Heterogeneous nucleation

This is the most common type of nucleation found in polymer systems containing additives. The efficiency of producing bubbles depends on several factors, such as the type and shape of nucleating particles and interfacial tensions of solid and solid-gas interface. Blander and Katz proposed a simple heterogeneous nucleation model for liquids in 1975.

$$G^*_{heter\,0} = \sigma_{lg}A_{lg} + (\sigma_{sg} - \sigma_{sl})A_{sg} - P \cdot V_b + n(\mu_g - \mu_l) \tag{7}$$

The primary benefit comes from the interface, which acts like a catalyst for nucleation. The presence of tiny particles and cavities reduces the activation energy required to achieve a stable nucleus. Figure 5 shows the reduction of Gibbs free energy associated with the heterogeneous nucleation process.
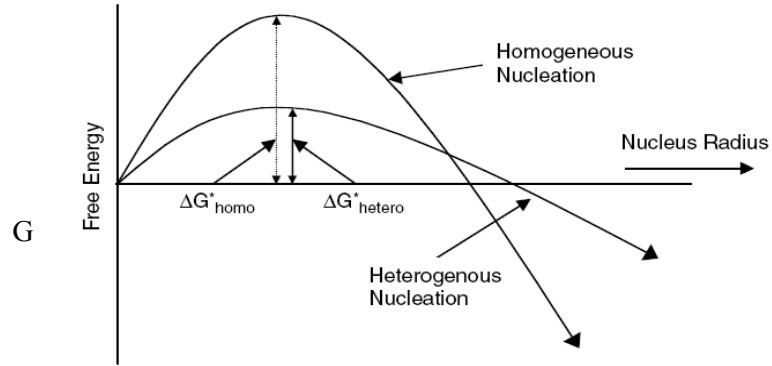
Figure 5. *Heterogeneous bubble nucleation. ΔG*_{hetero}< ΔG*_{homo}.*

The thermodynamics of heterogeneous nucleation and its mathematical analysis are given in Uhlmann and Chalmers [6]. The heterogeneity factor can be used to correct the activation energy term derived for homogenous nucleation, as shown in the following:

$$G^*_{heter\,0} = \; G^*_{\hom 0} \cdot f(\theta) \qquad\qquad (8)$$
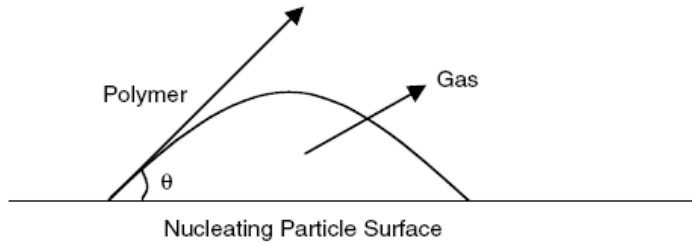
Figure 6. *Schematic of nucleating particle interaction with gas and polymer.*

For the configuration shown in Figure 6, Uhlmann and Chalmers derived an expression for $f(\theta)$ as:

$$f(\theta) = \frac{(2+cos\theta)(1-cos\theta)^2}{4} \qquad\qquad (9)$$

Then:

$$G^*_{heter\,0} = \frac{16\pi\sigma^3}{3\;P^2}f(\theta) \qquad\qquad (10)$$

where θ is the wetting angle, $f(\theta)$ is the heterogeneity factor, and σ represents the interfacial tensions of a polymer-gas bubble.

8

Cell growth

Bubble growth is the key step in polymer foam generation processes. The mechanical properties of foam polymers are closely related to the size of the bubbles created inside the material. However, cell growth is a phenomenon that is not fully understood. The classical theory suggests that the growth is controlled by diffusivity of the gas and by the stiffness of the substrate. The critical size of the bubble is dependent on the temperature because of the vapor tension. In particular, critical size of the bubble is inversely proportional to the difference between the vapor pressure and the liquid pressure. As the temperature increases the critical size of the bubble decreases because of the increase of the vapor pressure. For this reason, small bubbles are generated and start to grow at high temperatures of polymer melt. Another phenomenon occurs simultaneously with the opposite effect. The viscosity is also reduced with the increase of the temperature, increasing the diffusivity of the gas in the polymer. As a result of this effect, the possibility of a collapse of the bubbles increases (cell density decreases).

By applying the Laplace's law, it can be concluded that the gas pressure required to maintain a small bubble is higher than that of a bigger bubble. Therefore, the gas tends to diffuse from the smaller bubble to the larger one, resulting in a collapse of the small bubble, confirming the tendency that if they have enough time, the small bubbles will disappear. In 2009, Moon et al. [7] developed a theoretical framework to improve bubble growth rate and size predictions during microcellular injection molding process. Most common methods of analysis use a constant viscosity and surface tension to predict the size of the bubbles. Under actual situations, however, when the polymer contains gases, changes occur in the viscosity and surface tension that cause discrepancies between the estimated and observed bubble sizes. Moon and co-workers demonstrated that a model using variable bubble properties predicted bubble sizes that were closer to actual observations compared to results obtained from standard analysis tools.

Stabilization of the structure

The terminal phase of growth is dominated by the surroundings as the presence of molds or dies, internal pressure and gas permeability in the expanded cells and the mechanical properties of the material. Stabilization of bubbles is accomplished by cooling the foamed molten plastic to provide the necessary increase in viscosity. In particular in injection molding, since. it is a process of rapid cooling and with limited volume, the fluid pressure exceeds the pressure of the surrounding gas by increase the viscosity of the material, getting the bubbles unable to continue their growth.

1.3 Blowing agents

Polymeric foam is generally characterized by blowing agent indwelling and expansion within the polymeric matrix. Unstable foaming like boiling occurs and must be sustained by the surrounding polymeric material to form a stable cellular product. In most cases, blowing agent is virtually indispensable in the polymeric foaming process. There are a great variety of organic and inorganic blowing agents suitable for the process. From the nature of gas formation, it can be classified as physical blowing agent (PBA) and chemical blowing agent (CBA) [2]. CBA are generally solids at standard temperature and pressure (STP) and undergo a chemical transformation producing gas, while PBA, generally a liquid or gas at STP, undergo either a reversible change of state or expansion(Singh). Both PBA and CBA have been well established for specific foaming processes.

1.3.1 Physical blowing agents

Physical blowing agents (PBA) provide gas for the expansion of polymer by undergoing a change in physical state. The change may involve volatilisation (boiling) of a liquid or release of a compressed gas to atmospheric pressure after it was been incorporated into a polymer, generally at elevated temperature et/or pressure.

Physical blowing agents (PBAs) can be incorporated within the polymer matrix using various methods:
  (i)   physical blending and physical dissolution
  (ii)   physical blending and chemical decomposition
  (iii)   physical dissolution
  (iv)   chemical reaction and encapsulation.
Among these, physical blending and dissolution is considered the most commonly implemented method in the industry of polymeric foams.

Under high pressure, and sometimes elevated temperature, a physical blowing agent can be compressed as a critical or super critical fluid, depending on the processing temperature and the critical temperature of the fluid. It then contacts and dissolves into the polymeric melt to form a saturated polymer/gas system, which can foam when subjected to a lower pressure (or higher temperature) environment. When the solution is forced through an orifice to outside atmosphere, a sudden pressure reduction occurs, which automatically builds up a high supersaturation to convert the dispersed gas molecules into gas bubbles. Fast expansion and slow cooling are characteristic of the foam extrusion and foam injection molding. Namely, as soon as the polymer is cooled and sufficiently solidified to build up strength to hold the bubbles, a foam product is made. Due to the saturation of blowing agent in the fresh foam, a counter-diffusion with the surrounding air naturally occurs. As a result, blowing agent concentration in the cell

continues to decrease as opposed to the increase of air concentration. After a sufficiently long aging time, the foam will consist solely of air voids dispersed throughout the polymer matrix.

The most important physical blowing agents are:
- volatile organic chemicals (VOC)
- including hydrocarbons (HC)
- chlorofluorocarbons (CFC)
- hydrochlorofluorocarbons (HCFC)
- hydrofluorocarbons (HFC)
- Inert gases, such as carbon dioxide, nitrogen, and oxygen

High solubility of CFC in many thermoplastics has led to their use to make foams for many different thermoplastics. CFC were usually added as auxiliary blowing agents to enhance polyurethane foam expansion. Since it was discovered that CFCs cause ozone depletion issues, it has been a great challenge to find a proper replacement.

Currently inert gas are the most widely used blowing agent. This is partly because nitrogen is cheap, abundant and by far the most environmentally acceptable as it is simply borrowed from the atmosphere. The same is true for carbon dioxide even though it is greenhouse gas.

Table 2. *Properties of inert gases used as blowing agents*

	Carbon Dioxide	Nitrogen	Oxygen
Chemical formula	CO_2	N_2	O_2
Molecular weight	44	28	32
Boiling point [°C]	-78.3	-195.8	-183.0
Critical temperature [°C]	31	-146.9	-118.3
Critical pressure [MPa]	7.38	3.4	5.0
Heat of vapourisation at BP [kJ/mol]	6.8	-	-
Gas conducibility [mW/mK] at 25 °C	16.4	25.8	26.6
Vapour pressure [kPa] at 25 °C	6434	very high	very high
Flammable limit in air [vol%]	none	none	none

Many factor must be considered prior to selecting the PBA:

1. Environmental acceptability
- The stratospheric ozone depletion potential (ODP) of a blowing agent is an index defined as stratospheric ozone depleted per unit mass of a given product
- Global warming (GWPotential)
- Ground level air pollution
- Tropospheric degradation
- Long-term breakdown products
- Alogen content
- Acidification potential

2. Toxicity

3. Flammability

4. Compatibility with materials of construction

5. Boiling point

6. Molecular weight (lower costs per mole of PBA)

7. Vapour pressure in the temperature range used

8. High heat of vapourisation while still getting a high bowling efficiency is desired

9. Good solubility in raw material and poor solubility in finished foam

10. Compatibility with materials of construction

For thermoplastics, good solubility of the physical blowing agent means relatively lower minimum melt pressure to get and keep the BA in solution. This allows the melt temperature to be reduced which make it easier to cool the melt to the optimum temperature. If the BA has poor solubility, a high melt pressure and temperature is requested to force the BA into solution. This can degrade the polymer and make it more difficult to cool the melt to the optimum temperature, leading to poor cell structure, loss in blowing efficiency, surface imperfection, non-optimal closed cell content.

1.3.2 Chemical blowing agents

Some chemicals are capable of liberating gaseous components via reactions and/or thermally induced decomposition. When these occurrences take place within the polymeric melt, the decomposing chemical automatically acts as a blowing agent. Some chemicals fit certain polymer processing nicely. These kinds of chemicals are referred to as chemical blowing agents (CBAs). CBA refers more to process than product. In comparison to the requirements set for the suitability of PBAs for foaming applications, the requirements for the processing suitability of CBAs appear to be more stringent. This is so because chemical reactions and/or heat are involved, so that the dispersion of the blowing agent throughout the melt and the heat sensitivity of the polymer impose serious concerns that aggravate the processing of polymeric foams using CBAs. In other words, heat sensitive polymer and the required shear to attain dispersion are legitimate material and processing issues. Moreover, common CBAs possess a decomposition temperature 100°C above the melting point of the semi-crystalline polymers. Removing the extra heat usually becomes a serious processing bottleneck.

The decomposition of a CBA not only depends on the processing thermal profile, but also on its residence time under the decomposition temperature. If it requires too high a temperature to trigger its decomposition, or takes too much time to complete the decomposition reaction, it will be extremely difficult to incorporate to the plasticator.

Quite a few common CBAs are exothermic in nature. Exothermic reactions can promote gas expansion, but at the expense of weakening the polymeric melt strength due to the additional heating. At low expansion, polymer strength is usually not a concern, but strength becomes more critical as expansion ratio increases. Because the enthalpy plays a mixed role in the homogenizing, expansion, and stabilization stages of the foaming process, caution has to be exercised when selecting the CBA and foam fabrication method.

Most CBAs involve simple gases, which are very volatile. The inherent low solubility of the gas in the polymer combined with a high temperature profile may result in over-expansion and cell opening followed by collapsing. In contrast, PBA has less volatility and higher solubility to allow more dissolution in the melt. As a result, there are generally substantial plasticizing benefits, which renders more heat removal from the gas/melt possible. However, the volatile and less soluble CBAs virtually make a narrower foaming window. The density of the obtained foams would thus be relatively high. However, the volatile gas facilitates a sharp nucleation. If kept under control, it would be easier to obtain a fine-celled structure when using a CBA.

Many factor must be considered prior to selecting the PBA:

1. The gas release temperature closely matches the processing temperature of the polymer. If the CBA decomposition temperature is significantly above the polymer process temperature, little or no foaming will occurs. If the CBA decomposition temperature is significantly below the polymer process temperature, poor cell structure and surface skin quality is likely to result. Along with the correct decomposition temperature, the CBA must release the gas at a controllable but rapid rate.

2. The reaction products and residue of CBA must be compatible with material to be foamed and have little or no detrimental effect on properties or colour of the end product.

3. Performance

4. Cost-effectiveness and competitiveness of the finished product in a particular application

5. Kind and amount of decomposed gas(es)

6. Appropriate decomposition with other additives (i.e., peroxide)

7. Nucleating effects out of decomposed particles

8. Color from leftover or by-products

9. Type of the reaction occurring during the process (exothermic or endothermic).

Exothermic blowing agents are the organic origin substances, and as result of their decomposition nitrogen is emitted. During the decomposition of these blowing agents the heat emission occurs, which results in the increase of polymer temperature and gas pressure. Endothermic blowing agents are the inorganic origin and during their decomposition the carbon

dioxide is emitted. The use of endothermic chemical blowing agents activates the cooling of moulded parts and have impact on the decompression of gas inside moulded part, that contributes to the shortening of the cooling phase and time of the whole cycle of injection moulding process. When using the endothermic chemical blowing agents the porous structure with smaller pores sizes can be obtain, moulded parts have good surface quality and better mechanical proprieties than into the case of exothermic chemical blowing agents.[8]

Quite a few common CBAs are exothermic in nature. Exothermic reactions can promote gas expansion, but at the expense of weakening the polymeric melt strength due to the additional heating. At low expansion, polymer strength is usually not a concern, but strength becomes more critical as expansion ratio increases. Because the enthalpy plays a mixed role in the homogenizing, expansion, and stabilization stages of the foaming process, caution has to be exercised when selecting the CBA and foam fabrication method.

Most CBAs involve simple gases, which are very volatile. The inherent low solubility of the gas in the polymer combined with a high temperature profile may result in over-expansion and cell opening followed by collapsing. In contrast, PBA has less volatility and higher solubility to allow more dissolution in the melt. As a result, there are generally substantial plasticizing benefits, which renders more heat removal from the gas/melt possible. However, the volatile and less soluble CBAs virtually make a narrower foaming window. The density of the obtained foams would thus be relatively high. However, the volatile gas facilitates a sharp nucleation. If kept under control, it would be easier to obtain a fine-celled structure when using a CBA.

Table 3. *Chemical blowing agents [9].*

Blowing agent	Class	Volatiles produced	Decomposition range [°C]	Gas yield [ccm/g]
Azocarbonamide	Carbonamide	N_2, CO, CO_2	190-230	220
Dinitrosopenta-methylenethetramine	Nitrosoamine	N_2, NO, H_2O, CH_3, NH_2	160-200	210
Benzenesulphono-hydrazide	Hydrazide	N_2, H_2O	146	170-250
4,4'Oxybis(benzenesulphonohydrazide)	Hydrazide	N_2, H_2O	150	120-180
N,N'-Dimethyl N,N'-dinitroso terephthalamide	Terephthalamide	N_2, H_2O, CO_2	90-105	180
Azoisobutyronitrile	Azo	N_2	95-98	136
Sodium Bicarbonate	Inorganic	CO_2	100-130	125-130
Terephthalazide	Acid azide	N_2	85-112	107-311
Trihydrazinotriazine	Hydrazine	N_2, NH_3	275	225

Recently a new foam injection molding technology that enables the ease of processing of the CBA method with the foaming characteristics of a PBA, but in a cost-effective fashion was proposed [10]. In particular, a single screw extruder was used to produce CO_2 gas-laden polymer strands, that then will be used as feed in injection molding.

1.4 Batch foaming process

Foaming of polymers can be carried out in a batch apparatus by dissolving a blowing agent in the matrix. The solubility of the blowing agent is then reduced rapidly by producing a thermodynamic instability in the structure (e.g., a pressure decrease), to induce nucleation of the bubbles. To stabilize the bubbles, the foam cells are vitrified when the temperature is reduced below the Tg (glass transition temperature) of the polymer.

Various foaming strategies have been adopted to reduce density and improve foam mechanical properties.

About 25 years ago, Martini and his colleagues [11] reported microcellular polymeric foams by using gas (in particular CO_2) as physical blowing agent. Later on, other authors followed this research's line and Okamoto et al. [12] developed new technologies for producing nanocomposite polymeric foams by using poly(L-lactide) (PLA)/clay nanocomposite (PLACN) in a batch process by using supercritical CO_2 as physical foaming agent. This technology was used for different subsequent studies. In 2003, Ray and Okamoto [13], foamed pure PLA and PLA composite with organically modified MMT below T_m in batch mode, using supercritical carbon dioxide as physical-blowing agent, in order to study the difference in morphology of cell structures. Also Ema and Okamoto [14] incorporated nanoclay in semi-crystalline PLA for batch foaming using supercritical carbon dioxide as blowing agent. These researchers noted that the dispersed nanoclay acted as nucleating sites for the cell formation.

Recently, also other Authors [15] studied the batch foaming of modified (by chain extender epoxy functionalized) semi-crystalline PLA, using CO_2 as physical blowing agent. The system consisted in an autoclave with a volume of 300 ccm connected by means of a boost device to the gas tank (containing CO_2). The maximum working pressure was 200 bar and the limit in temperature was 350 C. The reactor was thermally regulated by temperature-controlled oil. A basket holding four samples was designed to simultaneously foam the neat and modified PLAs. The specimens were cut from the hot pressed plates into discs with 6 mm diameter and placed into the reactor. A CO_2 purge was performed prior to all experiments.

The foaming protocol was subdivided in several step: saturation of polymer with CO_2 under pressure, at the temperature of 165°C and at pressure ranging from 9.6 MPa to 14.2 MPa, for a time long enough to insure a sorption equilibrium in the entire sample; thermal stabilization of

the CO_2/PLA solution at the foaming temperature and then foaming by a pressure quench down to atmospheric pressure. This pressure drop allows the supersaturation of PLA matrix with CO_2, which led to cell nucleation and growth. Other authors [16] performed a preliminary study of non-isothermal crystallization behaviors of Poly(Lactic Acid) (PLA) under N_2 and compressed CO_2 (5-50 bar) at cooling rates of 0.2-2.0 °C/min by differential scanning calorimetry technique. The presence of compressed CO_2 postponed the crystallization peak to a lower temperature region (which resulted in about 20°C lower that under ambient N_2 at a given cooling rate) while effectively reducing the half-crystallization time and enhancing the crystallinity of the PLA specimen. The relevant matter is that on the basis of these findings, a new foaming strategy was proposed and utilized to fabricate PLA foams using the ordinary unmodified PLA by batch foaming approach.

The upper and lower temperature limits of this foaming strategy were shifted toward lower temperatures with respect to the common batch foam protocol used for PLA. The foaming tests were performed in high-pressure vessels immersed in an oil bath and rapidly heated to a desired saturation temperature. After the sorption of CO_2 into the PLA pellets reached a sort of equilibrium, the CO_2 in the high-pressure vessel was released from the foaming pressure to the ambient one.

As it appear, the most of part of Authors, referred to carbon dioxide for blowing physical agent in batch foaming of PLA. This is due to the greater solubility of CO_2 in PLA with respect to nitrogen, which could guarantee a faster solubilization in PLA matrix.

CO_2 solubility and diffusivity in many polymers tend to increase considerably under high pressure, thereby facilitating the plasticization of many polymers and enabling the forming process to be conducted at lower temperatures [17].This approach is based on the larger T_g depression effect of supercritical CO_2 on polymers, which keeps the polymer in the liquid state at relatively low temperatures. The sudden reduction in pressure leads to the formation of CO_2 nuclei which grow spontaneously. Meanwhile, as the pressure decreases, the T_g for the polymer also elevates and eventually rises above the foaming temperature, at which point the cellular structure is locked in place to produce a cellular network.

Consistently to this observation, other authors [18] stated that the different interaction of the two gases with the polymer melt led to different morphologies, in terms of foam density, cell number density, and cell size. Compared to N_2, CO_2 was much more soluble and plasticized the polymer more efficiently.

In the batch and the extrusion processes this means lower foaming temperatures and lower densities. Di Maio et al. observed that when N_2 was employed as blowing agent, at lower temperatures, the crystallization process of the polymer was too fast and the pressure developed in the nucleated bubbles was not enough for the expansion of the structure Foam

optimization based on the use of the mixture of the two gases led to a low-density microcellular structure.

On the basis of this study, a different approach was adopted by Di et al. [19] in batch foaming of semi-crystalline PLA. They used a mixture of N_2 and CO_2 (20/80%) as blowing physical agent, in order to obtain a foam with a better morphology and the lower density. In this case the batch system, which consist in a pressurized cylinder connected to the gas line, was suitably modified with a PID thermo-regulator and an acquisition system to record the pressure data, in order to allow measurement and control of the process parameters.

1.5 Foam injection molding

Foam injection molding is a relatively new process used to obtain light molded parts having good mechanical properties.

This process uses environmentally benign physical blowing agents in a high-pressure supercritical state to produce microcellular parts having small diameter cells and low density with respect to the unfoamed parts [20-22].

The gases commonly used in the foam injection molding process are nitrogen and carbon dioxide under supercritical conditions. The addition of a supercritical gas reduces both the viscosity [23-24] and the glass transition temperature of a polymer melt. So, the part can be injection molded with lower temperatures and pressures.

One further benefit of foam injection molding is the cycle time reduction: as the gas diffuses out of the polymer, the material recovers its larger glass transition temperature and vitrifies quicker; furthermore, the endothermic effect of cell nucleation and growth accelerates the cooling of the material. This certainly helps to reduce the cooling time as compared with conventional injection molding. Furthermore, it does not need a packing step as the system expands with time rather than shrinking and dimensional accuracy should improve [25-27]. On the other hand, the surface quality of molded parts is usually slightly inferior. Some studies show that the polymer-mold interfacial temperature can be manipulated and kept high enough during mold filling through a thermally insulated composite polymer film on the surface of the mold core to reduce or eliminate swirl marks, improving the surface quality of microcellular injection molding parts [28]. In 2012 a foaming control system using the Gas Counter Pressure (GCP) combined with mold temperature control during the microcellular injection molding was developed in order to investigate its influence on the parts' surface quality and foams structures [29]. In particular, a mold designed with proper sealing and installed with gas injection/release valves allowing high pressurized gas being injected/released from the mold cavity. Appropriate difference between the atmosphere and the pressure of the gas into the mold must be set: if the counter pressure is zero or one atmosphere, free foaming

occurs during the melt filling stage that usually leads to a silver-strike like flow mark on the part surface. If counter pressure is greater than one atmosphere and less than the critical pressure required for maintaining the nitrogen as SCF, the foaming will be restricted. If the gas counter pressure is higher than the critical pressure, then the melt may retain as a single phase without any foaming as long as the counter pressure applies. It was demonstrated that, for high GCP, part surface roughness for transparent polystyrene considerably improved. When GCP increased, the skin thickness also increased, the weight reduction decreased and the average cell size reduced. By increasing gas holding time, the cell density decreased and the cell size distribution became more uniform. The increase in amount of supercritical fluid foaming agent also increased the cell density. Turng et al. [30] have shown that by controlling the cell nucleation rate of the polymer/gas solution through material formulation and gas concentration, microcellular injection molded parts free of surface defects were achieved. In particular, by reducing the degree of supersaturation, the activation energy for cell nucleation will increase, thereby greatly reducing the cell nucleation rate. This retards cell nucleation during the mold filling stage, thus preventing bubble formation on the melt front of the polymer/gas solution, resulting in swirl-free microcellular injection molded parts. Altstädt et al. [31] present some possibilities to control the morphology of structural foams at high-density reductions by an intelligent mold and process design. Parameters affecting the morphology of the foamed part like the foaming temperature, the cavity pressure, cavity surface temperature and the expansion ratio were varied. In particular they have observed that elevated mold cavity surface temperatures can improve the surface finish and that increasing the mold opening distance, the cellular morphology becomes more inhomogeneous with an increasing part thickness.

If the control of the cell distribution in a complex process is achieved, also properties of the final object as dimensional accuracy, impact strength, toughness, and fatigue life can be increased.

There are a number of different systems and machines available for producing structural foams adopting either chemical blowing agents or supercritical gasses. The most important categories are low-pressure molding and high-pressure molding.

Low-pressure molding involves the use of supercritical gas or chemical blowing agents as expansion devices. In low-pressure systems, the molds, which are under very low pressure, are only partially filled with the melt. This results in a "short shot". The melt is then expanded by the supercritical gas, or by decomposing blowing agents, to fill the mold. With supercritical gas molding the resin, in pellet form, is fed into an extruder where it is plasticated and mixed with the nitrogen before it is injected into the mold.

High-pressure molding involves injecting the polymer melt and the blowing agents under higher pressures into the mold cavity to completely fill

it; the mold then expands or mold inserts are withdrawn to accommodate the foaming action [32].

Microcellular injection molding process involves the following four distinctive steps [33]:

- ***Gas dissolution***: supercritical nitrogen (or carbon dioxide) is injected into the machine barrel to form a polymer-gas solution for processing.

- ***Nucleation***: a large number of nucleation sites (orders of magnitude higher than conventional structural foaming processes) are formed by rapid and substantial pressure drop when material is being pushed into the cavity through the nozzle.

- ***Cell growth***: cell growth and cell coalescence take place during mold filling and post-filling stages and is controlled by the processing conditions such as melt pressure and temperature.

- ***Shaping***: the shaping of the part takes place inside the mold via solidification.

The first step regards the formation of a single phase polymer/gas solution. The solubility and the diffusivity of the gas in a molten polymer are critical properties in the production of foam injection molded parts. The gas solubility determines the maximum amount of gas that can be dissolved in a molten polymer at specific conditions of pressure and temperature. The diffusivity of the gas in the polymer melt affects the time necessary to obtain a single-phase solution. In particular, the diffusion rate and the total diffusion time for the gas to dissolve in the polymer are crucial aspects for the effectiveness of the foaming system. While the solubility of carbon dioxide is higher, nitrogen tends to provide finer cell structure and gives better surface finish [34]. In some cases, in order to obtain the promotion of uniform bubble nucleation, nucleating agents which may promote a fine distribution of bubble nucleation are added [35]. Incorporation of nanoparticles in matrix may affect the nucleation and bubble growth process. Further, nanoparticles will enhance the performance (stiffness, strength etc.) of matrix. The particles used in most of literature studies are of micron size [36], but the effect of nanoparticle dispersion on the foam cell morphology was also studied [19, 37]. In this case, due to their very high surface to volume ratio, is expected that also at very low concentration these nanoparticles can greatly enhance the bubble nucleation process. Indeed, the extremely fine dimensions and large surface area of nanoparticles provide opportunity of intimate contact between the particles, polymer matrix, and gas. It was also found that in presence of well dispersed nanoparticles, the cell size is reduced, as more bubbles start to nucleate concurrently [38-39]. In addition, the presence of nanoparticles may enhance mechanical and physical properties, the heat distortion temperature, and fire resistance of polymer foams [40].

Chapter 1

Ramesh and Lee [41] showed that, compared to the more traditional talc filling, organoclay nanofillers resulted less effective in polypropylene (PP) foaming. On the contrary, some works from the Toyota Technical Institute reported up to two orders of magnitude increase in the cell number densities on a polypropylene/clay system [42-43] and also reported successful results on a polycarbonate/fluoroectorite system [44] and on two poly(lactic acid)/organoclay systems [45], evidencing the different efficiency of different clay surface modifications to achieve micro to nano-cellular foams. In 2009 Hwang et al. [46] studied the effect of montmorillonite (MMT) and compatibilizers content on the on the microcellular foaming properties of low density polyethylene. Their studies has demonstred that, compared with the neat LDPE foams, the presence of a small amount of clay can significantly increase the tensile strength and the cell density, but decrease the cell size. The microcellular nanocomposites with higher organoclay content or MA content appeared to be more brittle. A very recent study [47] has quantitatively analyzed the improvements in mechanical properties of microcellular foam with the addition of nanoclay (MMT). Nanocomposite of polypropylene and nanoclay was prepared in a co-rotating twin screw extruder. Maleic anhydride grafted polypropylene (PP-g-MA) was used as compatibilizer. PP/nanocomposites were foamed in a microcellular injection molding machine, where supercritical nitrogen was mixed with plasticized PP/ nanocomposite inside the screw-barrel assembly. The foamed samples were tested for various mechanical properties, demonstrating that a considerable improvement occur in the property of microcellular polypropylene by the addition of a low percentage of nanoclay.

However, the nanoparticles can affect in a positive or negative way the crystallization behaviour of these composites influencing both the crystal nucleation and the chains mobility of the melt. The result of all these effects is hard to describe and predict.

From the process viewpoint, cell growth during shaping of the part is controlled by pressure. In injection molding, the pressure at each time is function of the position within the mold. The advancing front has the lowest pressure in the system, usually very close to atmospheric values, whereas upstream from the gate usually there is a quite high pressure. The pressure is held high during the packing stage and it is released at the end of the packing stage [48]. In foam injection molding, the cavity is not completely filled and a packing stage is not required because, as already mentioned, the system expands rather than shrinking.

Therefore, main variables for the control of cell growth are the degree of filling of the cavity and the temperature of the mold. Mold temperature should be low, but high enough to allow foaming [49].

During the time of cell growth in a foam, a number of properties of the system change greatly [50-51]. The following considerations are of primary importance:

20

- the fluid viscosity is changing considerably, influencing both the cell growth rate and the flow of polymer to intersections from cell walls;

- the pressure of the blowing agent decreases, falling off less rapidly than an inverse volume relationship because new blowing agent diffuses into the cells as the pressure falls off;

- the rate of growth of the cell depends on the viscoelastic nature of the polymer phase, the blowing agent pressure, the external pressure on the foam, and the permeation rate of blowing agent through the polymer phase;

- the pressure in a cell of small radius is greater than that in a cell of larger radius. There is thus a tendency to equalize these pressures either by breaking the wall separating the cells or by diffusion of the blowing agent from the small to the larger cells.

Mahmoodi et al. [52] observed that when the system pressure increases, the critical bubble size increases, and then those bubbles which have the size smaller than this critical size will tend to collapse. Increasing the pressure of system increases the critical bubble size, and then more bubbles tend to collapse until no bubble will survive in the system. The gas inside the bubbles diffuses back into the polymer matrix and dissolves in it. Concerning the mechanical properties of the molded structural foams, few recent studies consider the correlations among morphology and mechanical properties in the literature [53]. In 2012 some authors [54] studied morphology and the mechanical properties of polycarbonate samples produced through the variation of different processing parameters. The authors of this article come to the conclusion that all bending and tensile properties were influenced by the morphological structure in the same way. While improving one tensile property by the injection moulding process, all other tensile properties as well as bending properties are being improved at the same time.

The microcellular injection molding can be used advantageously for different applications, as injection molded automotive components, in which new and simplified principles of mold and part design are being applied to capitalize on the longer flow lengths and lower clamp forces, mold temperatures, and cavity pressures associated with microcellular foam molding. Designing specifically for the microcellular foam process routinely results in lower mold costs, reduced component costs, and optimized component functionality [55].

Another important application is the manufacture of porous scaffolds. Three-dimensional porous scaffolds fabricated from biodegradable polymers have been widely used as temporary extracellular matrices (ECM) and play critical roles in tissue engineering and in situ tissue reconstruction. High porosities and interconnected pores of porous scaffolds are required to facilitate cell seeding and adhesion, ECM secretion and eventual tissue

regeneration. On the other hand, complicated external shape is also highly desirable from the clinical point of view because the final anatomical shape of a regenerated tissue is basically dependent on the shape of the associated scaffold. Therefore, an ideal scaffolding technique should be able to simultaneously form internal interconnected pores and external anatomical shapes. Gomes et al. [56] reported an injection molding/gas foaming approach to prepare biodegradable starch-based polymeric scaffolds with a compact surface and porous cores. Moreover, L. Wu et al. [57] reported a room-temperature injection molding/particulate leaching approach for fabrication of biodegradable three-dimensional porous scaffolds. In 2012 different composites were injection molded and characterized [58]. The water soluble and sacrificial polymer, PEO, and NaCl particulates in the composites were leached by deionized water to produce porous and interconnected microstructures. The effect of leaching time on porosity, and residual contents of NaCl and NaCl/HA was investigated, demonstrating that the leaching time depends on the spatial distribution of sacrificial PEO phase and NaCl particulates. Furthermore, the HA addition at PCL improves the elastic and loss moduli of the scaffolds.

Recently experiments of new technologies were carried out. Between these, Turng et al. [59] proposed a new microcellular injection molding process for polycarbonate using water as the physical blowing agent and tiny salt crystals of 10–20 μm recrystallized during molding as cell nucleating agents. Distilled water with dissolved salt were fed through the hopper of an injection molding machine at a preset rate and mixed with polycarbonate (PC) in the machine barrel. Microcellular PC tensile bars were then injection molded with different shot volumes, water/salt solution feed rates, and salt concentrations. They have demonstrated that in comparison to commercial microcellular injection molded parts using nitrogen as the physical blowing agent, PC-water parts exhibit a smooth surface comparable to that of solid PC parts. PC-water parts also have a stronger specific Young's modulus and specific ultimate strength than commercial microcellular injection molded PC-N_2 parts.

1.6 Biodegradable polymers

Biodegradable polymers are a class of polymers made from various natural resources that are environmentally safe and friendly. These polymers have potential applications in the packaging and non-packaging industry. The expression "biodegradable polymer" refers to the susceptibility of a polymer to decomposition by living beings or by environmental factors. The American Society of Testing Materials defines biodegradable as capable of undergoing decomposition into carbon dioxide, water, methane, or biomass resulted from the enzymatic action of microorganisms, which can be

measured by standardized tests, in a specified period of time reflecting available disposal condition [60].

Natural environmental factors that cause decomposition include bacteria, fungi, molds and yeast. The degradability is defined as the ability of materials to break down by bacterial, thermal or ultraviolet (UV) light action. Degradation of polymers by UV light is also called photo-biodegradation, in which the polymer degrades into low molecular weight material and later is converted to carbon dioxide and water by bacterial action.

Some of the important properties of a biodegradable biomaterial can be summarized as follows [61]:

- The material should not evoke a sustained inflammatory or toxic response upon implantation in the body.
- The material should have acceptable shelf life.
- The degradation time of the material should match the healing or regeneration process.
- The material should have appropriate mechanical properties for the indicated application and the variation in mechanical properties with degradation should be compatible with the healing or regeneration process.
- The degradation products should be non-toxic, and able to get metabolized and cleared from the body.
- The material should have appropriate permeability and processability for the intended application

1.6.1 Biodegradable polymer: Poly(lactic) Acid

Poly-lactic acid (PLA) is a rigid thermoplastic polymer, a versatile polymer, recyclable and compostable, with high transparency, high molecular weight, good processability and water solubility resistance. In general, commercial PLA is a copolymer between poly (L-lactic acid) and poly (D-lactic acid), that can be semi-crystalline or totally amorphous, depending on the stereopurity of the polymer backbone. PLA is obtained from the controlled depolymerization of the lactic acid monomer obtained from the fermentation of sugar or feedstock or corn, and by the ri ng-opening polymerization of the cycle lactide dimer. The next Figure 7 shows the repeating unit of Poly-lactic acid.
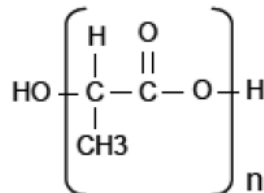
Figure 7. *Structure of Poly-lactic acid.*

Chapter 1

Poly-lactic acid is associated with two monomers, lactic and lactide. These two monomers have a chiral carbons, where the lactic acid has two stereoisomers, L- lactic acid and D-lactic acid .The lactide ,which is the cyclic diester of lactic acid, has different isomers: L-lactide (two molecules of L-lactic acid), D-lactide (two molecules of D-lactic acid), a racemic mixture of D-lactide and L-.lactide, that results in meso-lactide (one molecule of L-lactic acid and one molecule of D- lactic acid). In Figure 8 is possible to observe the combination of the different isomers mentioned above, resulting in PLLA, PDLA or PLA.
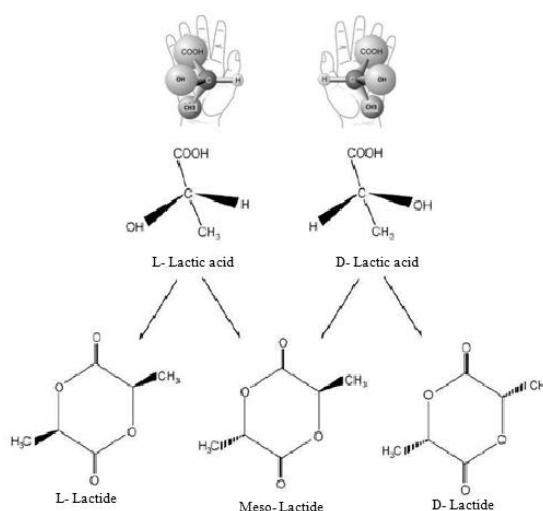
Figure 8. *Stereochemistry* [62]

Depending on the composition of the optically active L- and D,L-enantiomers, PLA can crystallize in three forms (α, β and γ). The crystal structure of PLLA homopolymer exists in α and β forms. PLA polymers with L-content greater than 90% tend to be crystalline while those with lower optical purity are amorphous. Moreover, Tm, glass transition temperature Tg, and crystallinity decrease with decreasing L-isomer content [63].

The synthesis of poly (lactic acid) is performed by the fermentation of glucose to yield lactic acid monomers D or L conformation. After through the condensation by polymerization there are presents oligomers of poly (lactic acid) that are pre–polymers of low molecular weight and average properties. Finally, the polymerization by ring opening the lactide will give rise to poly(lactic acid) high molecular weight and with better properties. Figure 9 shows all the process to obtain Poly(lactic acid).
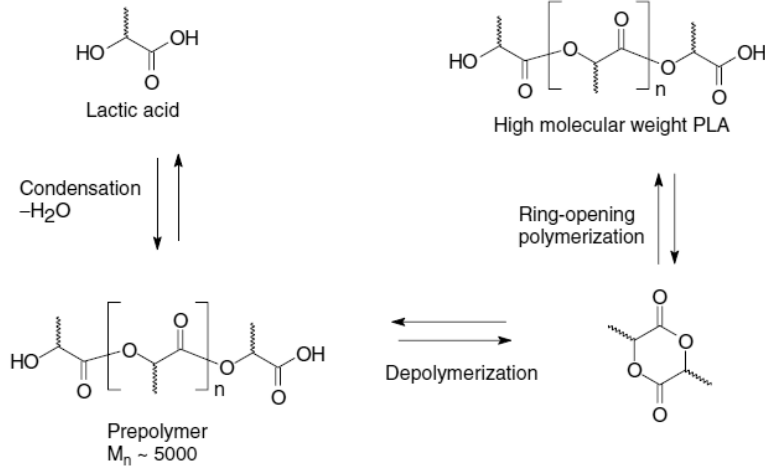
Figure 9. *Mechanism to obtain Poly(lactic acid).*

Biodegradation is a particular type of degradation, caused by the biological activity of bacteria, fungi, and their enzymes along with significant chemical alterations on the structure and properties of the materials. In order for biodegradation to occur, we need three essential elements: microorganisms, environment factors and substrate. The process of biodegradation is divided in two steps: scission of the main-chain in oligomers, and then assimilation of the oligomers by the micro-organisms. Biodegradation of PLA appens in three stages [64]:

1. degradation occuring by means of the diffusion of water intro the material (first in the amorphous zones) followed by random hydrolysis;

2. Fragmentation of the material to OLLA [oligo(L-Lactic acid)];

3. More extensive hydrolysis accompanied by phagocytosis, diffusion and metabolism.

In the first stage of degradation (Figure 10), a non-enzymatic random hydrolytic cleavage of the ester linkage lead to a quickly decrease of the MW, with little weight loss. The extent of hydrolysis depends on the size, hydrophilicity of the given polymer implant, crystallinity and environmental factors like, pH, temperature, moisture, and usually the degradation time is shorter for low-molecular-weight, morehydrophilic and more-amorphous polymers.
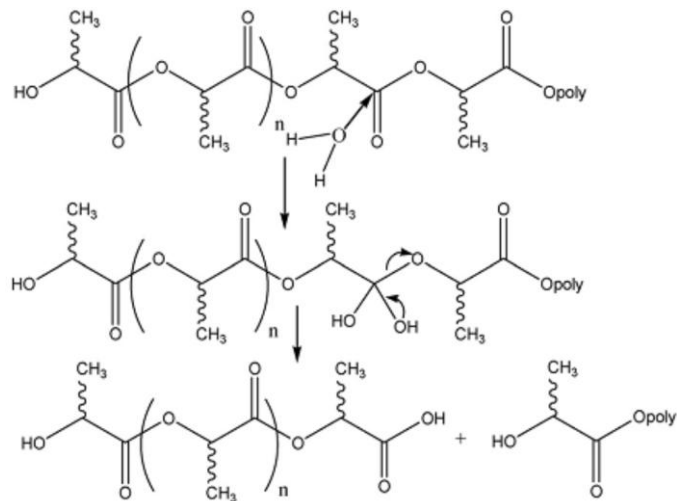
Figure 10. *Hydrolysis of PLA.*

During the second stage, the decrease in M_W slows and severe weight loss as well as the initiation of monomer formation are evident and the production of lactic acid occurs.

Finally, when total weight loss is experienced, about 50% of the polymer is converted to monomer, and continues the hydrolysis of the soluble oligomers, until all are converted in lactic acid. After hydrolysis, fragmentation and biodegradation, H_2O, CO_2 is produced and the end product is salts. [65].

1.7 Foam injection molding of biodegradable polymers

Biodegradable polymeric materials are gaining an increasing interest since they can contribute to reduce the environmental impact of all industrial products, of which the polymeric fraction represents a significant part. However, the higher costs with respect to those derived from non-renewable sources, the difficulties of processing these polymers due to the high viscosity, which requires for processing high pressures and temperatures close to those of degradation, and in some cases their inadequate properties represent key limitations for many applications.

The foam injection molding seems the ideal solution to adopt these materials for the production of low-cost, high quality articles. In fact, the use of physical blowing agents in a high-pressure supercritical state

increases the mobility of the polymer, thus allowing to process these polymers by conventional injection molding and possibly improving some physical properties by promoting a faster crystallization.

The addition of a supercritical gas allows the reduction of viscosity and glass transition temperature of polymer melt. So, the part can be injection

molded with lower temperatures and pressures. This is a very good advantage particularly for biobased plastics, which tend to be both thermally sensitive and have narrow processing windows.

In conclusion, combining biobased plastics and MIM would potentially enlarge the processing window of biobased materials with less thermal degradation due to the decreased temperatures required, and would decrease the amount of material while using an environmentally benign blowing agent. If the control of the microcell distribution in a complex process is achieved also properties of the final object as dimensional accuracy, impact strength, toughness, and fatigue life can be increased.

Among many biodegradable polymers, Polylactide (PLA) is a biobased, biodegradable and biocompatible aliphatic polyester and have found many applications in biomedical industries and packaging due to their unique set of properties. In a study of 2010 [66], PLA was injection molded and foamed by using supercritical nitrogen. Injection molding parameters such as mold temperature and SCF content were varied in order to investigate their effects on foam cell size. The effects of nucleating agent on the foam structure and cell size distribution were also elucidated by image analysis. Impact and dynamic mechanical performance of the foams were also evaluated. In the successive year Peng et al. [67] investigated the effect of gas content (in this case nitrogen) on the tensile properties and microstructure of two grades of poly (lactic acid) (PLA) that differ in terms of D-lactic acid (D-LA) content. They demonstrated that the mechanical properties and cell morphology of microcellular injection molded PLA were found to be dependent upon the D-LA content. This is attributed to the trend of a higher degree of crystallinity and nucleating capability. At a high gas content level, foams with small cell sizes and high cell densities could be produced.

1.8 Effect of gas on the rheology of a polymer

Gases are susceptible to interact with the polymers and change their rheological properties. Experimental results [68] indicate that the rheological properties of two phase gas-polymer suspensions are sensitive to shear rate, blowing agent concentration, melt temperature, and nozzle temperature.

A gas can act in two ways with the polymer. The gas particles can act as solid in the surrounding fluid , increasing the viscosity of the system. Conversely, if the bubbles are deformed under shear, the flow field is not adversely affected by the presence of the gas phase, and the system exhibits lower viscosity.

We can consider that besides the matrix viscosity, the viscosity of bubble bearing in the non-Newtonian fluid is a function of three variables: capillary number, volume fraction of the gas phase, and the bubble size distribution.

Chapter 1

The viscosity of single-phase gas-polymer solutions for these same polymers is lower than that of the two-phase system at the same temperature and shear rate conditions.

For the single-phase gas-polymer solutions, the dissolved gas increases the free volume of polymer molecules, thus allowing chain segments of the macromolecules to move more easily and reducing the viscosity of the system. Once the dissolved gas diffuses out of the melt there is an increase in polymer melt viscosity, reasonably attributed to a decrease in free volume. However, despite the resulting absence of the dissolved gas to plasticize the matrix, the viscosity of the suspension never fully increased to the value of the homogeneous melt. Since the gas bubbles had negligible viscosity, they deformed passively with the suspending medium, and their response to the local shear stress of the surrounding melt was viscous. This decreased the distortion of flow-lines around the bubbles resulting in a reduction in the viscosity of the suspension.

Conventionally, the shear viscosity is measured by means of a rotational or capillary rheometer. Alternatively, the shear viscosity measurements can be made using a die that is connected to real processing equipment. If the volumetric flow rate through the die and the pressure gradient in the fully developed region are known, the shear viscosity can be determined relatively straightforwardly, as in the case of a capillary rheometer. An obvious advantage of using the processing equipment as a rheometer is the fact that the thermo-mechanical history experienced by the test material is fairly similar to that in the actual processing operation. By contrast, in the conventional capillary rheometer the melting of the polymer takes place by means of heat conduction only and, consequently, there is practically no mixing and homogenization before the entry into the die. In past years, several developments have been directed toward performing rheological measurements in conjunction with injection molding machines [69-72].

In 2007, Aho et al. [73] carried out the viscosity measurements for two polystyrenes and two polypropylenes using a tailor-made slit die with adjustable height. Viscosity values calculated from the pressure recordings with all three dies showed satisfactory superposition and, for all the materials, the results were also very well comparable with the ones obtained by capillary rheometer and rotational rheometer.

In 2012, Turng et al. studied the effect of pressure and nitrogen under supercritical conditions on melt viscosity of LDPE in conventional and microcellular injection molding using a high-pressure slit-die rheometer [74]. In this work, shear viscosity of polymer/gas solution was found to be significantly lower than the only polymer. Furthermore, the pressure effect on viscosity was found to be more profound at high pressures, low shear rates and low temperatures.

1.9 Monitoring of cavity pressure and temperature profiles

It is very important to be able to accurately monitor the suitable variables in injection molding process, during each phase, in order to establish a key parameter for on-line quality control. In the 90s it was found that cavity pressure is the best factor to correlate with the quality parameters properties of the product. Rawabdeh et al. [75] stated that on-line monitoring of the injection molding operations required continuous measurements of different parameters while the machine was running.

More recently approaches have been proposed in the literature which are based on cavity pressure control during the different stages of the injection molding process [76-77].

Monitoring of thermo mechanical history variables, like temperature and pressure, inside the mold can represent a useful approach to understand what happens inside the cavity during the filling phase. Through the next Figure 11 is possible observe a typical qualitative pressure evolution inside the mold cavity plotted with its main features during a conventional injection molding process.
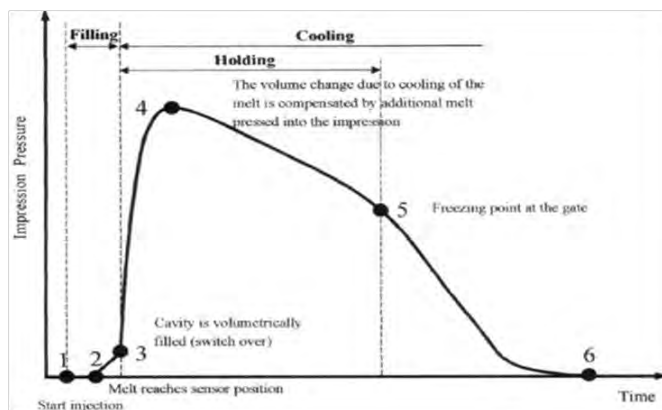
Figure 11. *Typical pressure evolution inside the mold′s cavity* [78].

In foam injection molding process the filling stage is even more important because of in this phase the gas expansion and the consequent formation of the foam takes occurs.

The blowing agent at high pressure and an amount of polymer to fill up to 50-80% of the mold, are injected into the "mixing chamber" to form a gas-polymer solution. The solution is injected into the mold where, due to a sharp reduction of pressure, the solubility of the gas in the polymer is reduced instantaneously and it has the de-mixing of the two phases.

The separation of the two phases leads to the nucleation and growth of gas bubbles. The process ends when the pressure forces that tend to expand the bubbles are balanced by the forces that instead oppose this process. The

opposing forces the expansion are essentially produced by the solidification of the polymer matrix and the possible formation of crystalline phases in the polymer. Figure 12 shows the different stages of the cavity filling.

(a)   (b)   (c)
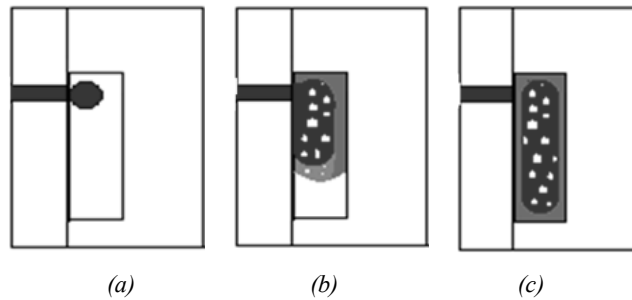
Figure 12. *Injection of polymer/gas solution (a); Cooling of skin on contact with the cold wall (b); Foaming of core inside the compact skin (c).*

In 2010 Berry and Kishbaugh [79] tested cavity pressure sensors and in-mold temperature sensors to determine their effectiveness for the process monitoring of microcellular foam injection molding . Piezoelectric pressure transducers were placed behind ejector pins, with direct exposure to the melt. Cavity pressure and melt temperature profiles at each position were measured and then analyzed relative to part weights and part dimensions.

Chapter 2
Materials and methods

2.1 Conventional polymers for injection molding

A preliminary study of molding conditions using two thermoplastic polymers commonly adopted for conventional injection molding and previously well characterized, a semi-crystalline polypropylene and an amorphous atactic polystyrene, was made, in order to obtain the appropriate knowledge of the microcellular injection molding and develop accurate foamed parts.

2.1.1 Polypropylene HIFAX BA 238 G3

A semicristalline heterophasic polypropylene Hifax BA238G3 with increased isotactic index, supplied by Montell, with Mn=55.6 103 and Mw=37.6 104 [80], was used. This grade of polypropylene is compounded with about 26% in weight of ethylene-propylene rubber (about 50% of ethylene and propylene) and 1.5% talc.

The relevant physical, mechanical, thermal and processing characteristics are summarized in the following Table 4 and Table 5.

Table 4. *Physical and mechanical properties for HIFAX BA 238 G3 [78, 81-83].*

	Method	Value	Unit
Physical property			
Density	D 792	900	$Kg\ m^{-3}$
Mechanical Property			
Flexural Modulus, 23°C	D 790	1000	MPa
Tensile Strength	D 638	20	MPa
Elongation at break	D 638	400	%
Poisson's coefficient ν	[-]		[-]
Notched Izod impact strength	D 256	80 (-30°C) 140 (0°C) >600 (23°C)	$J\ m^{-1}$

Chapter 2

Table 5. *Thermal properties and processing characteristics for HIFAX BA 238 G3*

Thermal Property			
Thermal Conductivity	ASTM C177	0.172	$Wm^{-1}K^{-1}$
Specific Heat	ASTM C351	2620	$J\,Kg^{-1}\,K^{-1}$
Vicat softening point (50°C/h 50N)	ASTM D1525	55	°C
Latent Heat of crystallization		$1.88\ 10^5$	$J\,Kg^{-1}$
Coefficient of linear thermal expansion α_L	ASTM D696	$2\ 10^{-4}$ (crystalline 72.5%)	K^{-1}
	ASTM D696	$6.55\ 10^{-4}$ (amorphous 72.5%)	K^{-1}
Linear Compressibility β_L	ASTM D696	$1.0\ 10^{-5}$ (crystalline 72.5%)	MPa^{-1}
	ASTM D696	$9.8\ 10^{-4}$ (amorphous 72.5%)	MPa^{-1}
Processing characteristics			
Melt Flow Index (230°C,2.2 Kg)	ASTM D1238	13	g/10min
Injection temperature range		180÷290	°C
Mould temperature range		20÷60	°C
Maximum shear stress		0.26	MPa
Minimum shear rate		24000	s^{-1}

2.1.2 Polystyrene PS 678E

The second material used was a general purpose Polystyrene (PS 678E) supplied by Dow Chemicals, commonly used in injection molding process. Polystyrene 678E presents a molecular weight distribution characterised by Mn=(87±4) 10^3, Mw=(250±20) 10^3 and Mz=(490±60) 10^3. The resin was well characterized and relevant properties [83-85] are summarized below. The thermal conductivity of the resin is reported [86] as essentially constant with the temperature; in particular at T =343K and T = 473 K (i.e. above and below glass transition temperature) the values 0.165 W/m K and 0.18 W/m K were reported, respectively. The Specific heat of resin, measured at different temperatures, is given in Table 6.

Table 6. *Specific heat of PS 678E [84].*

Temperature [K]	Specific heat [J/Kg K]
523	2300
473	2150
423	2000
373	1900
363	1600
353	1500
343	1450
333	1400

32

Typical properties of solid PS 678E are resumed in Table 7.

Table 7. *Properties for PS 678E [83-88]*

	Method	Value	Unit
Physical property			
Density	ISO 1183	1050	$Kg\ m^{-3}$
Mechanical Property			
Elasticity Modulus, 23°C	ISO 178	3255	MPa
Yield Stress	ISO 527-1/-2	43	MPa
Strain at break	ISO 527-1/-2	2	%
Poisson's coefficient ν	-	0.33	[-]
Ball indentation hardness	ISO 2391/-1	150	MPa
Thermal Property			
Thermal Conductivity	ASTM C177	0.17	$W\ m^{-1}\ K^{-1}$
Specific Heat	ASTM C351	See Table 5	$J\ Kg^{-1}\ K^{-1}$
Vicat softening point (50°C/h 50N)	ISO 306	86	°C
Coefficient of linear thermal expansion α_L	ASTM D696	$7.5\ 10^{-5}$	K^{-1}
Linear Compressibility β_L	ASTM D696	$1.04\ 10^{-4}$	MPa^{-1}
Processing characteristics			
Melt Flow Index (200°C, 5 Kg)	ISO 1133	11	$g\ 10\ min^{-1}$
Injection temperature range		200 ÷ 240	°C
Mould temperature range		20 ÷ 70	°C
Maximum shear stress		0.25	MPa
Minimum shear rate		40000	s^{-1}

In Table 8 the parameters of Cross-Vogel Model, determined by independent rheological measurements, are reported.

Table 8. *Parameters of Cross-Vogel Model.*

Table η* [Pa*s]	0.63
A [°C]	1348
T_{ref} [°C]	50.9
n [-]	0.17
τ* [Pa]	35201
k [1/Pa]	1.00E-05
T [°C]	220
T [K]	493.15
P [bar]	1
P [Pa]	1.00E+05

Chapter 2

2.2 Biodegradable polymers for injection molding

After the study on the process variable and the microcellular injection molding of polymers commonly utilized for injection molding, microcellular injection molding of two different grade of a biodegradable polymer was attempted.

2.2.1 Poly(lactic) Acid PLA 2002D

The material adopted in this work is a commercial grade PLA produced by Natureworks with the trade name 2002D. According to the material data-sheet the melt flow index is equal to 6, thus suitable for both extrusion and injection molding, and the D-enantiomer content is about 4%. The molecular weight distribution was determined by a size exclusion chromatography. It was found that $Mn = 145 \cdot 10^3$ g/mole and $Mw = 235 \cdot 10^3$ g/mole.

Before any test or processing, the material was dried for 24 h under vacuum at a temperature of 60°C.

Table 9 reports the relevant physical and mechanical properties of PLA 2002D.

Table 9. *Properties for PLA 2002D [89].*

	Method	Value	Unit
Physical property			
Specific gravity	ASTM D792	1.24	$g \, cm^{-3}$
Mechanical Property			
Tensile Strength at Break	ASTM D882	53.0	MPa
Tensile strength, Yield	ASTM D882	60.0	MPa
Elongation at break	ASTM D882	6	%
Tensile Modulus	ASTM D882	3.45	GPa
Izod Impact, Notched	ASTM D256	0.1281	$J \, cm^{-1}$
Processing characteristics			
Melt Flow (210°C, 2.16 Kg)	ASTM D1238	5– 7	$g \, 10 \, min^{-1}$

2.2.2 Poly(lactic) Acid PLA 4032D

The material adopted in this part of the work is a commercial grade PLA produced by Natureworks with the trade name of 4032D with a D-enantiomer content of approximately 2% and with a maximum degree of crystallinity of about 45%. PLA 4032D have a molecular weight distribution characterised by $Mn=119 \cdot 10^3$ g/mole and $Mw=207 \cdot 10^3$ g/mole.

34

Before any test or processing, the material was dried for 24h under vacuum at temperature of 60°C.

In Table 10 typical properties of solid PLA 4032D are resumed.

Table 10. *Properties for PLA 2002D [89-90].*

	Method	Value	Unit
Physical property			
Specific gravity	ASTM D1505	1.24	$g\ cm^{-3}$
Mechanical Property			
Flexural Modulus	ASTM D790	2.85	GPa
Flexural Strength	ASTM D790	44	MPa
Secant Modulus	ASTM D882	3.44	GPa
Thermal Property			
Melting Point	-	160	°C
Processing characteristics			
Melt Flow Index	ASTM D1238	7.72	$g\ 10\ min^{-1}$

2.3 Blowing agent: Nitrogen

The physical blowing agent adopted in this work is nitrogen under supercritical conditions.

Nitrogen Gas (N_2) gas is an inexpensive, nonflammable, nontoxic permanent gas. It can be made from the air and is chemically inert, which results in an environmentally safe blowing agent to replace some ozone depletion chemical blowing agents. Nitrogen in the gas state is commercially available at 13.8 MPa to 20.7 MPa. Therefore, the pressure of nitrogen gas in the vendor's tank already remains higher than critical pressure. The liquid state of nitrogen flow rate is stored in the dewars as a cryogenic liquid at about − 195.8 ˚C. For large nitrogen flow rates, cryogenic nitrogen is preferred. Overall, nitrogen is preferred in many, if not most, technical applications because it results in a more consistent and uniform microcellular part.

2.4 Batch foaming equipment

In the Figure 13 a foaming apparatus designed in the laboratory is schematically shown. This apparatus consists of a pressurized cylindrical vessel (about 200 ccm), made of stainless steel. A rigid sample holder, integrated into the cover closing, can be inserted inside the cylindrical part, and closed in it by means of 4 screws in order to guarantee the airtight seal of the reactor chamber.

Figure 13. *Hermetic system of batch process and your its constituents.*

The system is also provided by a cooling channel in order to operate the temperature quenching of the system by means of a cooling fluid, water or air. The heating of the vessel is performed by means of two cartridge heaters, which are operated by a temperature controller, which works in a feedback system logic controller. In fact, a thermocouple, placed in contact with the heaters, detects the current temperature, and comparing this value with the set-point, regulates the power for the heating. It is possible to operate at maximum heating rate of 15 °C/min. Two temperature values are monitored during the test by means of two type K thermocouples, with an accuracy of 0.02 °C: one in the upper part of chamber, and the other in the central part.

The upper part of the cylindrical vessel is connected by means of a boost device to the gas (physical bowing agent) tank. The vessel pressure (and consequently the amount of gas inserted) was measured at an accuracy of 1 bar by a pressure transducer, and ranged from 0 up to 65 bars.

The system is provided also for an exhaust valve which is used either for pressure control inside to the vessel, or to perform the pressure quench of gas, that is a decompression down to atmospheric pressure, during the foaming stage. It also permits to connect a vacuum pump for preventively elimination of moisture, in the case of hygroscopic materials.

2.5 Foam injection molding equipment

A traditional injection molding machine (a 70ton Negri-Bossi press) with screw diameter of 25 mm and L/D = 22 was adapted to carry out the microcellular injection molding process.

In particular, the screw of a traditional injection molding machine has the function to melt and drag out the material to the injection zone, where a check valve allows the injection of the material in the cavity. The screw for microcellular injection molding must be provided with a chamber for mixing

the gas with the molten polymer. The area of the screw before the mixing chamber must have fillets with a geometry that avoids the gas turn back. The cylinder within which the screw slides must be equipped with at least one gas injector connected to a pump which injects the gas into the cylinder.
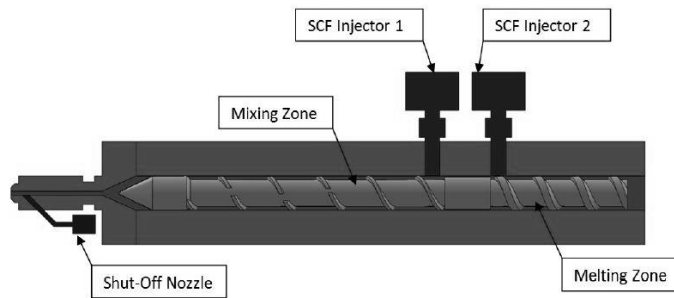
Figure 14. *Scheme of a typical screw for foam injection molding.*

The mold of a microcellular injection molding machine must be equipped with a good temperature control system, like in a batch process. A traditional mold is composed of several channels that bring the material to the cavity. In these channels the material cools and is oriented as a result of the flow. In the mold of a microcellular injection molding press it is necessary that the material arrives still hot in the cavity in order to avoid the foaming of the material already in the channels due to the lower temperature and the pressure drop. To this aim, the developed mold has a single channel, and a hot runner with a very small diameter. The hot runner is surrounded by a heating element that maintains a constant temperature and is thermally insulated from the mold.

The nozzle is also provided with a needle valve, to prevent the material leakage during the operations of mold opening and ejection.

The mold is thermally insulated from the machine through two layers of ceramic material with fiberglass. The mold temperature is controlled by a system of channels and a layer of electrical heaters.

A conventional injection molding press is typically provided with an ejection system in which the ejection pins move inside holes in mold. This system cannot be adopted if a control of cavity pressure is aimed at. Therefore a system was designed consisting of three ejector springs located inside the mold. In the future this system could also be used to enter a gas counter-pressure in the mold in order to control the foam inside the cavity. Two cavities having different thickness could be adopted: the geometry of the cavities is reported in Figure 15.
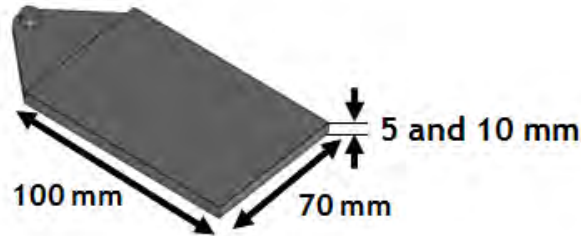
Figure 15. *Cavity geometry utilized in this work.*

2.6 Slit rheometer

The nozzle of the injection molding machine was modified to host a system for controlling the quantity of gas injected during the batching and the foaming process (Figure 16).
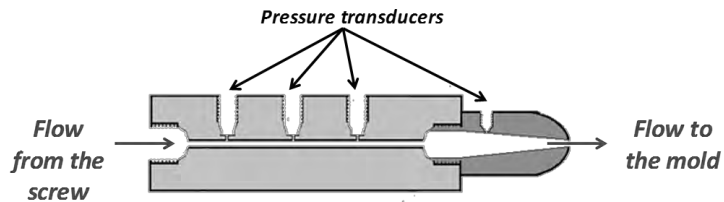
Figure 16. *Slit for rheological measurements.*

This system allows to obtain in-line rheological measurements by means of three pressure transducers which measure the pressure in a range from 0 to 2000 bars, and temperatures up to 450°C. These pressure transducers are housed along the flow direction, at a distance equal to 15, 60 and 105 mm from the inlet of the slit (Figure 17). In this work, slits with two different geometries were adopted (Table 11). The first slit, with a small thickness, allows to obtain shear rates higher than 10^4 s^{-1}, a typical limit for standard capillary rheometers. Then, a second slit was designed to obtain lower values of shear rate, comparable with shear rates of conventional rheometers.

Table 11. *Slits geometry.*

Slit dimension [mm]	First slit	Second slit
Length [mm]	120	120
Width [mm]	10	20
Thickness [mm]	0.75	2
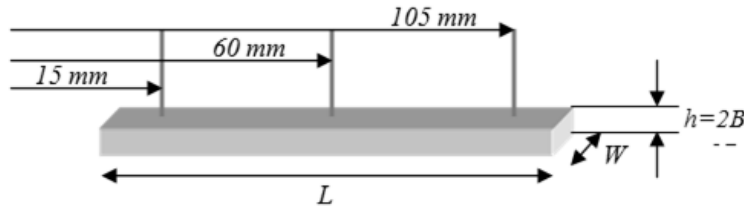
Figure 17. *Transducer position on the slit rheometer.*

The temperature inside the cylinder is measured by two thermocouples placed in appropriate holes in the cylinder, at the inlet and exit of the slit.

Inside the slit, with a balance of forces on a fluid element, a relationship can be obtained between the shear stress and the pressure gradient:

$$\tau(y) \equiv \frac{P \cdot y}{L} \tag{11}$$

where L is the length of the slit, h the thickness and W the width. The viscosity is:

$$\eta = \frac{\tau_w}{\dot{\gamma}_w} \tag{12}$$

The shear stress at the wall τ_w is:

$$\tau_w = -\tau(y = B) = -B\left(\frac{\Delta\wp}{\Delta x}\right) \tag{13}$$

The shear rate at the wall for a Newtonian fluid is:

$$\dot{\gamma}_w = -\dot{\gamma}_{xy}(y = h/2) = 6Q/(h^2 \cdot w) \tag{14}$$

So, the viscosity for a Newtonian fluid is:

$$\eta = \left(\frac{-\Delta P}{L}\right)\frac{h^3 w}{12Q} \tag{15}$$

To analyze the flow that is established within the slit, the equations of motion in rectangular coordinates can be used, with the simplifying assumptions of incompressible fluid, stationary flow and negligible edge effects. We can suppose that the flow takes place predominantly in the x direction, ie along the axis of the slide, and that B is the half thickness of the slit.

Chapter 2
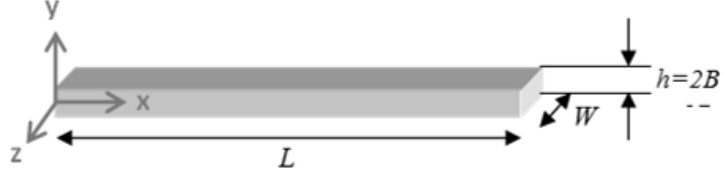
Figure 18. *Geometry of the slit.*

The relation between the shear stress and the pressure gradient is:

$$\frac{\partial \tau_{xy}}{\partial y} = -\frac{\partial \wp}{\partial x} \tag{16}$$

where $\wp$ is the dynamic pressure. At the conditions realized inside the slit depends only on x and we have:

$$\int_{y=0}^{y} \frac{\partial \tau_{xy}}{\partial y} dy = -\frac{d\wp}{dx} y \tag{17}$$

Whereas τ is zero at the axis, where $y=0$, we can obtain a linear stress profile

$$\tau_{xy}(y) = -\frac{d\wp}{dx} y \tag{18}$$

From the equation of the stress:

$$m\left(-\frac{\partial v_x}{\partial y}\right)^n = -\frac{d\wp}{dx} y \tag{19}$$

$$\frac{\partial v_x}{\partial y} = -\left(-\frac{1}{m}\frac{d\wp}{dx}\right)^{\frac{1}{n}} y^{\frac{1}{n}} = -\left(-\frac{1}{m}\frac{d\wp}{dx}\right)^{s} y^{s} \tag{20}$$

$$\int_{y=0}^{y} \frac{\partial v_x}{\partial y} dy = v_x|_{y=B} - v_x|_{y=y} \tag{21}$$

where B is the half thickness of the slit. Because at the solid-liquid interface the velocity is zero, the equation 11 becomes:

$$v_x = -\left(-\frac{1}{m}\frac{d\wp}{dx}\right)^{s} \frac{B^{s+1}}{s+1}\left(1 - \left(\frac{y}{B}\right)^{s+1}\right) \tag{22}$$

That is a parabolic velocity profile. The value of the stress at wall is:

40

$$\tau_{xy}\big|_{y=B} = m\left(-\frac{dv_x}{dy}\right)^n = m\left[\frac{V}{B}(s+2)\right]^n = m\left[\frac{V}{B}\frac{1+2n}{n}\right]^n \tag{23}$$

For a Newtonian fluid (n=1)

$$\tau_{xy}\big|_{y=B} = m\left[\frac{3V}{B}\right] \tag{24}$$

We can define an apparent shear rate

$$\dot{\gamma}_a = \frac{3V}{B} \tag{25}$$

In order to evaluate the average velocity V, we need to calculate the imposed flow rate, that is the product between the velocity of the screw and its section

$$Q_{imp} = v_{screw} * S_{screw} \tag{26}$$
$$S_{screw} = \pi * \frac{D^2}{4} \tag{27}$$

The average velocity inside the slit is:

$$V = Q_{slit}/S_{slit} \tag{28}$$
$$Q_{slit} = Q_{imp} \tag{29}$$
$$S_{slit} = W * h \tag{30}$$

So, the shear rate at wall in function of the apparent shear rate can be write

$$\dot{\gamma}_w = \dot{\gamma}_{xy}\big|_{y=B} = \dot{\gamma}_a\left(\frac{1+2n}{3n}\right) \tag{31}$$

$$\tau_w = \tau_{xy}\big|_{y=B} = m\left[\dot{\gamma}_a\frac{1+2n}{3n}\right]^n = -B\frac{\Delta\wp}{\Delta x} \tag{32}$$

This means that, at constant apparent shear rate, pressure drops depend on the ratio L/B.

Known the average velocity V, the slit geometry and the pressure drops, we can write:

$$\ln\left(-\frac{\Delta\wp}{\Delta x}\right) = \ln\left(\frac{m}{B}\right) + n\ln(\dot{\gamma}_a) + n\ln\left(\frac{1+2n}{3n}\right) \tag{33}$$

Chapter 2

This equation represent a straight line with slope *n* and from its intercept we can calculate *m*. If *n* is not constant, its value can be obtained from the local slope of the curve.

$$n = \frac{\partial \ln\left(-\frac{\Delta \wp}{\Delta x}\right)}{\partial \ln(\dot{\gamma}_a)} \qquad (34)$$

These equations allow to evaluate the viscosity (equation 2), known the measures of pressure obtained by the transducers inside the slit. Differently from the capillary rheometer, with the slit rheometer we can obtain a direct measure of the pressure. So, it does not need a Bagley correction.

The pressure transducers are connected to a software that allows to acquire all data during the different steps of the injection molding process. In particular, during the injection phase it acquires the pressure measured at the three transducers positions, the position of the screw and the pressure measured in the nozzle. From the screw position it is possible to evaluate the screw velocity, i.e. variation of screw position with time, that is the slope of the curve that represents the screw position versus time during the injection phase.

2.7 Density measurements: Archimedes' principle

Reduction in density of foamed samples in comparison with unfoamed parts was measured by means of Archimedes' principle.

A mechanism that simulates the operation of a two arms scale was formed in our laboratory: a weight ("basis weight") positioned on a automatic balance is hung to an arm, while a sample is hung to the other arm. The sample is immersed in a liquid having a higher density. In our case a solution of salt and water as was used. As a first step, the "basis weight" is measured with no sample hung to the other arm. This measure is recalculated once positioned the sample to be measured. This new measure will also take account of the buoyancy of the piece.
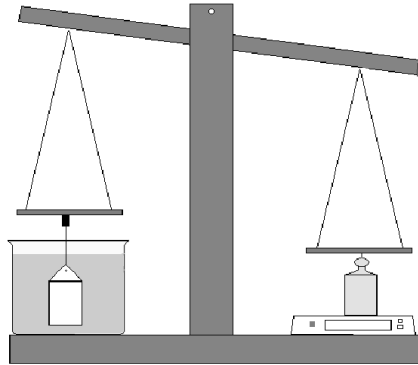
Figure 19. *Mechanism for density measurements.*

The measurement on the unfoamed sample is given by:

$$S_0 = (V_0 * \rho_L - P_0) \tag{35}$$

Where:

- S_0 = buoyancy of the unfoamed sample
- V_0 = volume of the unfoamed sample
- ρ_L = density of the liquid
- P_0 = weight of the unfoamed sample

Similarly, the measurement on the foamed sample is:

$$S_C = (V_C * \rho_L - P_C) \tag{36}$$

Where:
- S_C = buoyancy of foamed sample
- V_C = volume of the foamed sample
- P_C = weight of the foamed sample

Known the buoyancy and the weight of the foamed and unfoamed samples, one obtains the product of volume for density of the liquid. From the ratio between the two products:

$$\frac{V_C * \rho_L}{V_0 * \rho_L} = \frac{V_C}{V_0} \tag{37}$$

Knowing that:

43

$$\rho_0 = \frac{P_0}{V_0} \tag{38}$$

$$\rho_C = \frac{P_C}{V_C} \tag{39}$$

From the product of the result of the equation 27 and the ratio between the weights of the individual samples previously calculated, it is possible to obtain the relationship between the density of the unfoamed sample and that of the foamed sample (parameter A):

$$A = \frac{\rho_0}{\rho_C} = \frac{P_0}{P_C} * \frac{V_C}{V_0} \tag{40}$$

Using this parameter it is possible to calculate the percentage reduction in density:

$$\frac{\rho}{\rho} = \left(\frac{\rho_0 - \rho_C}{\rho_0}\right) * 100 = \left(1 - \frac{1}{A}\right) * 100 \tag{41}$$

2.8 Cross-Vogel Model

Viscosity of polymer melts varies with shear rate, pressure and temperature. The viscosity behavior of polymer melts can be extremely complex, much more than often appreciated when practitioners contemplate melt flow indices (MFI). Indeed, the MFI is a single point estimate of the viscosity, and may not be very representative of the behavior of the material than experiences a broad range of shear rates, temperatures, and pressures when it is being molded. For this reason, many viscosity models have been developed for plastics injection molding [91].

The mathematical description of the viscosity is fundamental for calculation and simulation of the flow in replication processes. In order to describe the shear thinning behavior, different empirical, semi-empirical, and theoretical models are used. The models allow the prediction of the shear thinning behavior of a polymer melt over a large range of shear velocity. One of these models is Cross-Vogel Model, that accounts for the effect of temperature, shear rate and pressure on the viscosity, over a wide temperature range. This is marked by two tangents and their point of intersection. This point defines the transition of the Newtonian behavior and the shear-dependent behavior. The gradient of the line in the shear-dependent area is defined by reciprocal flow exponent n, which is the inverse of the gradient of this line [92]:

$$\eta(T, \dot{\gamma}) = \frac{\eta_N(T)}{1 + \left(\frac{\eta_N(T) \cdot \dot{\gamma}}{\tau^*}\right)^{1-n}} \tag{42}$$

with

$$n = \frac{1}{m} = \frac{\partial \ln(\tau)}{\partial \ln(\dot{\gamma})} \tag{43}$$

where η_N, is the viscosity at zero rate of shear, $\dot{\gamma}$, is the shear velocity, τ^* is the shear stress at the intersection of the two lines defining the change between Newtonian fluid and shear thinning behavior, and n is the flow index.

The form of the Cross model is readily understandable since these three parameters, η_N, τ^* and n, can be estimated directly from a log-log plot of the viscosity as a function of shear rate as shown in this figure:
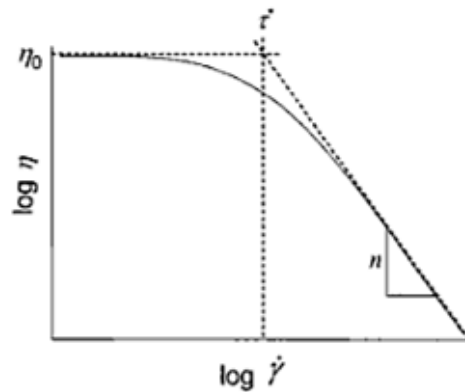
Figure 20. *Cross model terms [90].*

In the above equation, the Newtonian shear viscosity, η_N, is a function of temperature T, and pressure, P:

$$\eta_N(T) = \eta^* e^{\frac{A+kP}{T-T_{ref}}} \tag{44}$$

The model parameters are typically determined by curve fitting experimental shear-viscosity data taken by a capillary rheometer at shear rates from 10 to 10,000 1/s. The material properties for many thousands of plastics resins have been characterized, and the Cross-Vogel model coefficients for some representative materials are provided in many bibliography. The Cross-Vogel viscosity model for a medium viscosity PC is plotted as a function of shear rate for three different temperatures in this figure:
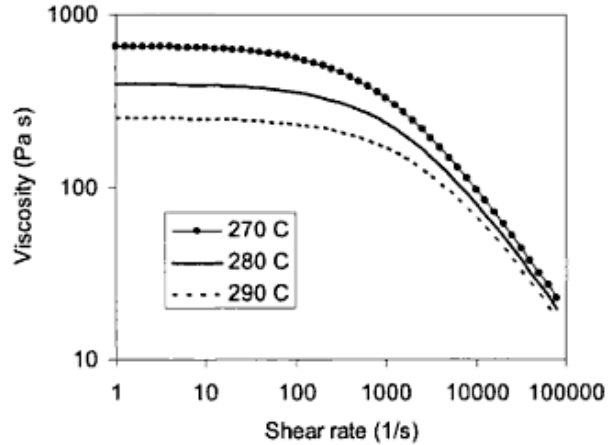
Figure 21. *Viscosity behavior of PC* [90].

As shown in this figure, the viscosity exhibits a Newtonian plateau for shear rates up to 100 1/s, then transition into a power law regime takes place. For a melt temperature of 280^0C, the viscosity decreases from 350 Pa.s at 100 1/s to 80 Pa.s at 10,000 1/s. Since the viscosity is strongly dependent on the shear rate, estimation of the filling time, melt velocity, and shear rate are vital to the predictions. The viscosity is also a strong function of temperature, with the zero shear viscosity increasing from 250 Pa.s at 290 ^{0}C to 660 Pa.s at 270^0C. Thus, knowledge of the processing temperature is also important to predicting the melt flow and pressure.

2.9 Test method for tensile properties

The tensile tests allow the study of the mechanical properties of the materials in quantitative way of form, being they able to be characterized. The test specimen is held with grips between the fixed base and the movable crosshead of the testing machine, in such way that slippage relative to the grips is not possible. The movable crosshead runs at a speed of 100 mm/min until the breaking of the specimen. The specified method allows obtaining data for the quality control, acceptance or rejection of products according to determined specifications, investigation and development.

In this test there is the solicitation of the material under the form of specimen of dimensions brought back to normal. This solicitation consists in the application of an axial force, which makes continuously traction of the material axially as it can be seen from the scheme in Figure 22.
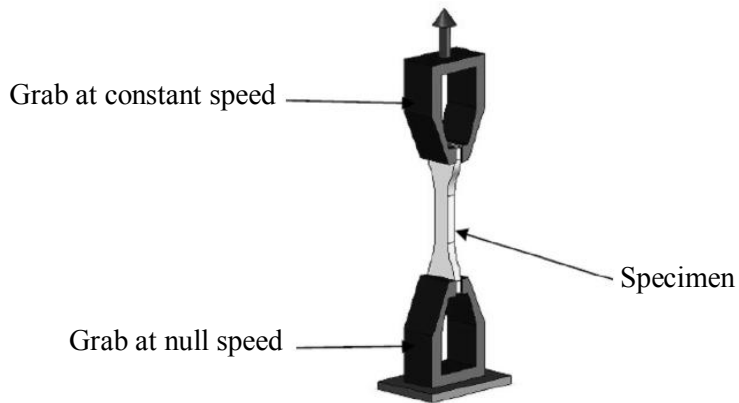
Figure 22. *Mechanism utilized in tests of traction.*

By this test a graph force *vs* elongation is obtained, but in order to obtain a graph of tensile stress- strain curve, it is necessary to calculate the values:

- Calculate the Strain [%]

$$\varepsilon_E = \frac{L}{L_0} = \frac{L_f - L_0}{L_0} \qquad (45)$$

$$\varepsilon_T = \int_{L_0}^{L} \frac{dL}{L} = \ln\left(\frac{L}{L_0}\right) = \ln(\varepsilon_E + 1) \qquad (46)$$

$\varepsilon_E = \varepsilon_{Engineering}$
$\varepsilon_T = \varepsilon_{True}$
dL = Increment of elongation when the distance between the gage marks is l.
ΔL = variation in length of the test piece caused by action of force application;
L_0 = Original distance between gage marks;
L_f = Distance between gage marks at any time;

- Calculate the Tensile strength [MPa]

$$\sigma_E = \frac{F}{A} \qquad (47)$$

$$\sigma_T = \sigma_E \times (\varepsilon_E + 1) \qquad (48)$$

σ = tensile stress [MPa];
F = axial force applied to the specimen [N];
A = sectional traction area [m^2].

Chapter 2

The graphs can be obtained to verify proportionality between the strength and elongation which is equal to proportionality between the tensile stress and strain. This can be derived according to Hooke's law:

$$= E \times \varepsilon \qquad (49)$$

σ = tensile stress [MPA];
E = Young's modulus or modulus of elasticity [MPa];
ε = strain.

The eq. (39) yields the value of Young's modulus corresponding to the portion of the graph from the starting point until the yield stress point. Up to this point deformation is reversible, in other words any deformation lower than the yield point can be recovered. This is due to elastic deformation in which from the yield point there is no proportional relationship and no longer reversible deformation, switching to a plastic domain.

The Young's modulus obtained from Hooke's law represents the slope of a line. This modulus, also known as the modulus of elasticity allows to obtain the value corresponding to the stiffness of the material. The higher is the modulus of elasticity, the lower is the elastic deformation resulting from the application of a given tension. Figure 23 shows a typical Stress-strain curve.
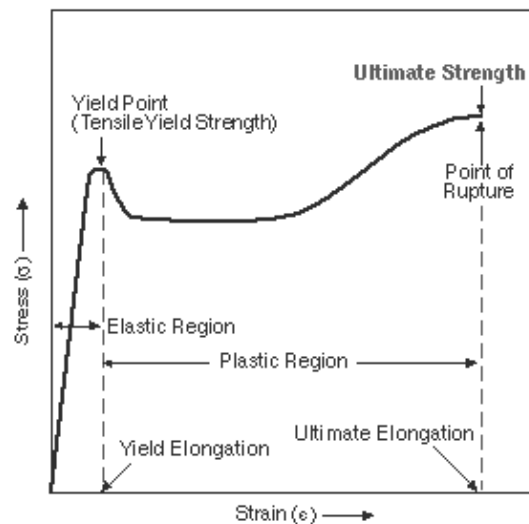
Figure 23. *Stress-strain curve for a typical thermoplastic.*

When the polymers are tested mechanically by means of tensile tests, different behaviors are possible: ductile or fragile (Figure 24).
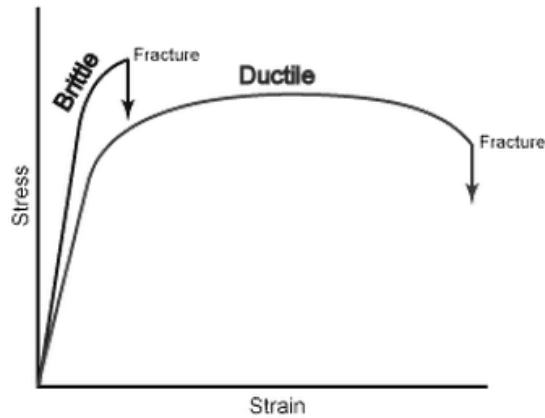
Figure 24. *Ductile behavior and fragile/brittle behavior.*

If a material breaks to deformation values much low and does not present constant deformation, this one suffers fragile rupture. A material can present a constant plastic deformation before breaking, presenting so flexible rupture.

In order to correctly conduct the test, it is necessary to define some conditions, such as the distance between the clamps and the deformation velocity. This velocity must increase with the reduction of the rigidity of the material. The test temperature is the room temperature. The norm used to perform the development of the results is **ASTM D 638 – 03.**

The next Figure 25 shows the typical equipment utilized to perform these tests.

Figure 25. *Test machine of tensile testing.*

2.10 Test method for impact resistance

The impact resistance test determines the capacity that a material has to support loads of impact at elevated speed and thus to estimate the brittleness or toughness of notched or unnotched specimens within the limitations inherent in the test conditions. It may also be used for the determination of comparative data from similar types of material. The norm used to perform the development of the results is **ISO 179-1:2000.**

Unnotched specimens

The Charpy impact strength of unnotched specimens, $a_{cU,}$ expressed in joules per square meter, is calculated using the following equation:

$$a_{cU} = \frac{E_c}{h \times b} \tag{50}$$

Where,

E_c = corrected energy, in joules, absorbed by breaking the test specimen;
h = thickness, in millimeters, of the best specimen;
b = width, in millimeters, of the test specimen.

The next Figure 26 shows the typical equipment adopted to perform these tests.

Figure 26. *Impact testing machine.*

2.11 Test method for flexural properties

The data of flexural tests are often used to select materials for parts that will support loads without inflecting. Flexural modulus is used as an indication of a material's stiffness when inflected. Since the physical

properties of many materials (especially thermoplastics) can vary depending on ambient temperature, it is sometimes appropriate to test materials at temperatures that simulate the intended end user environment. The norm used to perform the development of the results is **ASTM D 790 – 03.**

The next equation allows to calculate the flexural stress:

$$f = \frac{3PL}{2bd^2}$$

(51)

σ = Stress in the outer fibers at midpoint, [MPa];
P = Load at a given point on the load-deflection curve, [N];
L = support span,[mm]
b = Width of specimen tested, [mm];
d = Depth of specimen tested, [mm];

Calculate the flexural strain:

$$\varepsilon_f = \frac{6Dd}{L^2}$$

(52)

ε_f = Strain in the outer surface,
D= Maximum deflection of the center of the beam,[mm];
L = support span,[mm]
d = Depth, [mm]

Calculate the flexural modulus:

$$E_B = \frac{L^3 m}{4bd^3}$$

(53)

E_B = Modulus of elasticity in blending, [MPa];
L = support span, [mm]
b = Width of specimen tested, [mm];
d = Depth of specimen tested, [mm];
m = Slope of the tangent to the initial straight-line portion of the load-deflection curve, [N/mm] of deflection.

In Figure 27 it is possible to observe typical curves of flexural stress versus flexural strain. Through these curves the results obtained from bending tests can be analyzed.

Curve a: Specimen that breaks before yielding.
Curve b: Specimen that yields and then breaks before the 5 % strain limit.
Curve c: Specimen that neither yields nor breaks before the 5 % strain limit
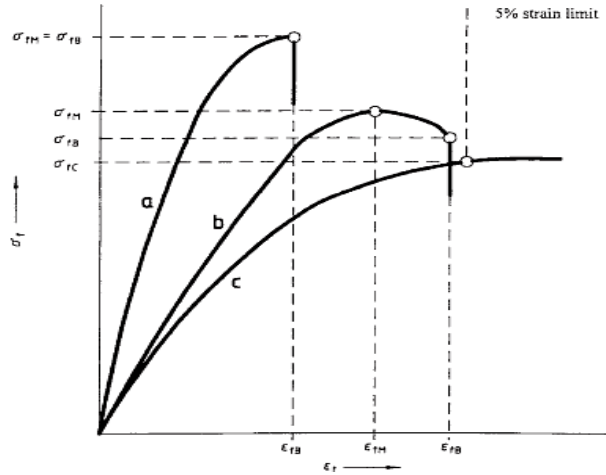
Figure 27. *Curves of Flexural Stress Versus Flexural Strain.*

The following Figure 28 shows the type of equipment used for bending tests as well as a schematic diagram.
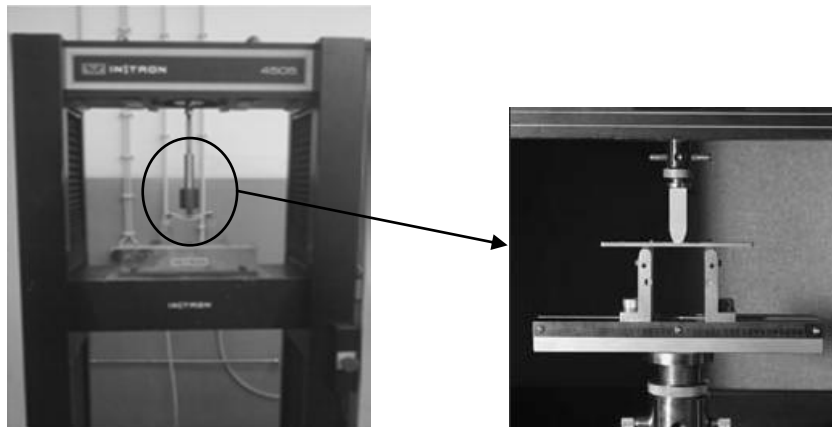
Figure 28. *Flexural Testing Machine and schematic representation of the test.*

Flexural tests were made on the samples in order to know the capacity of the foamed samples to endure a load 10 kN before to flex and break. The specimen is positioned on two supports with a distance of 42 mm and is loaded by means of a loading nose midway between the supports that approaches a speed of 10 mm/min. The specimen is deflected until rupture occurs in the outer surface of the test specimen. The schematic representation of such a test is shown in Figure 29. In it is also represented the direction of the flow in the specimen during the injection molding process.
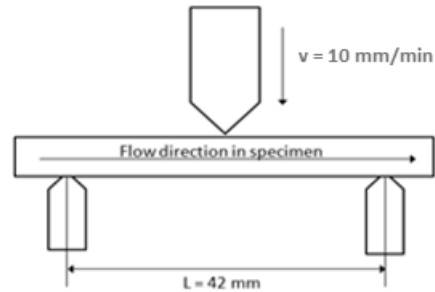
Figure 29. *Scheme of flexural test.*

2.12 SkyScan 1174 for Tomography

Thanks to the Polymer Centre of the Faculty of Technology, Thomas Bata University in Zlin (CZ) it was possible to use the SkyScan1174 compact micro-CT (Figure 30) to obtain a tomography, procedure that utilizes computer-processed X-rays to produce tomographic images or slices of specific parts.
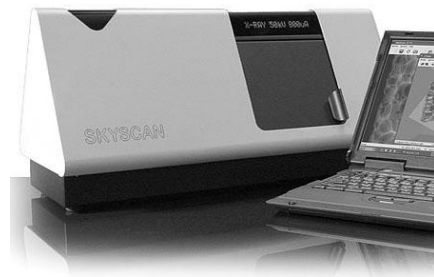
Figure 30. *SkyScan1174 compact micro-CT.*

This scanner uses an x-ray source with adjustable voltage and a range of filters for adaptation to different object densities. A 1.3 megapixel x-ray camera allows scanning of the whole sample volume. Variable magnification (6-30 µm pixel size) is combined with object positioning for easy selection of the object part to be scanned. The scanner, connected to a PC, is combined with a SkyScan software that allows to obtaining fast volumetric reconstruction and quantitative analysis.

The micro-positioning stage shown in Figure 31 helps to achieve exact positioning of small objects in the middle of the scanning field. Precise object centering improves all aspects of scan quality, enabling the

achievement of maximum magnification and the optimization of the scan speed [93].

Figure 31. *Micro-position stage.*

Scanning was carried out without using any filter. In Table 12 the operative conditions utilized for this work were shown.

Table 12. *Operative conditions of SkyScan.*

X-ray source	**Voltage [kW]**	**28**
	Current [µA]	800
	Power [W]	23
Zoom	pixel size [µm]	11,66
Camera mode	small pixel size	1304x1024
Scanning options	rotation step [deg]	0,7
	Averaging [frames]	4

Chapter 3
Batch foaming process

Batch foaming experiments were used to determine a correlation between foaming conditions and morphology. The information coming from batch foaming activity will be used to optimize the process variables of microcellular injection molding.

Batch process is a physical foam processing strategy that consists of four stages:

1. N_2 saturation in the sample at desired Temperature and Pressure;

2. Cooling of batch to reach the foaming temperature ($T_{foaming}$) and subsequent cell nucleation when the release of N_2 pressure started (positive supersaturated N_2);

3. cell growth to an equilibrium size during the release of N_2;

4. cell stabilization via cooling process of the foamed system.

These stages are schematized in Figure 32.
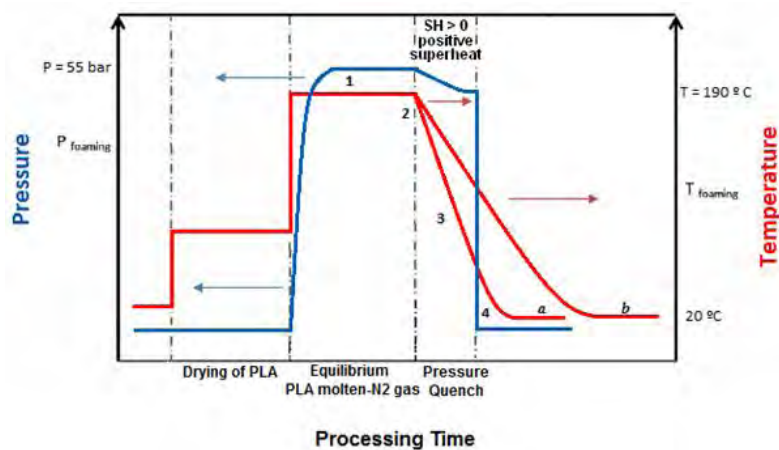
Figure 32. *Steps of the process about pressure and temperature; a-process by water, b-process by air.*

Chapter 3

Since PLA has an hygroscopic behaviour, before each test the PLA samples were vacuum-dried overnight at 60°C in the sealed vessel. Then there is the expansion of about 2 g of material in pellet in a pressure vessel.

1. PLA pellets vacuum-drying overnight at 60°C in the sealed vessel;

2. Introduction of N_2 gas in the vessel at 55 bar and heating to T=190°C; solubilization of N_2 (keeping the pressure value at 55 bar for 5 hours). Further analysis focused on shorter solubilization time (1-2 hours) in order to study its effect on foaming process.

3. Cooling of system (-10°C/min), to reach the foaming temperature (variable in a range 150÷80°C). Further analysis concerned a faster cooling (-60°C/min) of the system in order to study its effect on foaming process.

4. Expansion at foaming temperature by Pressure Quenching from 55 bar to atmospheric pressure.

A scheme of the foaming procedure proposed in this work is reported in Figure 33.
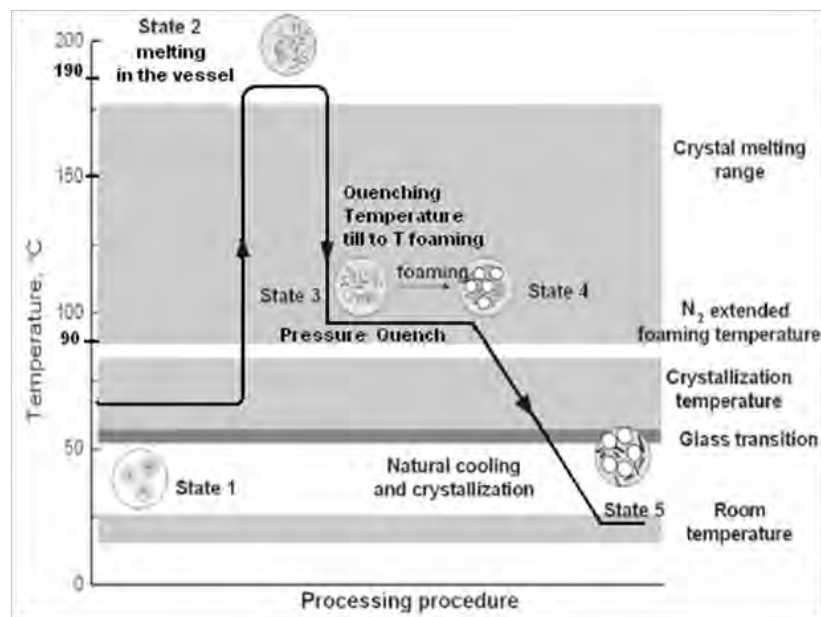
Figure 33. *Scheme of the foaming procedure.*

After drying of sample and gas introduction, the temperature of the vessel was increased to reach 190°C. The temperature increment leads to a better diffusivity of gas inside to the melt, but the gas solubility decreases. The gas solubility into the PLA can be improved by an increment of pressure, but in performing the tests it needs to take in account the structural limit of the apparatus (upper pressure limit 63 bar).

56

Therefore, it was necessary to find a compromise in setting the parameters. Differential scanning calorimetric (DSC) tests indicated that to completely overcome the melting peak of PLA (T_{melt}=169°C), it was necessary to set a temperature value greater than 180°C (Figure 34).
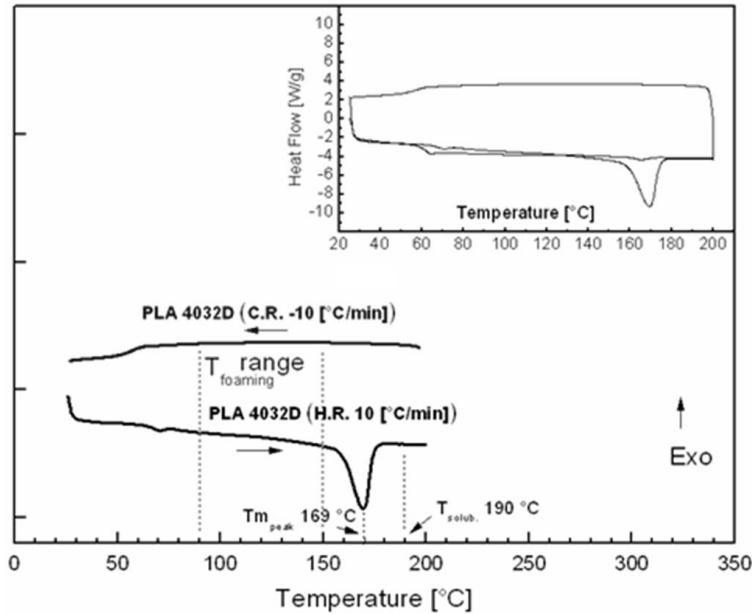
Figure 34. *DSC of the PLA 4032D.*

Therefore, the introduction of N_2 (55 bar), which guarantee a margin of safety for the vessel, and the stabilization in temperature of 190°C (state 2) were set.

On the basis of literature data [94], at this conditions, the solubility of N_2 in PLA is about 0.004 g N_2/g PLA (Figure 35). Moreover, the solubilization time is another pivotal parameter, since the process involves a suitable contact time between the phases.

Following the literature indications, a solubilization time of about 5 hours was adopted for the purpose. In the second instance, also the effect in decreasing of this parameter will be evaluated.
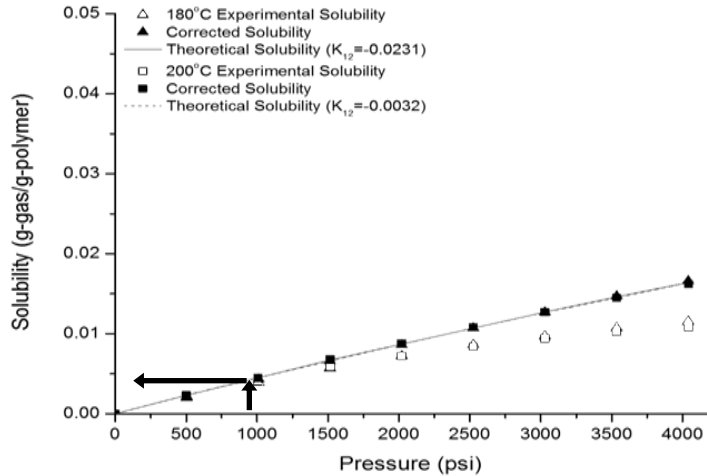
Figure 35. *Solubility of nitrogen into PLA at temperatures of 180 and 200°C.*

The next stage is the cooling till to reach a suitable temperature for operating the gas evacuation (state 3). Since the aim is that the foaming of the PLA occurs when it is melt, it is need to preliminarily evaluate if crystallization occurs for PLA, in order to roughly estimate the foaming temperature range.

In contrast with some authors [95], no crystallization peak in cooling scanning was detected for PLA samples. Therefore, a wider operative window for foaming temperature was investigated. Starting from solubilization temperature, the system was cooled by compressed air (average speed of -10°C/min). Then, the stage 4 was performed at temperatures ranging within 150÷80°C.

Nitrogen injection is performed by means of a discharge valve which leads to the pressure quench, as soon the temperature reaches the desired value T_{foam}. The subsequent cooling of the system to reach the room condition guarantees the structural stabilization of foam (state 5 in fig. 31). In this way, it is possible to obtain the formation of bubbles within the material thus creating the desired foam.

Also, the effect of a faster cooling (-60°C/min) was investigated, operating a quench of temperature by means of water. Some of these tests were repeated using a different polymer, an amorphous polystyrene, in order to compare the outcome with the results obtained with PLA.

3.1 Sample identification

After each experiment, all samples were identified with a code that takes into account the processing variable used.

Below, the meaning of each term in the label is explained.

✓ First part "A" or "W" refers respectively to cooling of the vessel by compressed air or by circulating water;

✓ second part (e.g. "P55") indicates the corresponding gas pressure value in *bar* in the vassel (P_{sol});

✓ third part (e.g. "T190") indicates the solubilization temperature (T_{sol}) adopted in the test;

✓ fourth part (e.g. "5H") refers to the solubilization time (t_{sol}) imposed in performing the tests and finally is the foaming temperature used;

✓ latter part (e.g. "F120") indicates the foaming temperature ($T_{foaming}$) at which the release of gas is performed.

Furthermore, the samples of PS amorphous are detect by the first label "PS". All labels in which the material is not specified (PS) refer to samples of PLA.

3.2 Experimental conditions

Several experimental tests were carried out in order to understand how the most important experimental parameters affect the morphology of the foamed PLA. In Table 13 and

Table *14* the tests performed by Batch foaming process are reported.

Table 13. *Summary of the I step of tests performed by Batch foaming process.*

Series	P_{sol} [bar]	t_{sol} [h]	T_{sol} [°C]	$T_{foaming}$ [°C]	$P_{foaming}$ [bar]	Cooling Rate [°C/min]	Cooling Method
I Step – Foaming Temperature							
A_P55_T190_5H_F150	55	5	190	**150**	44	10	AIR
A_P55_T190_5H_F140	55	5	190	**140**	40	10	AIR
A_P55_T190_5H_F130	55	5	190	**130**	45	10	AIR
A_P55_T190_5H_F120	55	5	190	**120**	40	10	AIR
A_P55_T190_5H_F110	55	5	190	**110**	43	10	AIR
A_P55_T190_5H_F100	55	5	190	**100**	40	10	AIR
A_P55_T190_5H_F090	55	5	190	**90**	37	10	AIR
A_P55_T190_5H_F080	55	5	190	**80**	33	10	AIR

Table 14. *Summary of the next tests performed by Batch foaming process.*

Series	P_{sol} [bar]	t_{sol} [h]	T_{sol} [°C]	$T_{foaming}$ [°C]	$P_{foaming}$ [bar]	Cooling Rate [°C/min]	Cooling Method
II Step – Solubilization Time							
A_P55_T190_2H_F110	55	**2**	190	110	43	**10**	**AIR**
W_P55_T190_2H_F110	55	**2**	190	110	43	**60**	**WATER**
A_P55_T190_1H_F110	55	**1**	190	110	41	**10**	**AIR**
III Step – Cooling Type							
W_P55_T190_1H_F110	55	**1**	190	110	43	**60**	**WATER**
W_P55_T190_1H_F90	55	**1**	190	90	30	**60**	**WATER**
W_P55_T190_1H_F80	55	**1**	190	80	43	**60**	**WATER**
W_P55_T190_1H_F70	55	**1**	190	70	43	**60**	**WATER**
W_P55_T190_1H_F60	55	**1**	190	60	43	**60**	**WATER**
W_P55_T190_1H_F50	55	**1**	190	50	43	**60**	**WATER**
Polystyrene							
PS_W_P55_T190_1H_F110	55	**1**	190	110	43	**60**	**WATER**
PS_W_P55_T190_1H_F90	55	**1**	190	90	38	**60**	**WATER**

As reported in Table 13 and Table 14, a series of tests that differed on the basis of several parameters, like foaming temperature or solubilization time, were performed, in order to individuate a suitable operative window for the PLA 4032D in the batch system.

3.3 Experimental Results

3.3.1 Foaming temperature effect

The morphological analysis permits to study the effect of foaming temperature on cellular structure size. In Figure 36 it can be observed that the morphologies of foamed samples were very different exhibiting larger cell diameters in samples foamed at higher temperature. This behaviour was already observed in literature by Matuana et al. [96], who supposed that a higher temperature accelerates the rate of gas diffusion, which favors bubble growth. The melt viscosity of the polymer has a strong influence on the rate

of gas diffusion between cells. At an elevated temperature, the melt strength of the polymer and its extensional viscosity decrease significantly. When the melt viscosity is low, the diffusion of gas through the matrix is favored and the cells can grow more easily. In contrast, high melt viscosity offers high resistance to cell growth in the polymer matrix [97]. Consequently, the rate of cell growth during foaming at lower foaming temperature resulted in foamed samples with lower void fraction and smaller ratio between the density of unfoamed sample and the density of foamed sample. All these samples were obtained using a slow cooling rate (cooling by air), before the foaming of gas. In this case, the lowest temperature utilized was 80°C, since further decrement in foaming temperature did not allow to expand the PLA (Figure 37). Similar behaviour of PLA in batch foaming process was observed in literature by Correa et al., [98] who performed the batch foaming experiment using PLA and CO2 as physical foaming agent. The cellular morphology of the foam was tailored by adjusting the molecular architecture through reactive extrusion with a multifunctional epoxy, as well as by tuning the crystallinity of PLA and the foaming parameters in the batch reactor. Test was performed in a narrow range of temperature foaming (150÷110ºC). Microscope analysis confirmed that the higher foaming temperature induce larger cellular size.
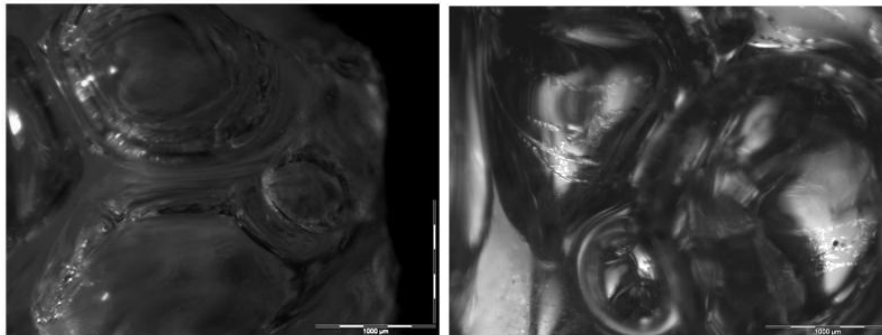
A_P55_T190_5H_F150

A_P55_T190_5H_F130
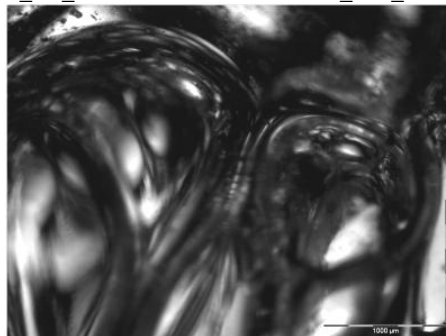
A_P55_T190_5H_F120

Chapter 3

Figure 36. *Samples of PLA with foaming temperature between 150-120℃ (scale 1000 µm)*

A_P55_T190_5H_F110	*A_P55_T190_5H_F100*
A_P55_T190_5H_F90	*A_P55_T190_5H_F80*
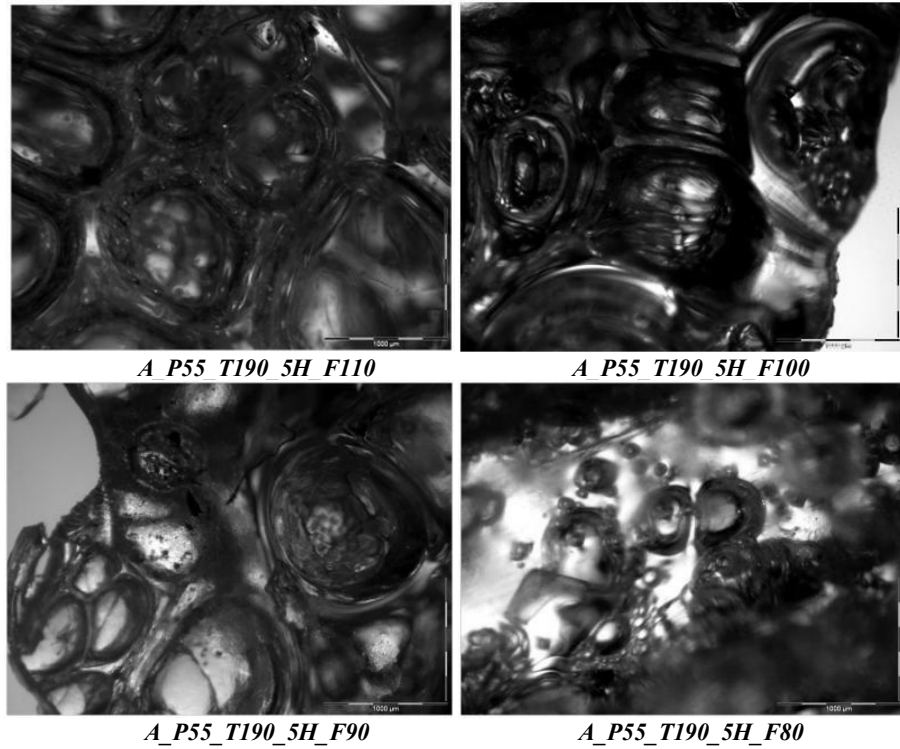
Figure 37. *Samples of PLA with foaming temperature between 110-80℃ (scale 1000 µm)*

Regarding the density, the apparent density range of samples obtained by batch foaming process is very wide. As expected, the lowering of foaming temperature leads to a more non-uniform cell distribution with smaller size, and consequently a progressive increment in foaming density of PLA samples. In Figure 38, the effect of foaming temperature, when the cooling of vessel was performed by compressed air (slow cooling rate) is shown.
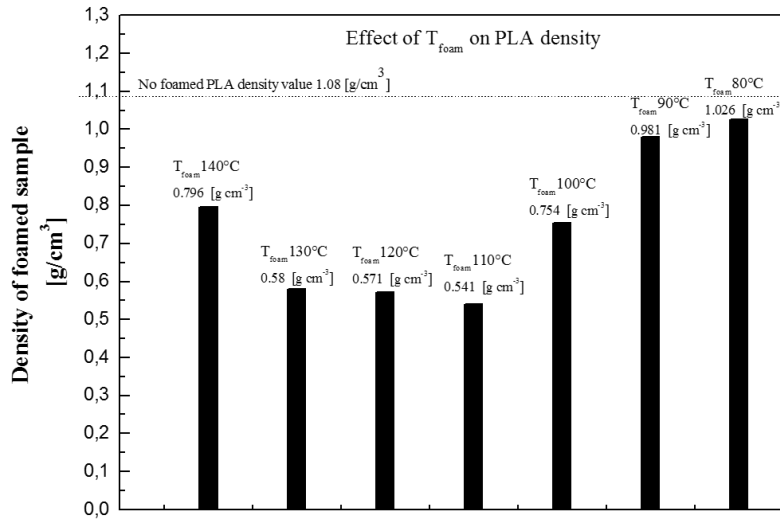
Figure 38. *Effect of foaming temperature for t_{sol}=5h and cooling by air.*

The figure shows that increasing the foaming temperature, there is a reduction of apparent density. For temperatures above 110°C it can be observed a slight increase in density up to 130 °C, and a sharp increase to 140 °C, which suggests that this is the upper limit in the range of foaming temperatures. As it appears, both the morphological analysis and the apparent density values suggest that 110°C is the condition to adopt as a standard reference for the study task. Starting from this position, further analysis regarding the effect of processing conditions on PLA foam characteristics, was developed (see Table 13 and

Table *14*).

3.3.2 Cooling by water

Similar results (Figure 39) were obtained by cooling the vessel by water. This process causes a faster cooling rate. It was observed that the rapid cooling of the vessel by water quenching did not allow the relaxation of material during the gas release. On its turn, this leads to a stabilization of the bubble structure around of nucleation sites and allows to obtain foaming of PLA at temperatures very close to Tg (T_{foam} 60°C), while at foaming temperature below glass transition temperature (see micrograph at 50°C) the formation of foam was not observed.

W_P55_T190_1H_F110

W_P55_T190_1H_F100

W_P55_T190_1H_F90

W_P55_T190_1H_F80

W_P55_T190_1H_F70

W_P55_T190_1H_F60

W_P55_T190_1H_F50
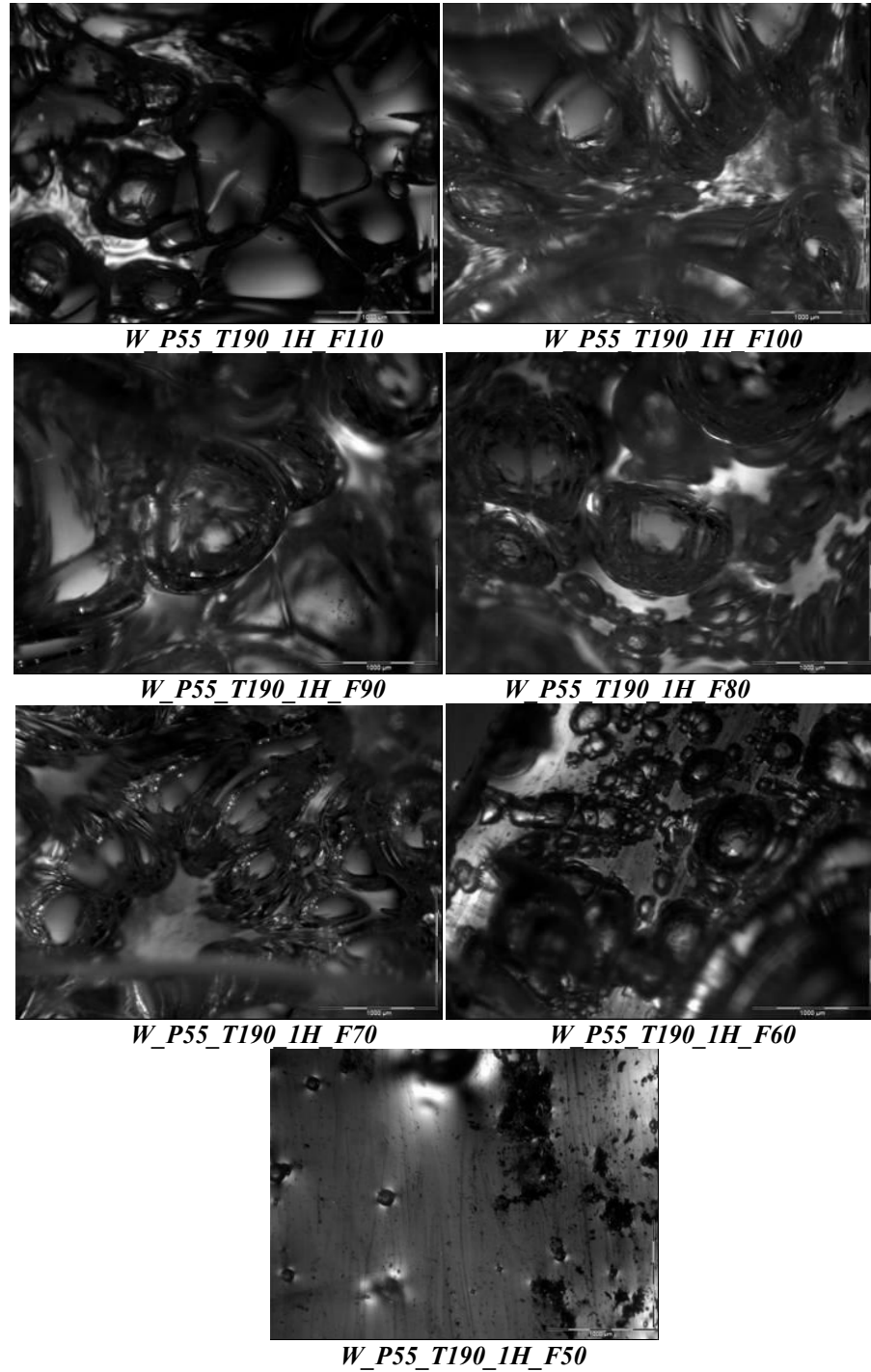
Figure 39. *Samples of PLA with foaming temperature between 110-50ºC (scale 1000 μm)and fast cooling rate.*

In Figure 40, the effect of foaming temperature, when the cooling of vessel was performed by water (fast cooling rate) and time of solubilization equal to one hour, is shown. Also in this case, as the foaming temperature increases, the density decreases, consistently with the progressive bubble growth highlighted by microscope analysis.
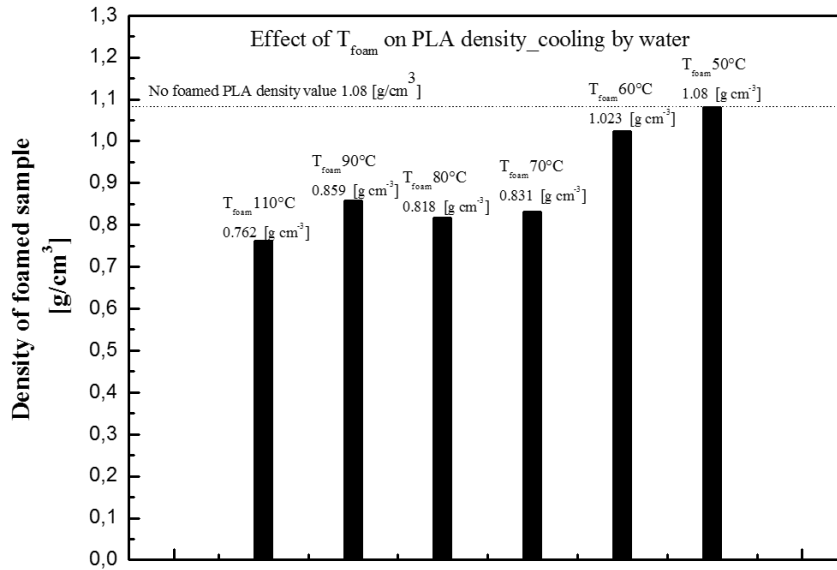
Figure 40. *Effect of foaming temperature for t_{sol}=1h and cooling by water.*

Figure 41 shows a comparison between a sample cooled by air (a) and a sample cooled by water (b) in the same experimental conditions. A faster cooling leads to the formation of smaller and better-defined bubbles.

(a) *(b)*
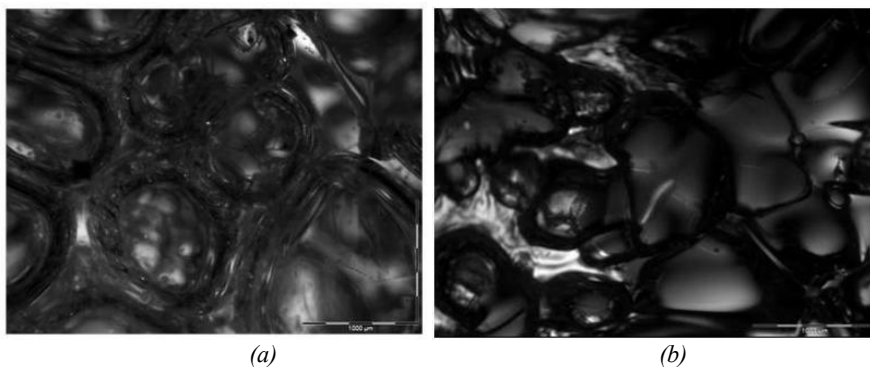
Figure 41. *Comparison between samples of PLA cooled by air (a) and by water (b) at foaming temperature of 110°C.*

3.3.3 Solubilization time effect

Regarding the solubilization time effect on the foam characteristics, Figure 42 highlights that a worse quality of the cellular structure was observed in samples with shorter gas/polymer contact time. The foamed sample obtained in a solubilization time equal to 5 hours exhibits a uniform cells size distribution, while in the samples with a shorter solubilization time, respectively 2 and 1 hours, the cell size distribution is not regular and in the last case unfoamed zones are detectable in the sample. The need for a longer time for an effective penetration of gas within polymer matrix is evident.

A_P55_T190_5H_F110   *A_P55_T190_2H_F110*

A_P55_T190_1H_F110
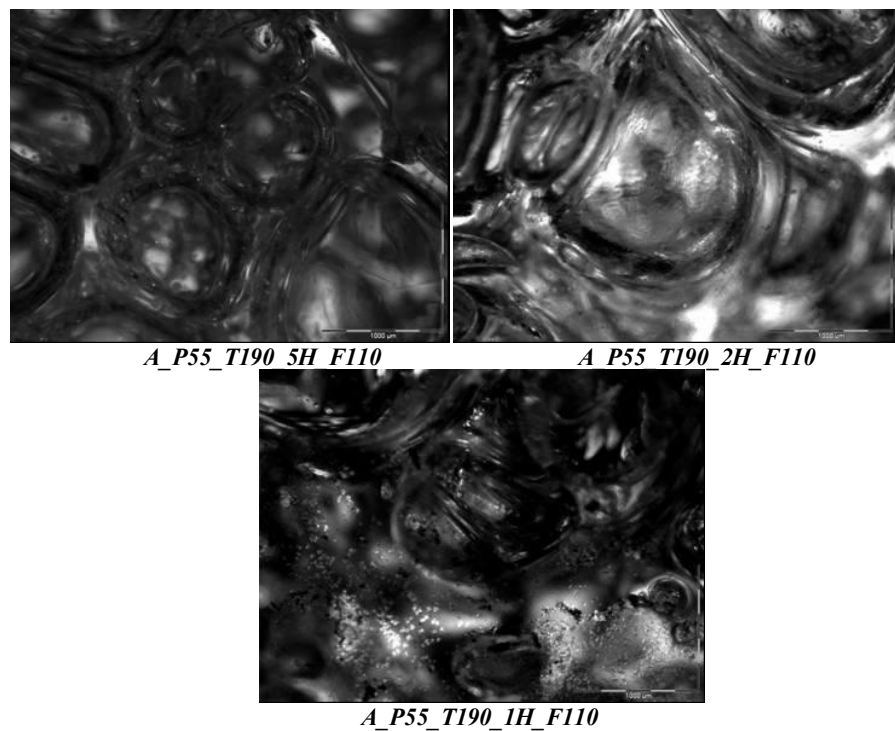
Figure 42. *Samples of PLA with solubilization times equal to 5, 2 and 1h and foaming temperature of 190°C (scale 1000 μm).*

The corresponding density values shown in Figure 13 confirmed that, increasing the solubilization time there is a decrease of the apparent density, and then a better foaming structure.
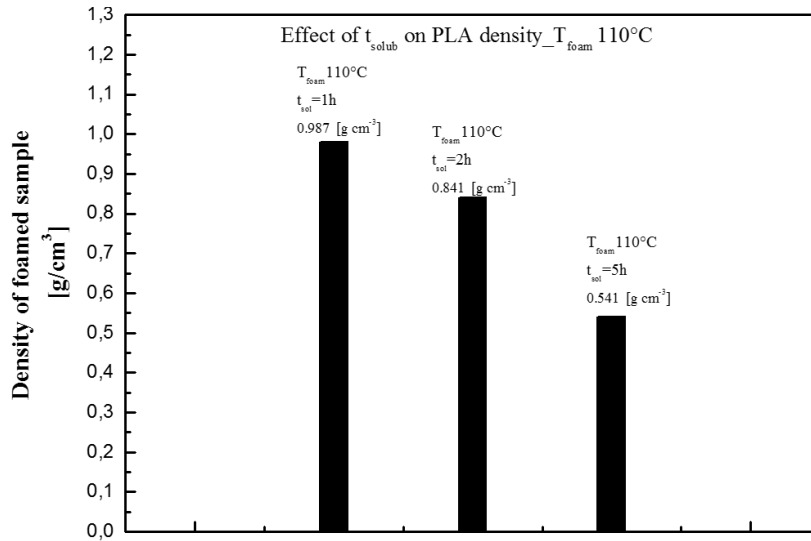
Figure 43. *Effect of solubilization time at $T_{foaming}$=110°C and cooling by air.*

3.3.4 Comparison between Cooling Rate and Solubilization Time

In Figure 44 it is possible to observe how the variation of both Cooling Rate and Solubilization Time take effect on the cellular morphologies. The microscope analysis confirmed that unfoamed zones can be observed in samples obtained imposing a lower solubilization time. Furthermore, for the same solubilization time, by means of a sudden cooling allowed by water, an improvement in the quality of the cellular structure also in the critical solubilization time conditions can be obtained.

A_P55_T190_2H_F110   *W_P55_T190_2H_F110*

A_P55_T190_1H_F110   **W_P55_T190_1H_F110**
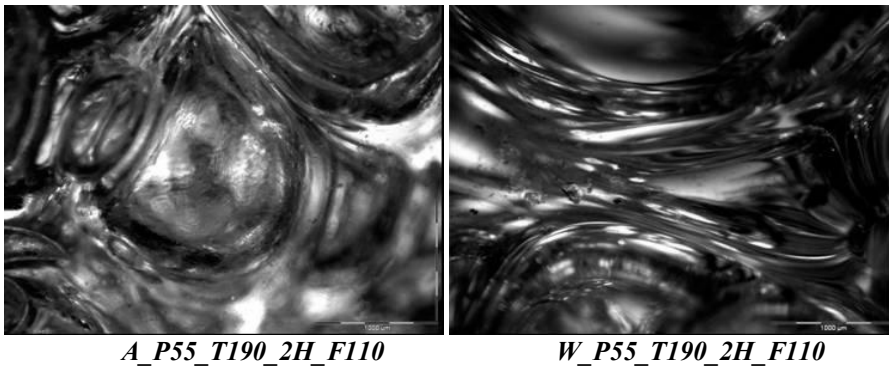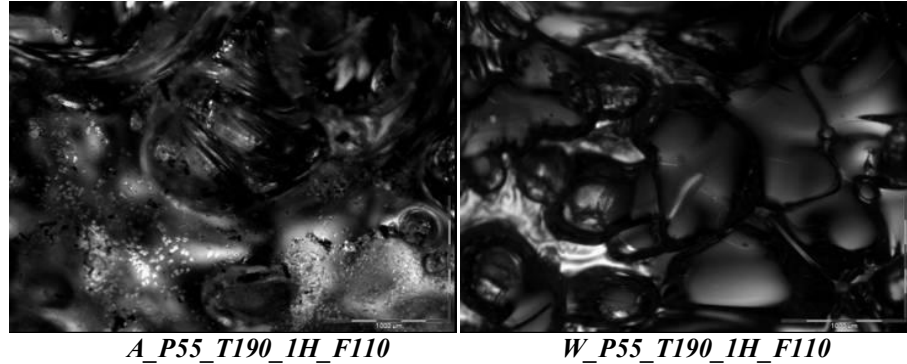
Figure 44. *Samples of PLA with different cooling type (air and water) and different solubilization time (2h and 1h) at $T_{foaming}$=110°C (scale 1000 μm).*

In Figure 45, density values for the abovementioned samples are displayed. For both temperatures, lower density values were obtained for the samples cooled by water, confirming a better foaming from melt state also for short solubilization time.
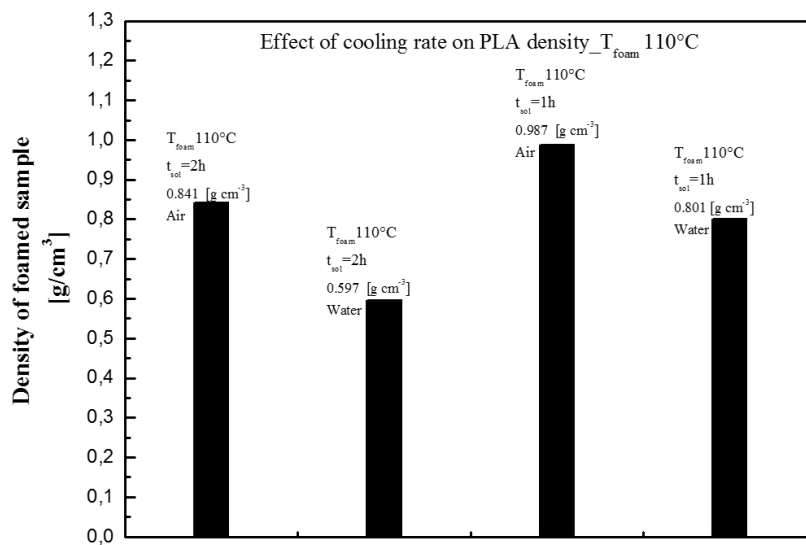
Figure 45. *Effect of cooling rate and solubilization time for $T_{foaming}$=110°C.*

3.3.5 Comparison between PS with PLA

A comparison between foams of PLA and amorphous Polystyrene by adopting two different temperature conditions (T_{foam} 90÷110°C) was made (Figure 46).

PS_W_P55_T190_1H_F110   *PS_W_P55_T190_1H_F90*

PLA_W_P55_T190_1H_F110   *PLA_W_P55_T190_1H_F90*
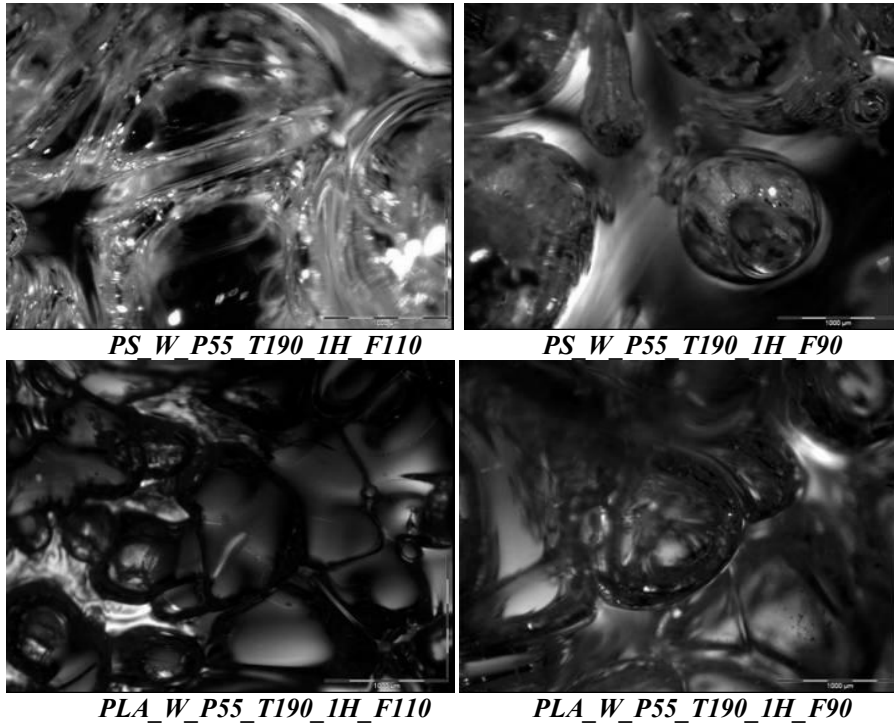
Figure 46. *Samples of PS with different foaming temperature (110 and 90°C) and t_{sol}=1h (scale 1000 μm).*

Differently to the PLA matrix, PS samples exhibited high foamability at T_{foam} 110°C, due to lower viscosity value at this temperature. By contrast, as soon as foaming temperature imposed is close to glass transition value for PS (above 100°C), wide unfoamed zones are detectable in Polystyrenic sample. This occurrence involved, in the case of PS, a doubling in density value compared to the samples obtained at higher foaming temperature (Figure 47), with values of density quite similar to the values obtained for PLA samples.
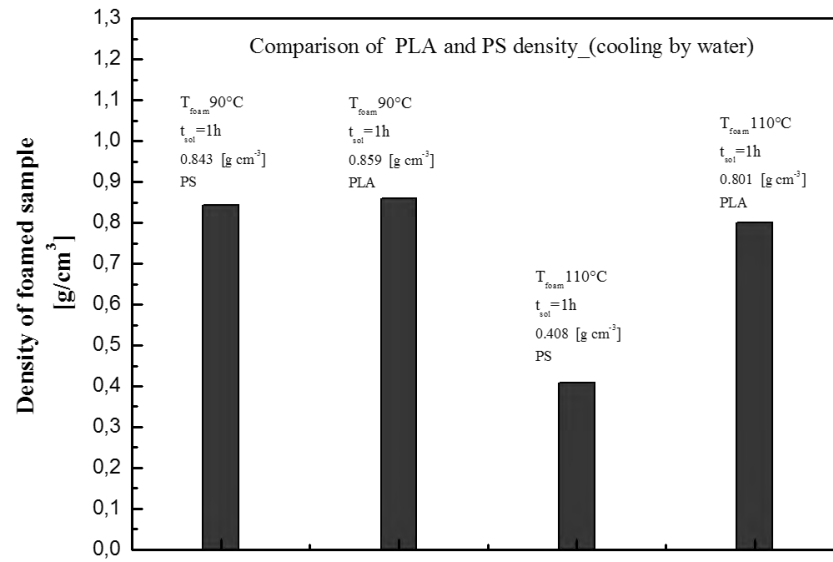
Figure 47. *Comparison between PLA vs. PS.*

Chapter 4
Polypropylene
HIFAX BA 238 G3

Preliminary tests were carried out on an industrial polypropylene, in order to analyze the workings of alla the systems and the effect of several process variables and to understand the best molding conditions.

Experiments with different volumes of batching were carried out to find the volume that allows to completely fill the cavity in absence of blowing agents. Then, for the experiments in presence of gas, the volume of the shot was fixed at 70% of this value in order to allow the free blowing of the molded part. The injectors of the blowing agent are in a fixed position in the cylinder. At the beginning of the batching step, they are opened by a valve that allows the injection of gas from the pump to the cylinder during the entire batching step. At the end of the batching step, the valve can be closed.

The first experiments of injection molding with a blowing agent have shown a density much lower than that of the samples molded in the absence of gas. In particular, a reduction in density as high as 35% was found.

During these preliminary tests, the effect of the application of a holding pressure was analyzed.

The results show that the application of this pressure leads to samples with higher density and greater unfoamed skin. Therefore subsequent experiments were performed in the absence of packing step.

Another important variable in the injection molding process is the back pressure, namely the pressure applied inside of the cylinder while the screw returns back to prepare a new shot of material to inject. Some experiments have shown that, on increasing the back pressure, the density of the sample significantly increases, as shown in Figure 48. Therefore, in the subsequent experiments the back pressure was fixed at 2 bar (pressure of the hydraulic system) in order to obtain a good equilibrium between the density of the material and the facility of the dosage step. In fact, by imposing a pressure equal to zero, which would allow a lower density, problems arise when loading the material during batching.
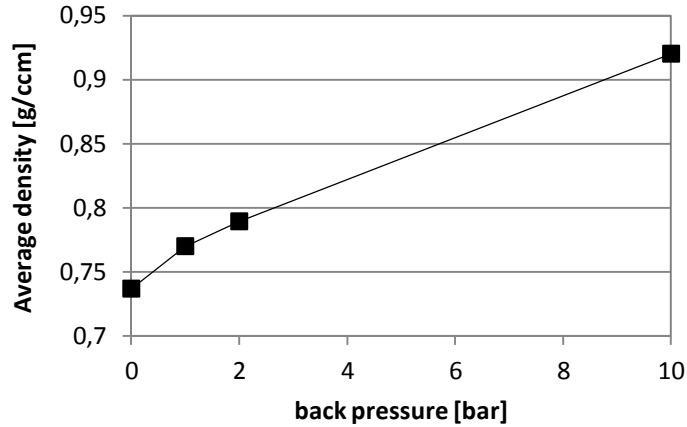
Figure 48. *Effect of back pressure on the sample average density.*

The rotation speed of the screw during the batching step is another variable analyzed in this part of the work. The blowing agent is injected at a fixed position in the cylinder during the entire dosage step. A higher rotation speed leads to a shorter time of the dosage step, therefore less amount of gas injected into the polymer melt. Hence, the rotation speed for all the experiments was set at 200 rpm.

From these considerations, first experiments of injection molding with a blowing agent were carried out. These experiments have shown a density much lower than that of the samples molded in the absence of gas. In particular, a reduction in density of 35% was found.

4.1 Experimental conditions

The first experiments of microcellular injection molding with rheological measurements by using the thinner slit were carried out in order to observe the rheological behavior of the polymer/gas solution.

Table *15* shows the experimental conditions adopted for injection molding tests with BA and nitrogen.

Table 15. Experimental conditions

Injection Temperature [°C]	220	220
Gas Pressure [bar]	-	100
Flow Injection [ccm/s]	4, 9, 17, 36, 66, 72	4 , 9, 17, 36, 66, 72
Shot volume [ccm]	44	44
Rotation speed [rpm]	200	200
Back pressure [bar]	2	2

4.2 Analysis with Cross Model

Some experiments without gas at different injection velocity were carried out. The data of viscosity and shear rate obtained from the rheological analysis were compared with rheological measurements well described by the Cross-Vogel Model. In particular, the parameters of the model were determined on the basis of independent measurements carried out by capillary and rotational rheometers for the same material at the same temperature. Figure 49 shows a perfect match between the experimental data and the model. So, the data of viscosity obtained by slit rheometer are compatible with the experimental data of viscosity in the same conditions present in literature.
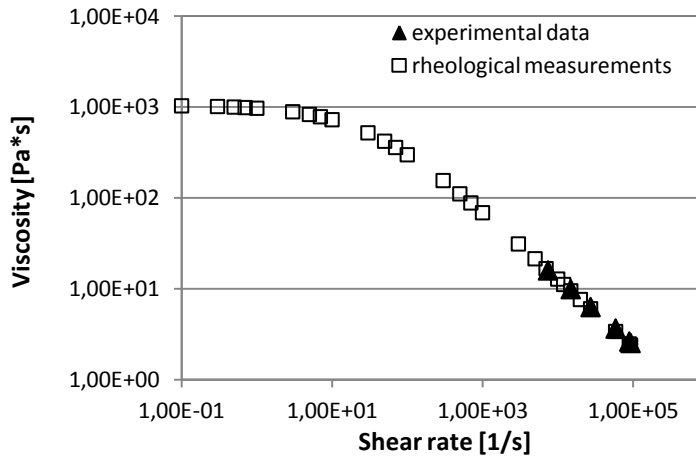
Figure 49. *Comparison of the experimental data of BA238G without gas with the Cross-Vogel Model which describes independent viscosity data for the same material at the same temperature (T=220°C)*

4.3 Rheological measurements

The Kistler "Data Flow" system allows the acquisition of the pressure data by the three transducers and of the screw position during the cycle.
Figure 50 shows the pressure profiles during the injection phase.
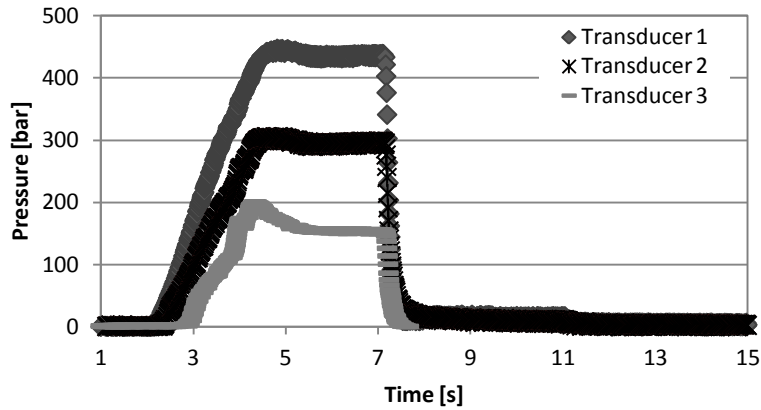
Figure 50. *Pressure profiles during the injection phase.*

Figure 51 shows the pressure drops, namely the difference between the pressure values of two consecutive transducers after the injection phase, in absence of foaming gas and with 0.8 g of nitrogen, at different injection flow rates. This graph allows to observe that, in presence of nitrogen the pressure drops are lower than for the polymer without gas.
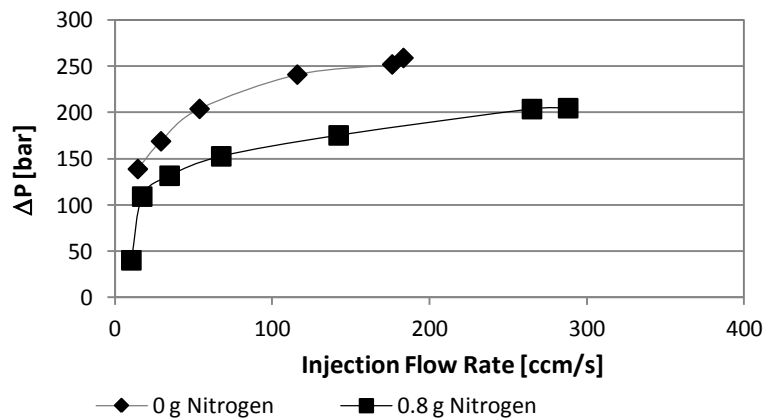
Figure 51. *Pressure drops vs screw velocity for BA238G with gas and without gas (T=220°C).*

The shear rate and viscosity were calculated from the differences in pressure between the transducers (P). In Figure 52 viscosity is reported versus shear rate for tests with gas and without gas: at the same shear rate a lower viscosity is measured for the material in presence of foaming gas. The viscosity reduction is equivalent to a temperature increase of 15°C. This means that, to have with BA the same values of viscosity obtained by BA/N_2 solution at 220°C, it should work at 235°C.
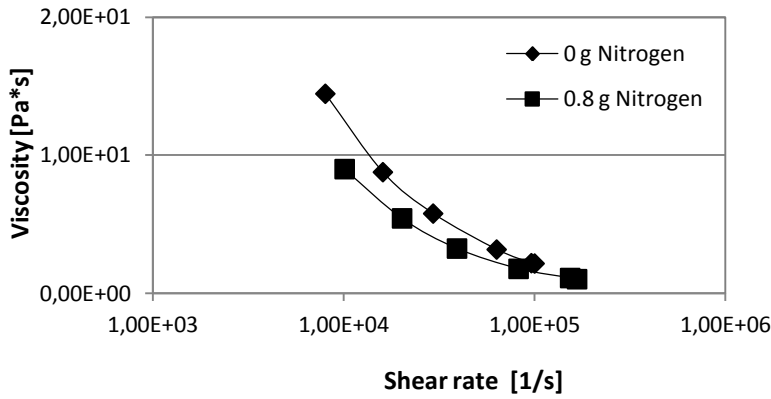
Figure 52. *Viscosity vs shear rate for BA238G with gas and without gas (T=220°C).*

4.4 Morphological analysis

In Figure 53 the densities of the three zones of the sample are compared. As is possible to see, the density decreases on increasing the distance from the injection point, which means that, moving away from the injection point, the sample appears increasingly more foamed.
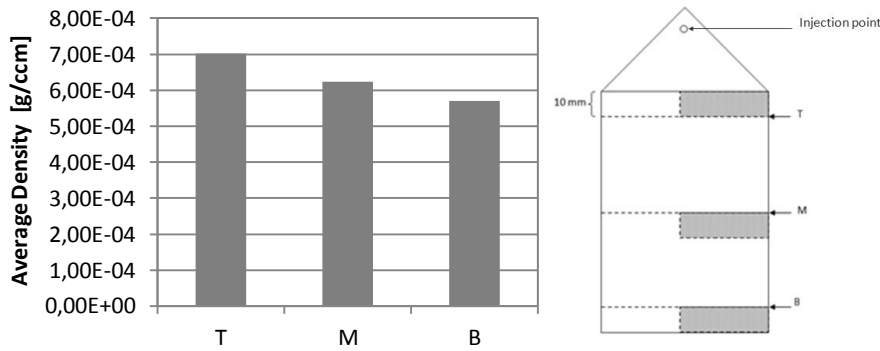
Figure 53. *Average density of parts taken at different distances from the injection point.*

The top of the sample has the largest skin of unfoamed material and un-homogeneous distribution of bubbles, making this zone denser than the others. Going away from the injection point, the samples present lower density because they have a more homogeneous morphology and a thinner layer of compact skin.

Chapter 4

A first analysis of the morphology and the skin thickness was made on all the samples obtained from these experiments. The samples were cut at three different distances from the injection point. In Figure 54 the characterization of the sample, obtained at 240°C with a shot volume of 36 ccm and 1.5 g of nitrogen injected, is reported.
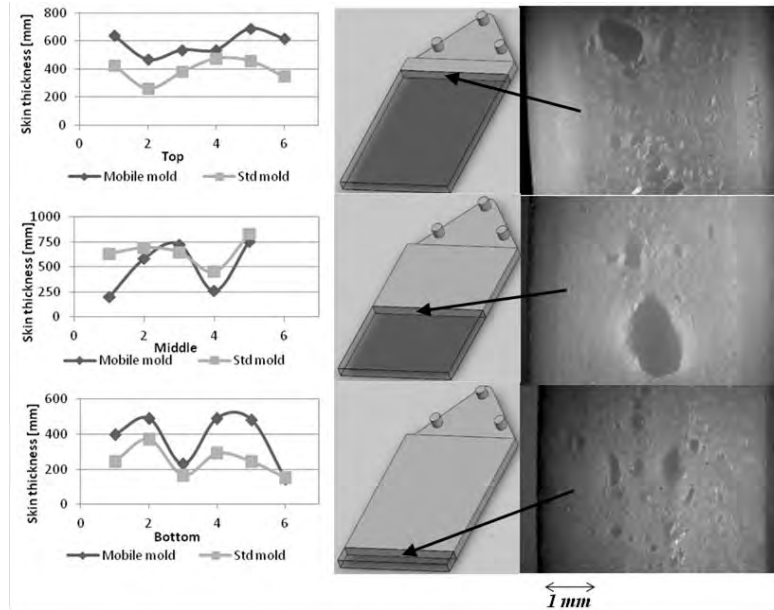
Figure 54. *Skin thickness analysis and cells distribution for the sample of BA238G obtained at 240°C with shot volume of 36 ccm and 1.5 g of nitrogen injected.*

Chapter 5
Polystyrene 678E

In this part of the work, a polymer commonly used in the conventional injection molding process, polystyrene 678E, was adopted to make foam injection molding with nitrogen as physical blowing agent.

Experiments were carried out by use of cavity with two different thicknesses and two slit rheometers, in order to analyze a wider range of shear rate.

5.1 Thicker cavity

First experiments were carried out by use of a cavity with thickness of 10 mm, as shown in Figure 55.

Figure 55. *Samples geometry utilized in the first set of experiments with PS 678E.*

The experiments were performed by changing several process variables in order to study their effect on the rheological and physical properties of injected material. In particular, three injection temperatures and polymer/gas solutions with different percentages of nitrogen were investigated. The higher thickness of the cavity imposes a great volume of dosage. Table 16 shows the experimental conditions of the tests made with the thicker cavity.

Table 16. *Experimental conditions.*

Injection Temperature [°C]	220	240	260
Gas Pressure [bar]	0, 60, 80, 100	0, 60, 70, 80	0
Injection Flow Rate [ccm/s]	4, 9, 16, 35, 69, 74	4, 9, 16, 35, 69, 74	4, 9, 16, 35, 69, 74
Rotation speed [rpm]	200	200	200
Shot volume [ccm]	44	44	44
Back pressure [bar]	0, 2	2	2
Mold Temperature [°C]	30	30	30

Chapter 5

5.1.1 Analysis with Cross Model

The comparison between the experimental data obtained by slit rheometer in absence of gas at the three temperatures and the Cross-Vogel model, whose parameters were determined by independent rheological measurements, was shown in Figure 56.
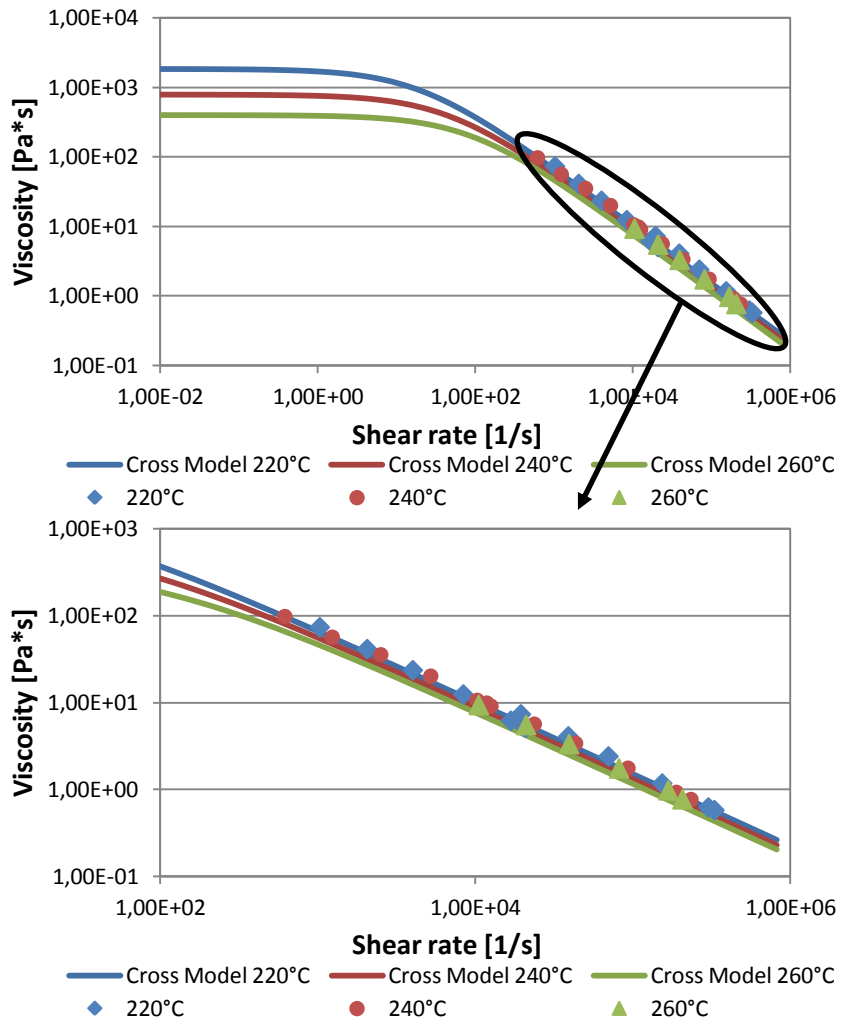
Figure 56. *Comparison of the experimental data of unfoamed PS 678E with Cross-Vogel Model at different process temperatures.*

It is possible to observe that the experimental data of pure PS are very close to the lines which describe independent rheological measurements in all the three cases. So, the rheological measurements obtained by slit rheometer can be considered reliable.

Injection temperature 220°C

Different amounts of gas, corresponding to different pressures imposed by the volumetric pump, were used in order to compare the properties and the morphology of the samples foamed with increasing amount of nitrogen. In particular, knowing the values of pressures and volumes before and after the injection of gas by means the pump, the molar volume of nitrogen allows to obtain the numbers of moles injected. Figure 57 reports the amount of nitrogen injected at injection temperature of 220°C.
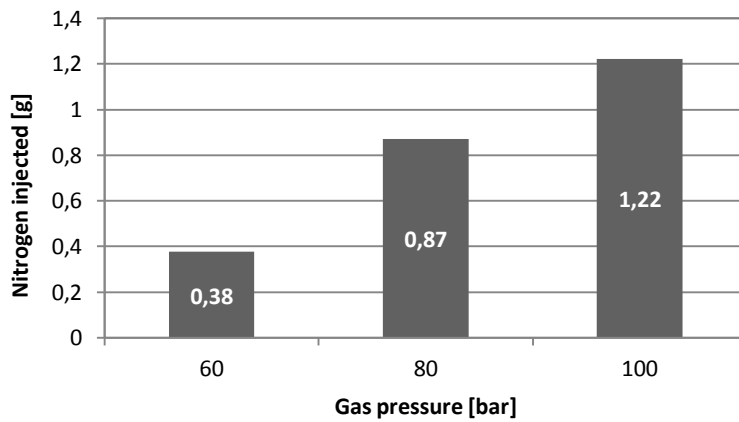
Figure 57. *Amount of nitrogen injected in PS 678E at T= 220°C.*

As explained in paragraph 2.6, slit rheometers with two different geometries were utilized, in order to study a wider range of shear rates. Figure 58 and Figure 59 show the profiles of pressure drops obtained with the two slits.
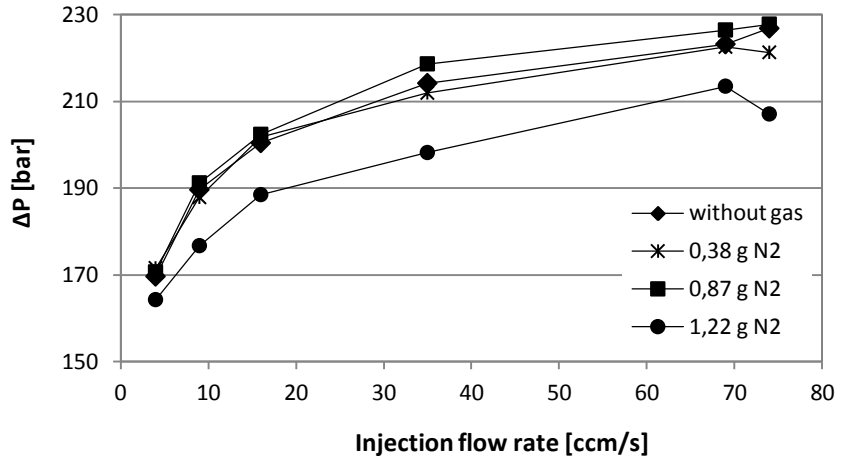
Figure 58. *Pressure drops of measured in the thinner slit (thickness=0.75 mm; width=10 mm) for PS 678E with different amounts of nitrogen (T=220°C).*
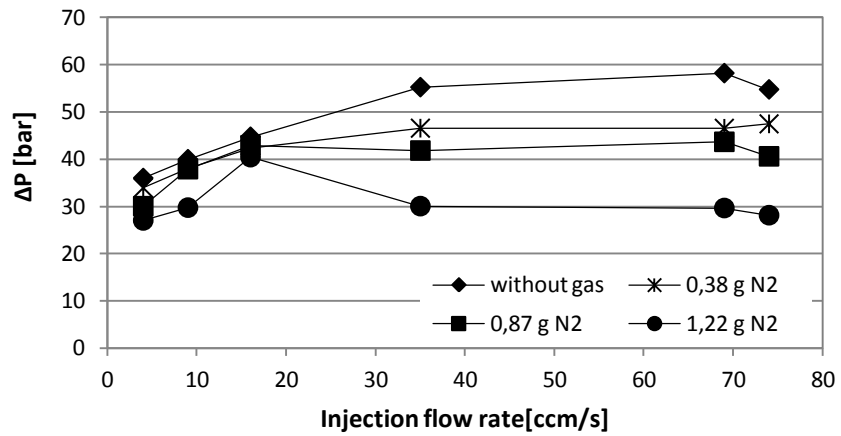
Figure 59. *Pressure drops measured in the thicker slit (thickness=2 mm; width=20 mm) for PS 678E with different amounts of nitrogen (T=220°C).*

The values of the pressure measured by transducers of the slit are reported in
Table 17 and
Table *18*.

Table 17. *Pressure values measured by pressure transducers in the thinner slit (thickness=0.75 mm; width=10 mm).*

Injection flow rate [ccm/s]	Without gas		0.38 g Nitrogen		0.87 g Nitrogen		1.22 g Nitrogen	
	P_1 [bar]	P_2 [bar]	P_1 [bar]	P_2 [bar]	P_1 [bar]	P_2 [bar]	P_1 [bar]	P_2 [bar]
4	358,8	205,0	333,2	161,7	319,7	149,1	300,1	135,9
9	409,4	236,8	369,8	182,0	366,8	175,6	346,5	169,8
16	460,5	268,9	410,1	208,3	405,3	202,9	379,7	191,2
35	539,4	318,2	449,1	237,2	454,7	236,0	426,1	228,0
69	553,4	329,1	509,8	287,3	513,7	287,3	469,1	255,7
74	558,4	334,0	537,7	316,4	528,9	301,1	458,8	251,7

Table 18. *Pressure values measured by pressure transducers in the thicker slit (thickness=2 mm; width=20 mm).*

Injection flow rate [ccm/s]	Without gas		0.38 g Nitrogen		0.87 g Nitrogen		1.22 g Nitrogen	
	P_1 [bar]	P_2 [bar]	P_1 [bar]	P_2 [bar]	P_1 [bar]	P_2 [bar]	P_1 [bar]	P_2 [bar]
4	196,4	160,4	171,8	137,9	161,1	131,1	146,9	119,9
9	230,5	190,5	200,4	162,5	192,6	154,8	184,2	154,5
16	269,6	224,9	244,7	202,4	241,9	199,0	256,2	215,8
35	315,2	260,0	280,6	234,0	272,8	231,0	274,0	244,0
69	366,7	308,6	318,1	271,6	316,3	272,7	337,2	307,6
74	381,2	326,5	341,8	294,4	334,6	294,1	341,7	313,6

From the pressure drops, by means of the equations given in paragraph 2.6, it is possible to obtain the evolution of the viscosity with the shear rate. The two slits allowed to explore a wide range of shear rates: from 760 s^{-1}, values comparable with shear rates obtained with conventional rheometers, to 40000 s^{-1}, values higher than the limit for standard capillary rheometers. In Figure 60 values of viscosity at different shear rates are shown.
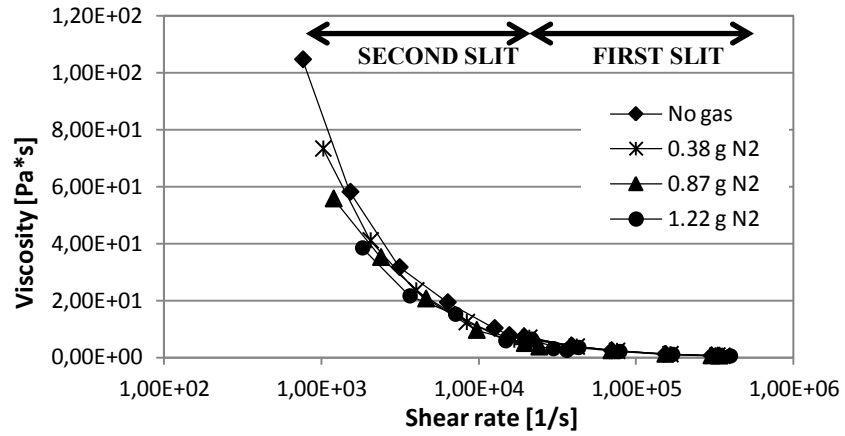
Figure 60. *Evolution of viscosity with shear rate for PS 678E with different amounts of nitrogen (T=220°C).*

On increasing the amount of nitrogen injected, there is a reduction of viscosity that can be quantified through an equivalent increment of temperature. In fact, it is interesting to know at which temperature the curve without gas can reach the position of the curve with gas. So, we need calculate the temperature T^* at which it is possible to obtain, without gas, the same viscosity values obtained in the experiments in the presence of gas. The increase of temperature is calculated as:

$$\Delta T = T^* - T \tag{54}$$

Where T is the injection temperature at which the experiments in absence of gas were made. Through the equations of the Cross-Vogel Model it is possible to obtain T^* as:

$$T^* = \frac{A + T_{ref} \cdot \alpha}{\alpha} \tag{55}$$

where A and T_{ref} are constant data and α can be calculated with:

$$\alpha = ln\left(\frac{\eta_N}{\eta_0}\left(\frac{\Delta P_1}{\Delta P_0}\right)^{1/n}\right) \tag{56}$$

ΔP_1 is the pressure difference obtained from the gas/polymer solutions and ΔP_0 is the pressure difference obtained from pure polystyrene. So, the increments in temperature equivalent to a reduction in viscosity, calculated for two amounts of gas in solution, were reported in Table 19.

Table 19. *Increment in temperature equivalent to the reduction in viscosity.*

Injection flow rate [ccm/s]	T-0.38 g Nitrogen	T-0.87 g Nitrogen
4	5,87	19,46
9	5,23	5,50
16	5,36	3,93
35	17,92	31,69
69	24,43	32,92
74	14,89	34,79

From the Table 19 it is possible to deduce that, in order to obtain in absence of gas the same values of viscosity obtained at 220°C with 0.87 grams of nitrogen and injection flow rate of 74 ccm/s, the machine should operate with a temperature of about 255°C.

Another important result of the gas injection into a polymer matrix is the production of a part with lower density compared to a sample having the same volume, molded in the same conditions in absence of gas. The reduction in density compared to the density of an unfoamed part was measured using the Archimedes' principle described in the section 2.7 above.

Reductions in density of the foamed samples compared to samples of pure polystyrene molded in the same conditions are reported in Table 20, from which it is possible to notice that, at high amounts of gas injected, it can reach a reduction in density larger than 40%.

Table 20. *Reduction in density for samples of PS 678E with different amounts of nitrogen (T=220°C).*

Injection flow rate [ccm/s]	0.38 g Nitrogen	0.87 g Nitrogen	1.22 g Nitrogen
	REDUCTION IN DENSITY [%]		
4	17,5	44	46
9	30,5	33	42
16	42	48,5	45
35	37	33	46
69	39	48	40
74	42	40	40

Injection temperature 240°C

The same polymer was processed at an injection temperature of 240°C. Also in this case, samples of pure polystyrene were compared with samples obtained by a solution of polystyrene with 0.51 g of nitrogen.

Figure 61 shows the difference between the pressure drops measured for pure polystyrene and those of the PS/N_2 solution. Also in this case the unfoamed sample has higher pressure drops that the foamed one.
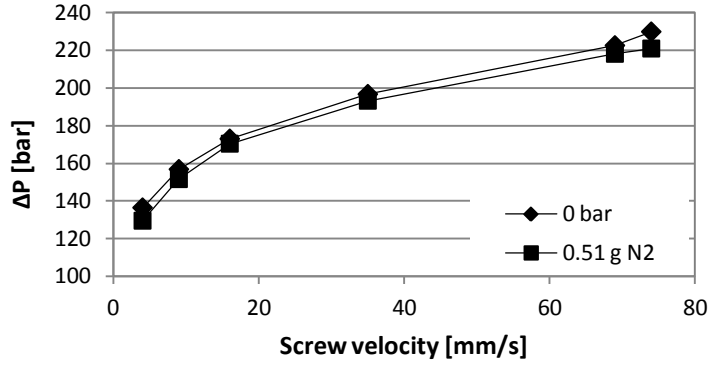
Figure 61. *Pressure drops of PS 678E with different amounts of gas (T=240°C).*

The values of pressure measured by slit are reported in Table 21.

Table 21. *Pressure values measured by pressure transducers in the slit.*

Flow Injection [ccm/s]	Without gas		0.51 g Nitrogen	
	P_1 [bar]	P_2 [bar]	P_1 [bar]	P_2 [bar]
4	151,9	124,8	130,7	106,6
9	179,1	147,8	173,5	142,7
16	223,2	183,3	201,6	164,8
35	266,5	219,5	227,2	186,1
69	306,1	257,4	268,7	223,4
74	323,0	271,9	287,6	244,8

In Figure 62 the evolution of the viscosity with the shear rate at 240°C is shown. The reduction of viscosity at lower values of shear rate correspond to an increment of temperature equivalent to 19°C.
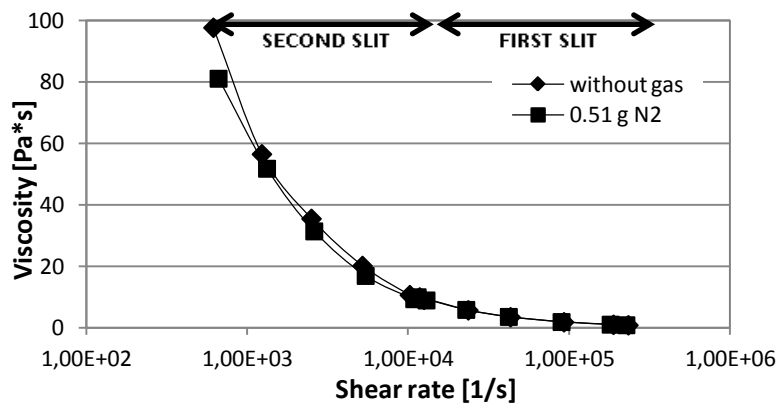
Figure 62. *Viscosity vs shear rate for PS 678E with different amounts of nitrogen (T=240°C).*

Also in this case, the reduction in density compared to the unfoamed sample was measured. As shown in Figure 63, it is increasing with the injection flow rate and reaches values greater than 45%.
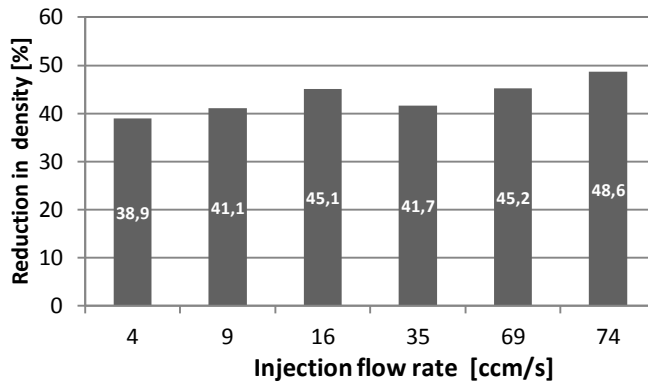
Figure 63. *Reduction in density for samples of PS 678E with different amounts of nitrogen (T=240°C).*

5.2 Thinner cavity

All the experiments reported below were carried out using only the second slit (higher thickness and width), in order to observe the effect of gas on viscosity at lower shear rates. After the previous set of experiment, the cavity has been changed. In particular, the thickness was reduced from 10 mm to 5 mm.
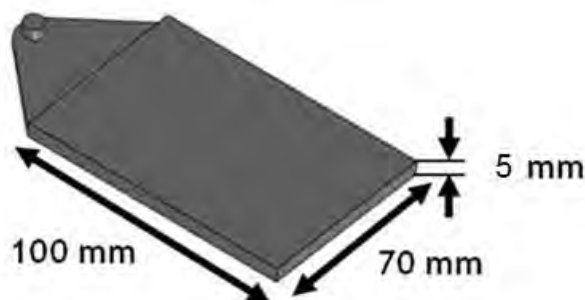
Figure 64. *Samples geometry utilized in the second set of experiments with PS 678E (T=220°C).*

Table 22 shows the experimental conditions adopted in this case. The shot volume was decreased because of the lower volume to fill.

Chapter 5

Table 22. *Experimental conditions.*

Injection Temperature [°C]	**220**
Gas Pressure [bar]	0, 40, 60, 80, 100
Injection Flow Rate[ccm/s]	4, 7, 15, 30, 60, 74
Shot volume [ccm]	29.5
Rotation speed [rpm]	200
Back pressure [bar]	2
Mold Temperature [°C]	30

The unfoamed samples were compared with samples obtained from injections of gas at four increasing pressures, that correspond to four amounts of nitrogen injected, as shown in Figure 65.
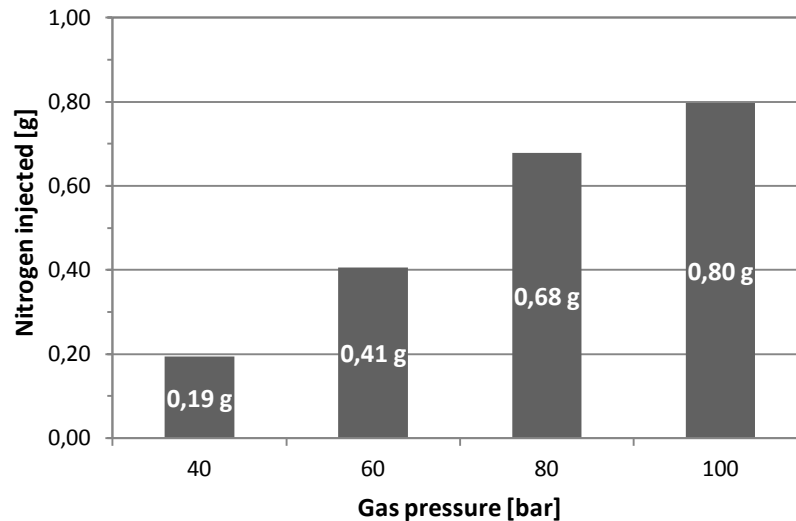
Figure 65. *Amount of nitrogen injected corresponding to different gas pressures, for PS 678E at injection temperature of 220°C in a thinner cavity (thickness=5mm).*

5.2.1 Analysis with Cross Model

Figure 66 shows the comparison between the experimental data in these conditions and the Cross-Vogel Model whose parameters were determined by independent rheological measurements.

Polystyrene 678E
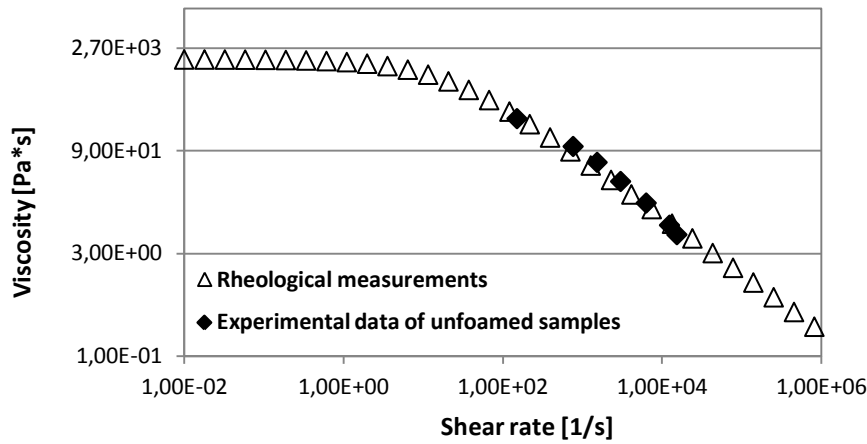
Figure 66. *Comparison of rheological data of unfoamed samples of PS 678E with Cross-Vogel Model (second slit; T=220°C).*

The comparison shows a good agreement between the experimental data and the model.

5.2.2 Solubility

The minimum and maximum values of solubility, calculated as ratio between grams of nitrogen and grams of polystyrene injected, were compared with the limit of solubility of nitrogen in PS during the different phases of the process. In particular, at high pressure established in the injection chamber, the amount of nitrogen is below the solubility curve present in literature. When the solution arrives into the slit rheometer, the pressure decreases. The minimum value of nitrogen stays still below the limit curve, but at low pressures the maximum value crosses above that curve. So, at low pressures and high amount of nitrogen it may occur a partial foaming already into the slit, instead of in the cavity.
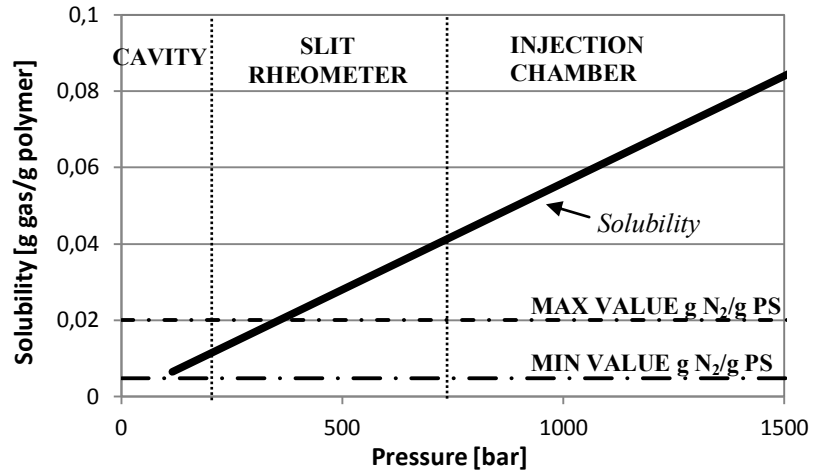
Figure 67. *Solubility of nitrogen inside of PS 678E (T=220°C).*

5.2.3 Rheological measurements

As in the previous case, increasing the amount of nitrogen in solution, decreasing pressure drops can be measured (Figure 68).
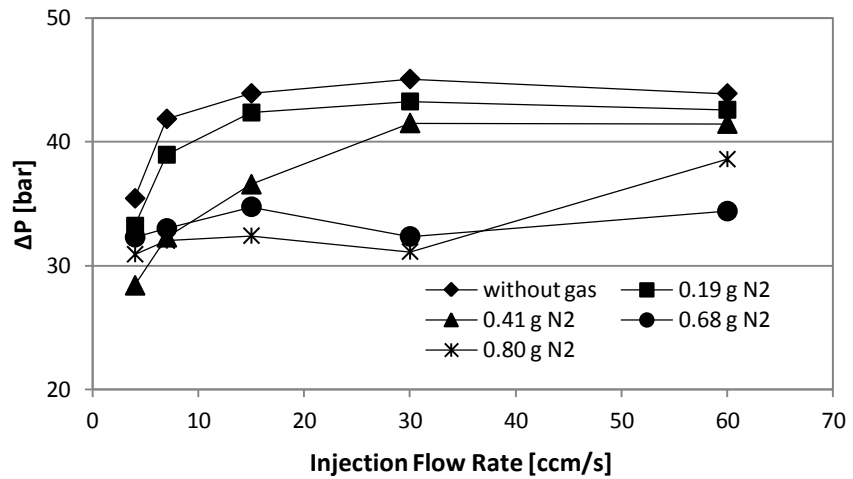
Figure 68. *Pressure drops at different injection flow rates for PS 678E with different amounts of nitrogen (second slit; T= 220°C).*

It can be observed also that the curves at 0.68 and 0.80 grams of nitrogen in solution are almost similar. The anomalous trend of the curve with 0.80 g could be due to a partial foaming already inside the slit.

Table 23 reports the values of pressure measured by pressure transducers in the slit rheometer, from which the pressure drops were obtained.

Table 23. *Pressure values measured by pressure transducers in the slit (PS 678E at 220°C).*

Injection flow rate [ccm/s]	Without gas		0.19 g Nitrogen		0.41 g Nitrogen		0.68 g Nitrogen		0.80 g Nitrogen	
	P_1 [bar]	P_2 [bar]	P_1 [bar]	P_2 [bar]	P_1 [bar]	P_2 [bar]	P_1 [bar]	P_2 [bar]	P_1 [bar]	P_2 [bar]
4	207,9	172,4	177,9	144,7	171,3	142,9	155,1	122,8	168,4	137,5
7	241,3	199,5	210,8	171,8	207,2	174,9	194,5	161,5	195,4	163,4
15	279,3	235,4	247,2	204,8	242,9	206,3	231,6	196,8	229,8	197,4
30	332,0	287,0	292,1	248,9	279,7	238,2	269,6	237,3	275,8	244,7
60	382,5	340,1	353,9	311,3	319,3	277,8	328,4	294,0	321,7	283,2
74	403,6	365,2	374,7	336,6	348,4	316,5	318,9	285,0	335,0	301,6

The variation of viscosity with the shear rate for solutions at different amounts of gas is shown in Figure 69.
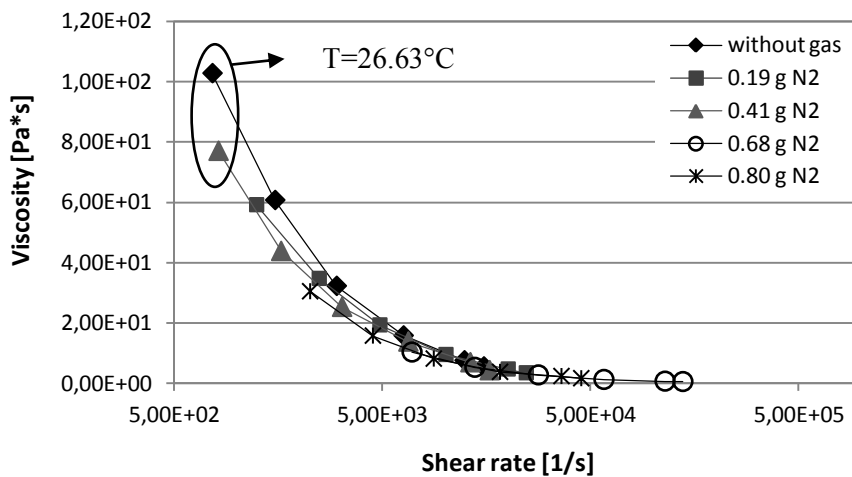
Figure 69. *Viscosity vs shear rate for PS 678E with different amounts of nitrogen (second slit; T= 220°C).*

Also in this case, increasing the amount of gas in solution, it can be observed a reduction of the viscosity values. This reduction compared to viscosity of the pure PS molded in the same conditions can be quantified through the equivalent temperature increase. As reported in Table 24, considering the solution with 0.41 grams of nitrogen and an injection flow rate of 74 ccm/s, it should work at about 246°C to obtain without gas the same viscosity values.

Chapter 5

Table 24. *Reduction in temperature equivalent to the reduction in viscosity (PS 678E at 220°C).*

Injection flow rate [ccm/s]	T-0.19 g	T-0.41 g	T-0.68 g	T-0.80 g
4	8,32	32,85	12,30	9,34
7	9,33	39,91	35,81	28,49
15	4,48	26,27	35,15	41,48
30	5,16	10,78	54,61	54,10
60	0	2,70	30,74	13,10
74	0,61	26,63	17,09	18,27

5.2.4 Density measurements: Archimedes' principle

Density measurements showed a significant reduction in density of the foamed samples compared to the unfoamed ones. The samples with 0.80 grams of nitrogen in solution have, at all the injection flow rates, larger apparent densities if compared with the samples with 0.68 grams.

The data of apparent density can be used to calculate the reduction of density with respect to the unfoamed samples. In Figure 70 it is possible to observe a larger reduction of density on increasing the injection flow rate. On increasing the amount of gas, the reduction in density increases. But for too high amount of gas, the reduction in density begins to decrease again, probably due to a premature foaming in the adduction channels, as noted in Figure 67.
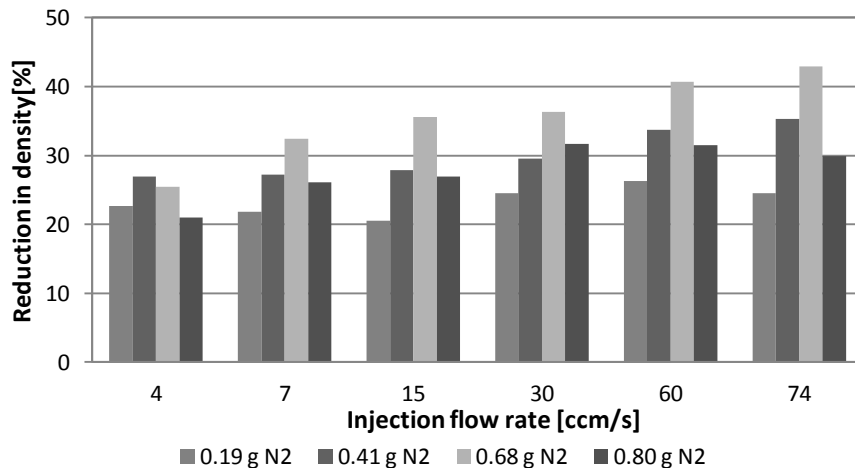
Figure 70. *Reduction in density for PS 678E with different amounts of nitrogen (T= 220°C).*

Furthermore, the reduction in density reaches a maximum for the solution obtained with 0.68 grams of gas.

90

5.2.5 Mechanical properties

The presence of gaseous bubbles (cells) in foamed polymers generates unique physical and mechanical properties in comparison with the base unfoamed polymer. The lower density grants buoyancy to foamed-polymer parts, whereas the softness, energy absorption, and thermal insulation capability open possibilities for a great variety of applications such as floatation, construction, automotive, transportation, sports, medical, furniture, and so on. Their performances are closely associated with material properties. The relationship becomes extremely important when new foamed are developed for more intensively performance-oriented applications [99].

In this part, mechanical properties of the polystyrene/nitrogen solutions in all experimental conditions are investigated.

Flexural test

Flexural tests were carried out in order to compare the flexural modulus of the foamed samples with the one of unfoamed polystyrene. In Figure 71 it is possible to observe two curves of flexural stress versus flexural strain: one corresponds to the sample of pure PS while the other to the solution with 0.80 grams of nitrogen. Both curves are referred to samples obtained by injection at a flow rate of 74 ccm/s.
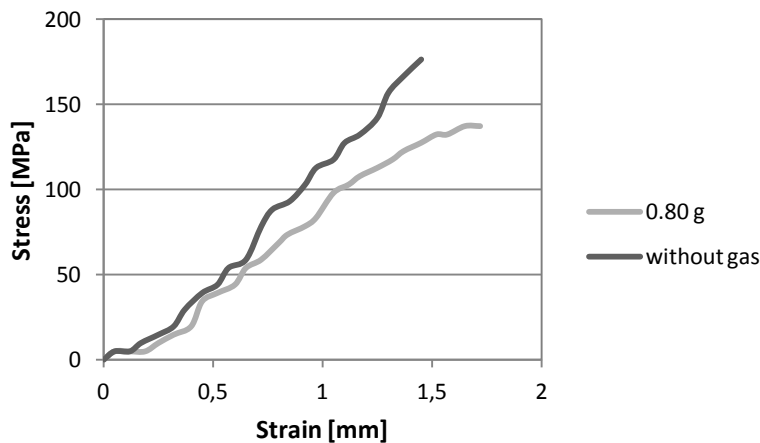
Figure 71. *Flexural stress versus flexural strain of foamed and unfoamed samples of PS 678E injected at 74 ccm/s (T=220°C).*

As it is possible to observe, the curve of the foamed sample has minor slope than the curve of the unfoamed one. So, from the equation in paragraph 2.11, a lower modulus compared to the unfoamed one was

91

measured. Figure 72 shows the modulus of elasticity obtained from these tests.
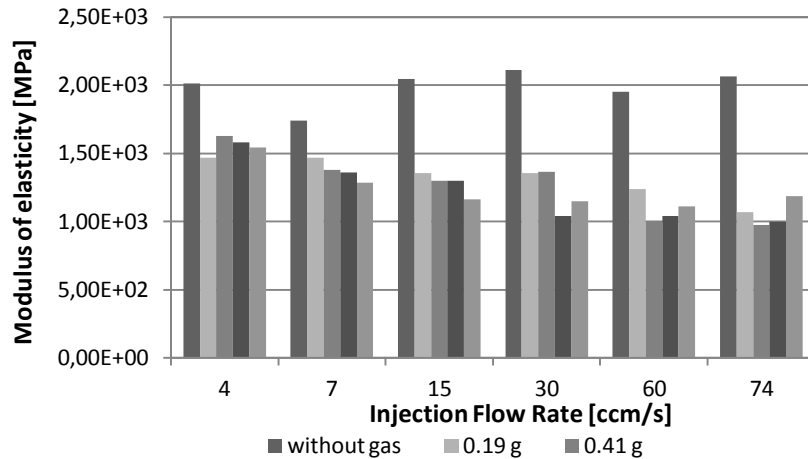
Figure 72. *Flexural modulus at different injection flow rates for PS 678E with different amounts of nitrogen (T= 220°C).*

It is possible to observe that the modulus decreases with the increase of the amount of gas in solution. These modules were multiplied for the ratio between the density of pure PS and the density of the foamed samples, in order to compensate the reduction in density compared to the unfoamed parts (Figure 73). In this way the difference between the modules of foamed and the unfoamed parts strongly decreases.
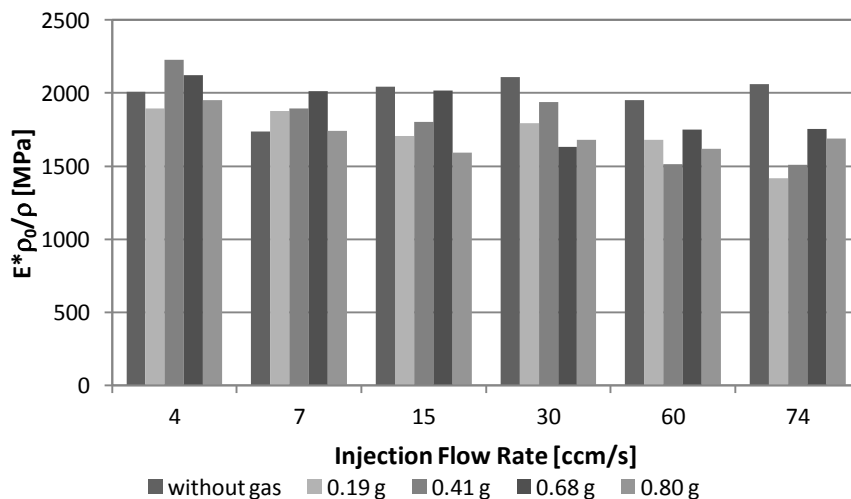
Figure 73. *Modules of elasticity multiplied for the ratio between the density of pure PS 678E and the density of the foamed samples (T=220°C).*

Impact Resistance

The resistance test to the impact were carried out on foamed and unfoamed parts. Figure 74 shows the impact resistance multiplied for the ratio between the densities respectively for unfoamed samples and samples with 0.68 grams of gas in solution.
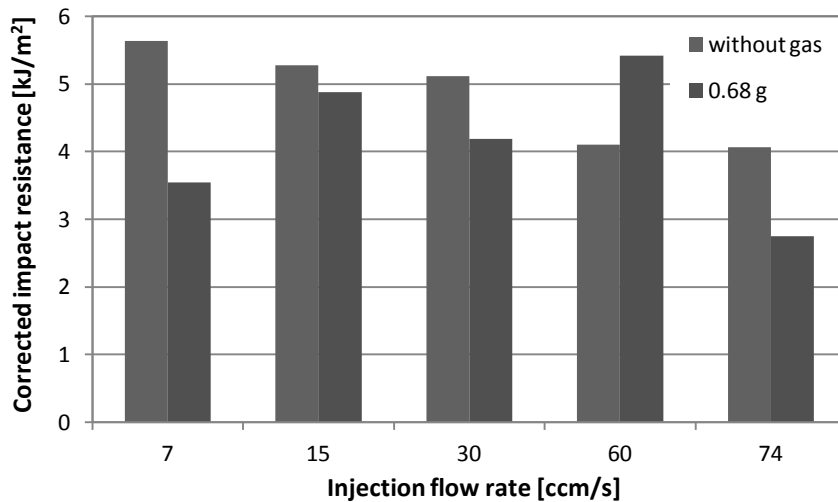
Figure 74. *Impact resistance multiplied for the ratio between the density of pure PS 678Eand the density of the foamed samples (T=220°C).*

It can be observed that the resistance of the sample with 0.68 grams of nitrogen, if it is corrected with the ratio of the densities, increases up to reach the values obtained from the unfoamed samples.

5.2.6 Morphological analysis

From the previous analysis only marginal variations of physical and mechanical properties with the flow were observed, especially for high flow rates. So, it was decided to conduct the morphological analysis only on the samples processed with an injection flow rate of 60 ccm/s. This series of samples was cut as shown in Figure 75 and analyzed by means of tomography and a software for image analysis, ImageJ, in order to observe cell size, cell distribution and thickness of the unfoamed skin layer.

Chapter 5
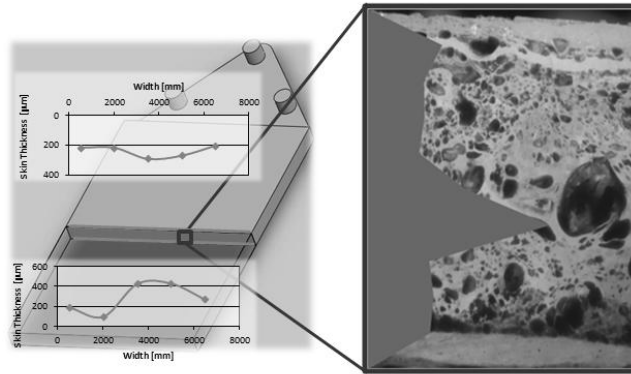
Figure 75. *Position of the morphological observations (length=50 mm).*

Cell size and distribution

The fundamental parameters characterizing the morphology of the foams is the cell size and their distribution. The samples were observed by optical microscopy, from which images of the sample section were obtained (Figure 76).

0.19 g N₂   *0.41 g N₂*

0.68 g N₂ 0.80 g N₂
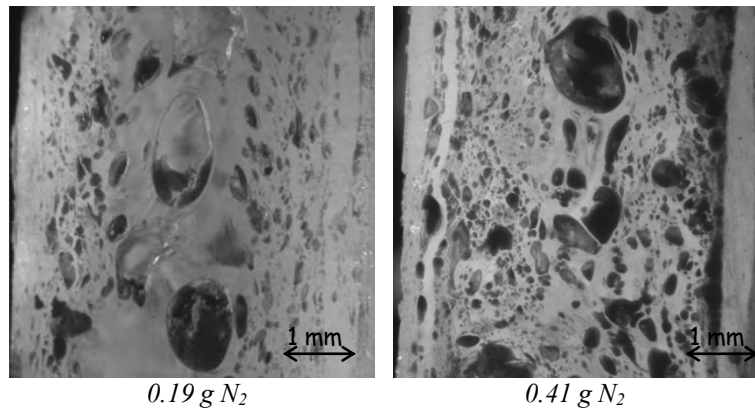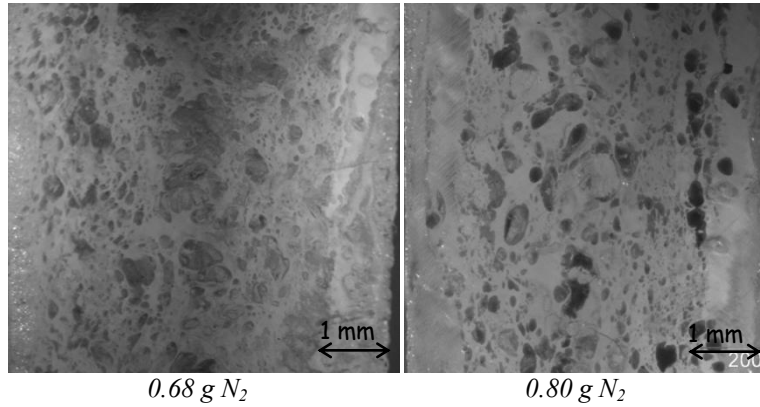
Figure 76. *Micrographs of PS 678E foamed at 220°C with different amount of gas.*

These images were analyzed with the aim of counting the number of cells, their size and their location along the sample thickness. The following graphs show the percentage of void due to cells with radius included in a defined range. Above each column the number of cells with radius included in that range is reported. A software allowed to identify cells and indicate the corresponding area. The percentage of voids V, i.e. space occupied by cells with radius including at a given interval   x, was calculated as:

$$V = \frac{A_i}{A_{tot}} \cdot 100 \qquad\qquad (57)$$

Where A_i represents the area of each cell whose radius is within the range x and A_{tot} is the sum of the areas of the cells of any size.

This analysis was carried out for each amount of gas injected in the polymer matrix. From the Figure 77, that shows the results obtained from samples with 0.19 grams of nitrogen, it is possible to observe that there are cells with very different sizes and great part of the void space is occupied by the cells with radius higher than 500 micron.
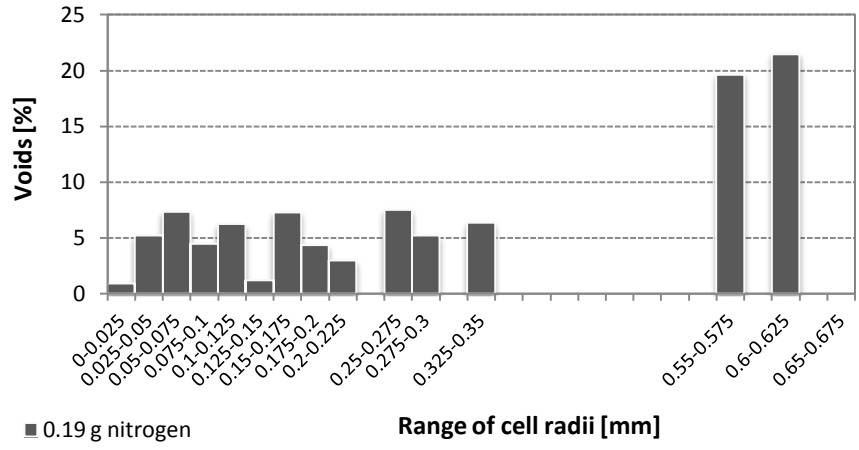
Figure 77. *Percentage of void due to cells with radius included in defined ranges for samples of PS 678E with 0.19 g of gas.*

Increasing the amount of nitrogen in solution to 0.41 grams (Figure 78), the void space of the small cells increases, but it can still observe a large percentage of space occupied by big cells.
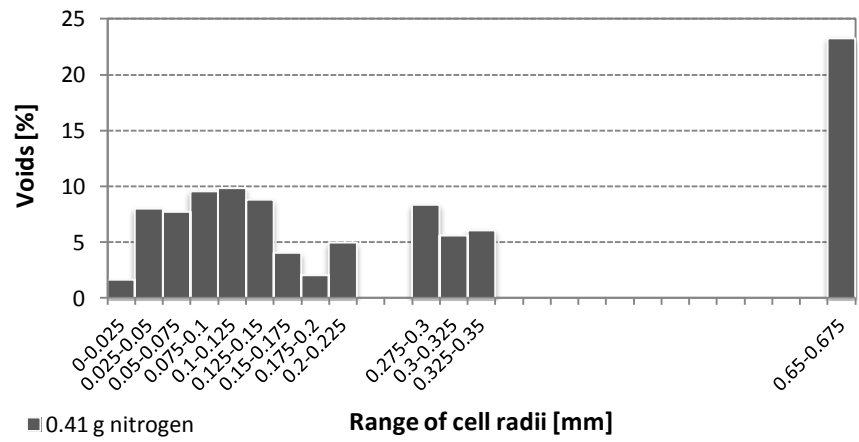
Figure 78. *Percentage of void due to cells with radius included in defined ranges for samples of PS 678E with 0.41 g of gas.*

The best condition can be observed in the case of samples with 0.68 g of gas. In fact, as shown in Figure 79, the great percentage of void space is occupied by cells with radii included in the range 100-200 micron and no big cells are detected.
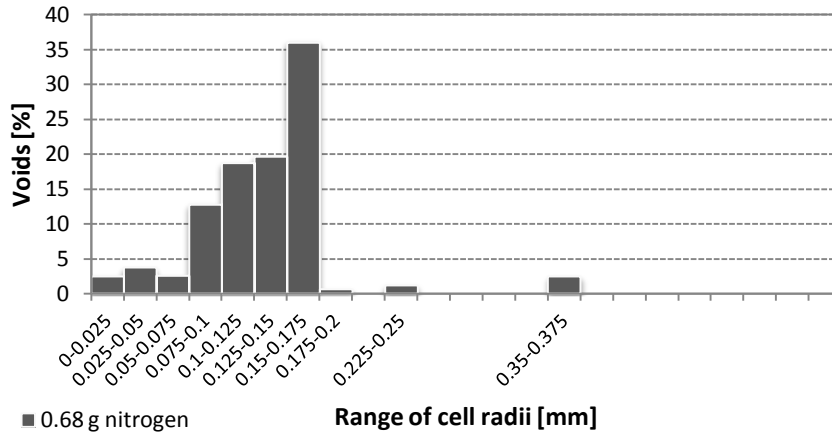
Figure 79. *Percentage of void due to cells with radius included in defined ranges for samples of PS 678E with 0.68 g of gas.*

Good results were also obtained from samples with 0.80 grams of nitrogen injected (Figure 80), where the largest part of the cells have size less than 200 micron. However from the fourth image of Figure 76, representing this condition, a large layer of compact skin can be observed.
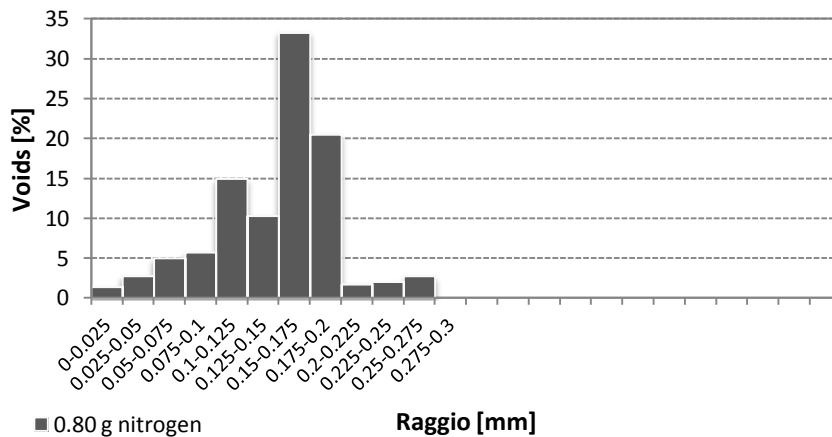
Figure 80. *Percentage of void due to cells with radius included in defined ranges for samples of PS 678E with 0.80 g of gas.*

For a complete morphological analysis of the foamed samples is necessary to know the distribution of the cell radii along the sample thickness. In cellular polymers foamed by injection molding the cell diameter in the middle of the sample is larger than the one in edge areas, because of the cooling rate change. In fact, during the filling of the cavity,

97

Chapter 5

part of the polymer/gas solution, on contact with the cold walls of the mold, quickly cools creating a compact skin. Moving towards the center of the cavity, the cooling rate decreases as shown in the scheme in Figure 81.
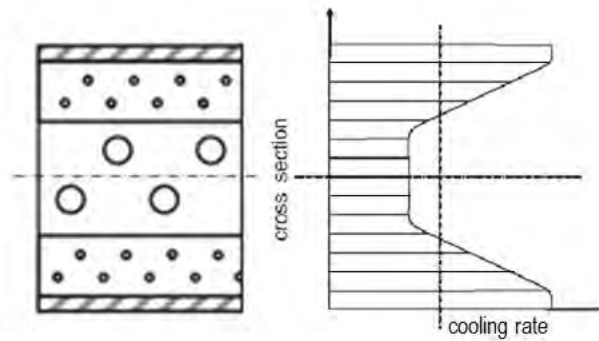
Figure 81. *Cooling rate change over the cross section of an injection molded foam.*

Then, the center of the sample cools more slowly, allowing the cells to grow and coalesce forming larger cells at the center and smaller as they approach the wall. Being the sample thickness equal to 5 mm, the average of the radii included in intervals of 500 micron was calculated. The presence of a lot of small cells around the more visible bubbles greatly decreases the average values of the radii.

The radii distribution profiles were matched to the respective images. From Figure 82, in which the distribution of the radii along the thickness of the sample with 0.19 grams of nitrogen is shown, it is possible to observe that cell radii in the center of the sample have an average radius much higher than that measured at greater distances from the center. Moving from the walls to the center, the average radius increases up to a central peak.

Figure 83 reports the average radii along the thickness of the sample with 0.41 g of nitrogen. In this image it is possible to notice a peak lower than that observed in the previous sample. Moving from this peak to the wall, cells with smaller sizes and quite similar to each other are found, and a sudden decrease of dimensions in proximity of the walls.
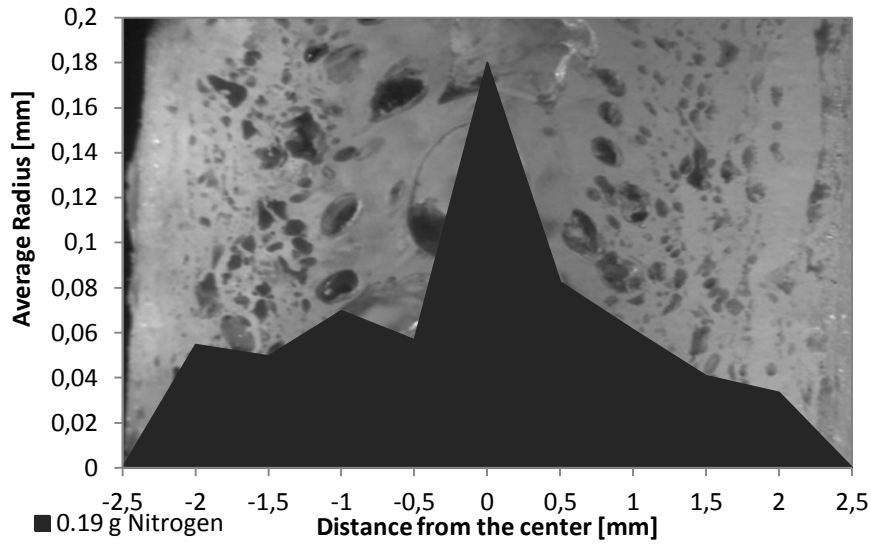
Figure 82. *Radii distribution along the thickness of the sample of PS 678E with 0.19 g of nitrogen.*
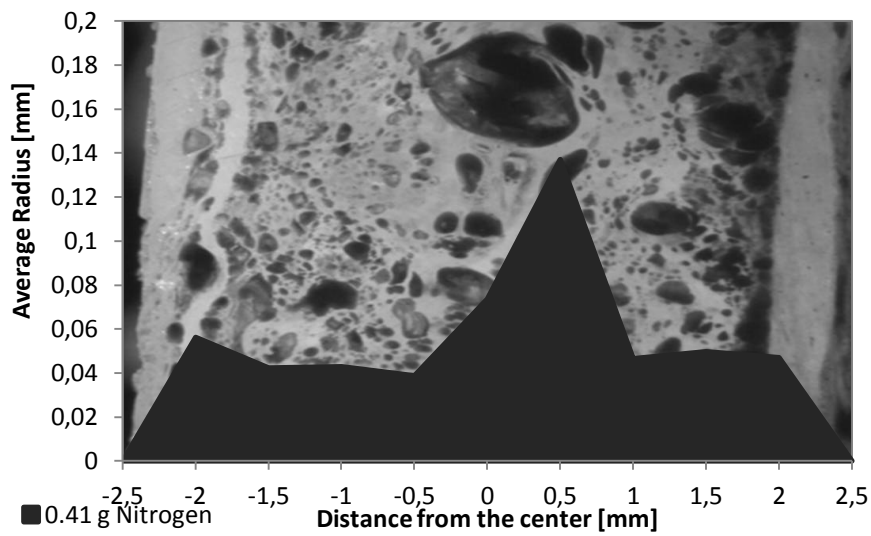
Figure 83. *Radii distribution along the thickness of the sample of PS 678E with 0.41 g of nitrogen.*

In
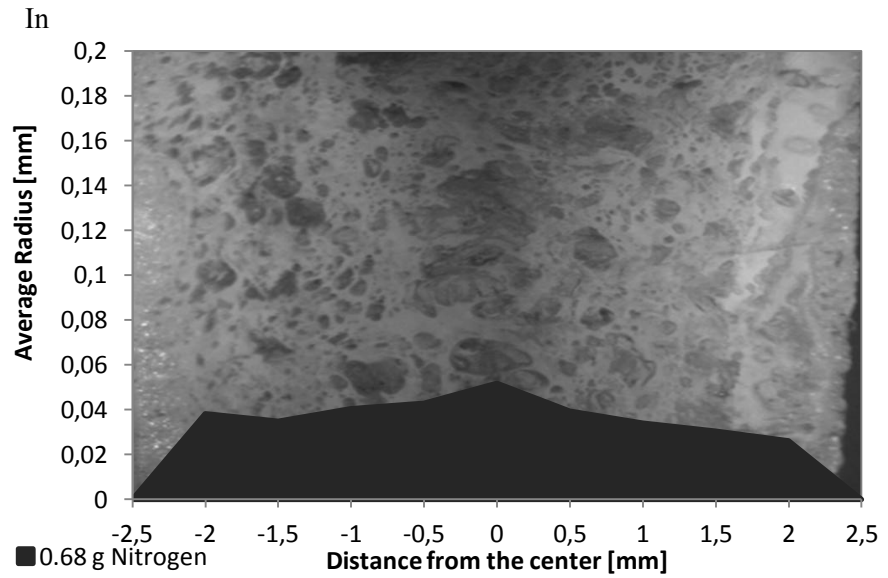
Figure *84*, reporting the average radii along the thickness of the sample with 0.68 grams on nitrogen, the profile flattens.
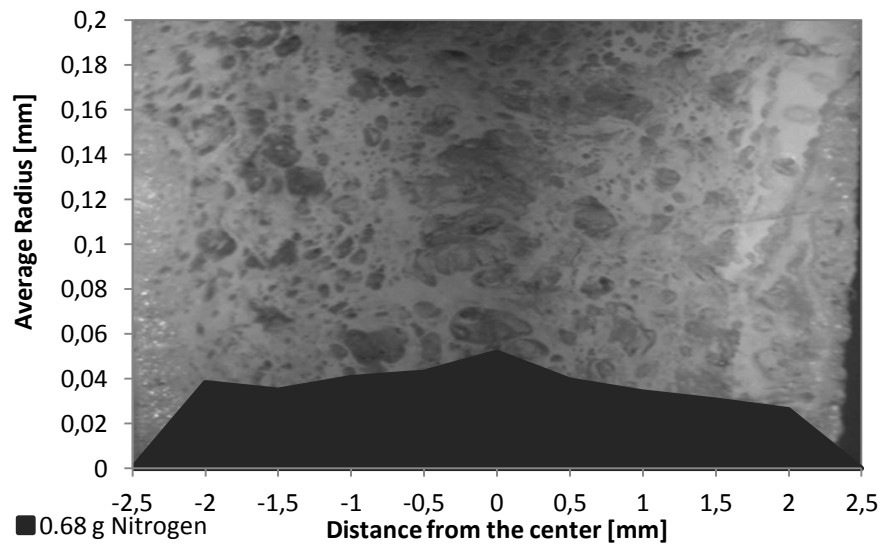
Figure 84. *Radii distribution along the thickness of the sample of PS 678E with 0.68 g of nitrogen.*

In Figure 85 a large layer of compact skin and an almost homogeneous cell distribution in the foamed core can be observed.
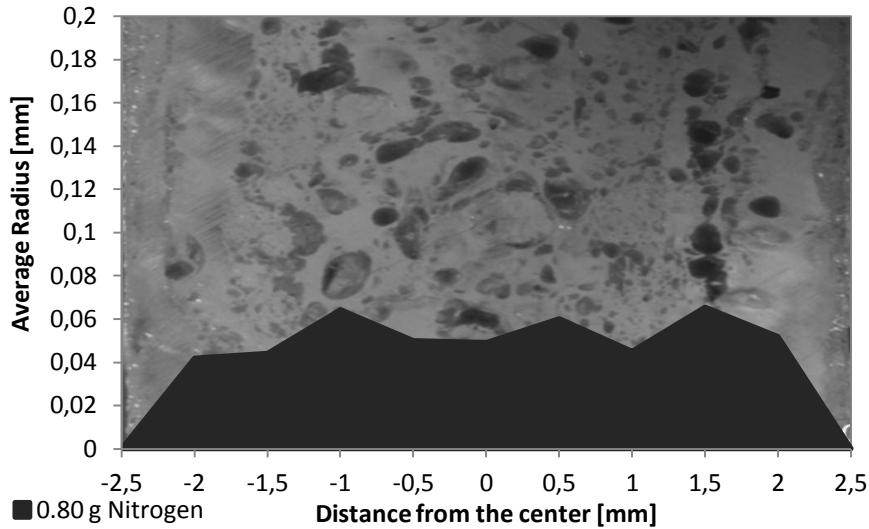
Figure 85. *Radii distribution along the thickness of the sample of PS 678E with 0.80 g of nitrogen.*

In Figure 86 the radii distribution along the sample thickness for all four quantities of gas injected were reported, in order to make an easier comparison between them.
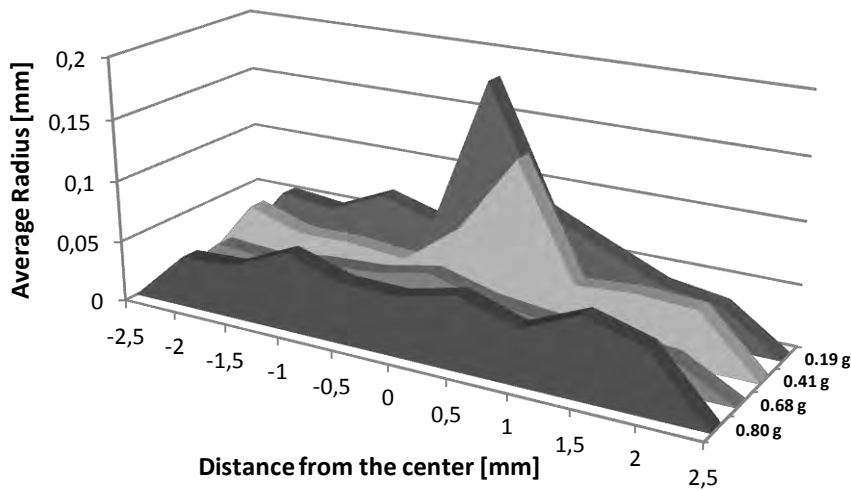
Figure 86. *Radii distribution along the sample thickness for PS 678E with different amounts of nitrogen (T=220°C).*

It is possible to observe that the two profiles with the lower amount of gas show a peak in the center, which means that the cells in that position are larger than those nearer to the wall. Increasing the amount of gas, the profile tends to flatten. Also from morphological point of view, the solution with

101

Chapter 5

0.68 grams of nitrogen appears the best solution, as well as for rheological and physical properties (Figure 68 and Figure 70).

Skin distribution

As explained above, the high cooling rate near the walls leads to the formation of a layer of unfoamed skin. These layer were measured for the four cases by a software for image analysis. The measurements are shown in the following figures.
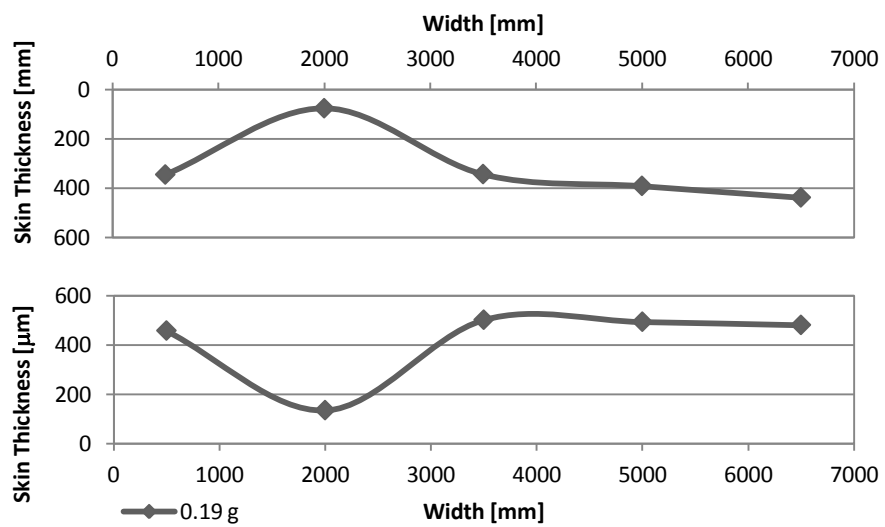
Figure 87. *Skin thickness of the sample of PS 678E with 0.19 g of gas.*
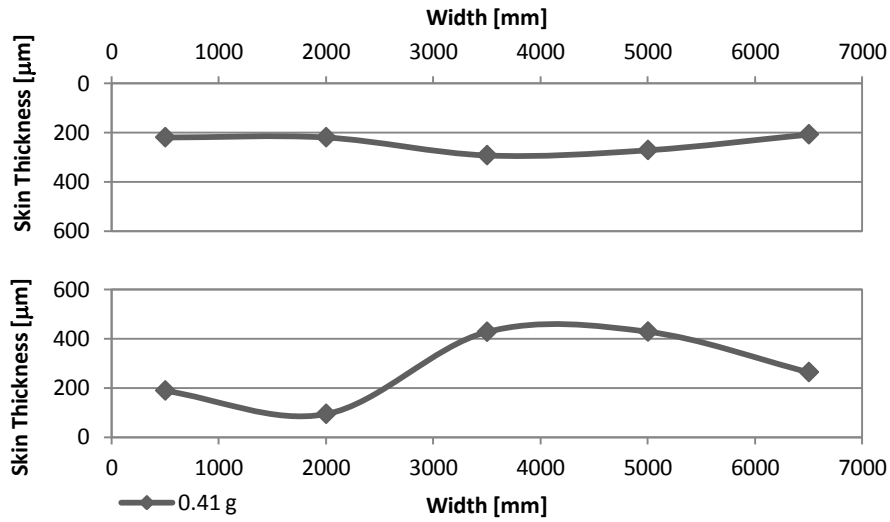
Figure 88. *Skin thickness of the sample of PS 678E with 0.41 g of gas.*
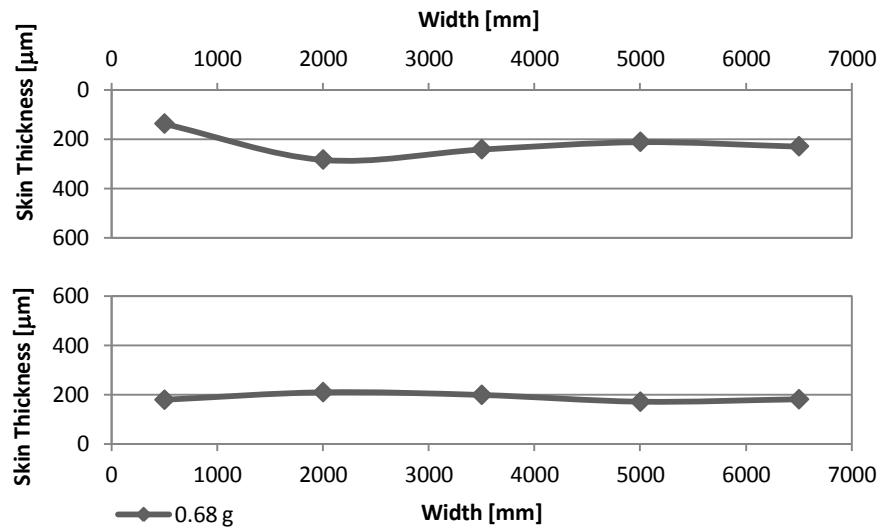
Figure 89. *Skin thickness of the sample of PS 678E with 0.68 g of gas.*
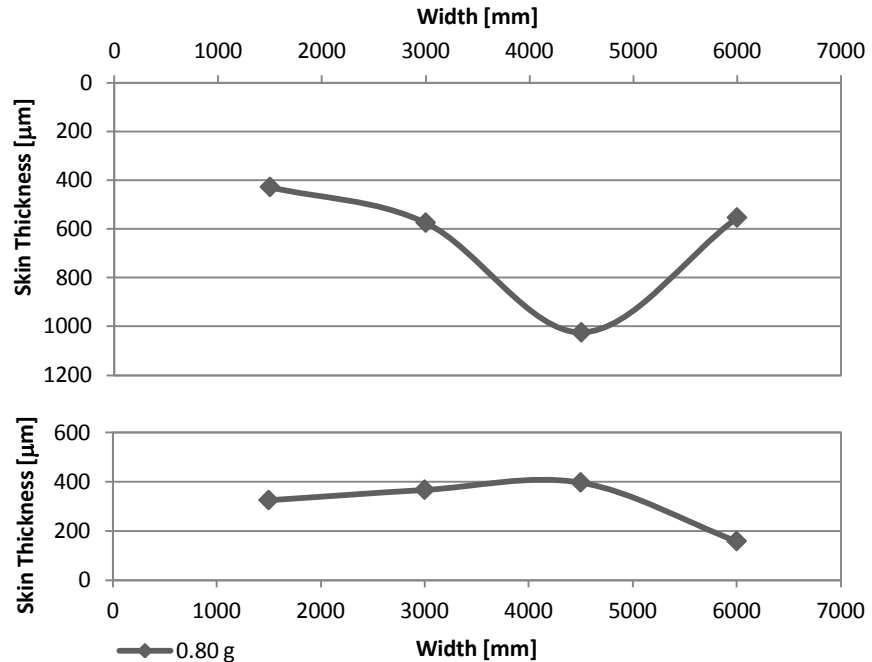
Figure 90. *Skin thickness of the sample of PS 678E with 0.80 g of gas.*

Also in this case the sample with 0.68 grams of nitrogen presents the best profiles. From the Figure 89, in fact, it is possible to observe that the thickness of the unfoamed skin is almost constant at 200 microns along the entire width of the sample (70 mm). From Figure 90, instead, it is possible to observe how the profile of skin thickness of the sample with 0.80 grams of gas is different in the two sides and is not homogeneous along the width.

Tomography

Samples molded with the two best conditions (solutions with 0.68 and 0.80 grams of nitrogen into polystyrene) were analyzed by tomography, procedure that utilizes computer-processed X-rays to produce tomographic images or slices of specific part, with the help of the Polymer Centre of Faculty of Technology of Thomas Bata University in Zlin (CZ). Tomography was carried out by means of a SkyScan1174 compact micro-CT. In Figure 91 and Figure 92 it is possible to observe two series of images obtained from tomography of samples with 0.68 and 0.80 grams of nitrogen respectively. The images are scanned at a distance of 3 mm from each other.
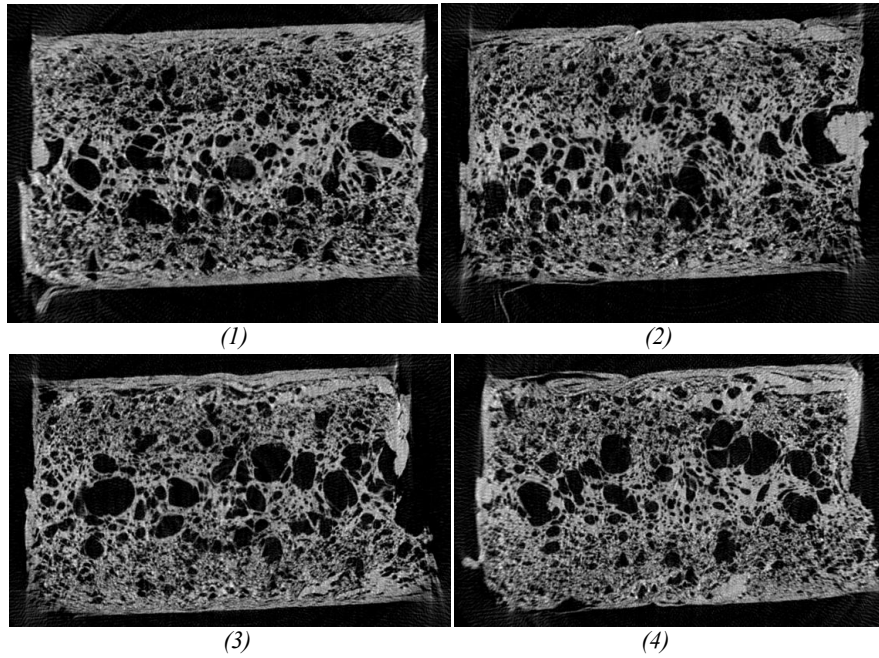
Figure 91. *Thin slices of the sample with 0.68 g of N_2 taken every 3 mm from a length of 38 mm to a length of 50 mm (direction of flow perpendicular to the section).*

In Figure 91 it is possible to observe a cellular structure with a thin layer of compact skin and foamed core with cells of increasing sizes as it move toward the center of the sample. In Figure 92 the skin is thicker than in the previous case and there are more large cells in the center of the sample, as already seen previously in cell distribution.

(3)   *(4)*
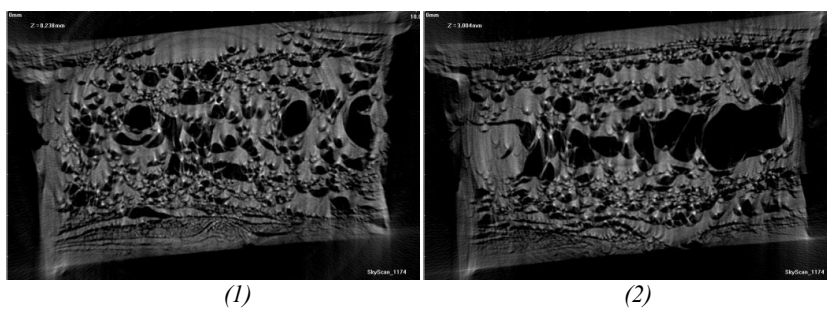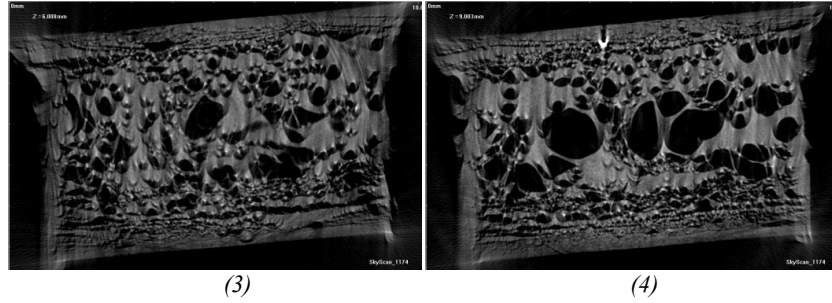
Figure 92. *Thin slices of the sample with 0.80 g of N_2 taken every 3 mm from a length of 38 mm to a length of 50 mm (direction of flow perpendicular to the section).*

Chapter 6
Poly(lactic) acid 2002D

Foam injection molding experiments were conducted also on a biodegradable polymer, polylactic acid (PLA). The utilization of the foam injection molding process, in fact, seems the ideal solution to problems of moldability of biodegradable polymers caused by their high viscosity and operative condition very close to those of degradation.

Two different grades of PLA were used for subsequent experiments. In this paragraph, the experimental part performed with PLA 2002D is explained.

6.1 Experimental conditions

In Table 25 the experimental conditions utilized in this part of the work are reported. Preliminary tests at different injection temperatures were carried out and, based on the results obtained, it was chosen to work at 220 °C.

Table 25. *Experimental conditions.*

Injection Temperature [°C]	220
Gas Pressure [bar]	0, 60, 80
Injection Flow Rate [ccm/s]	4, 8, 15, 33, 65, 75
Rotation speed [rpm]	200
Shot volume [ccm]	32
Back pressure [bar]	2
Mold Temperature [°C]	30

In this part, the volume of dosage was increased from 30 ccm, volume utilized in the experiments with polystyrene, to 32 ccm, in order to obtain the complete filling of the cavity after foaming of gas/polymer solution inside of it. The other operative conditions were unchanged compared to the case of

polystyrene. The polymer was loaded with two different amounts of gas corresponding to different gas pressures, as shown in Figure 93.
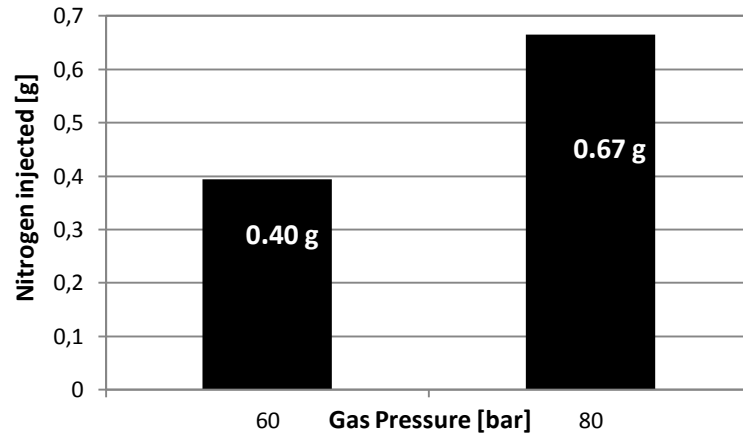
Figure 93. *Amount of nitrogen injected in PLA 2002D at different gas pressures (T=220°C).*

The cavity utilized in this part of the work has a thickness of 5 mm, as shown in Figure 94.
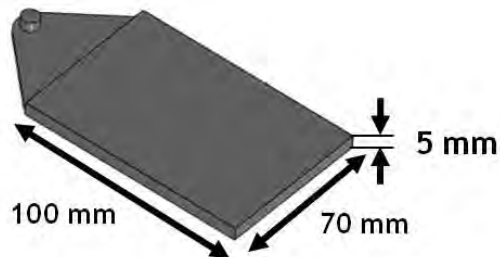
Figure 94. *Geometry of the mold cavity utilized in experiments with PLA 2002D (T=220°C).*

6.2 Rheological measurements

The slit allows to monitor the rheological parameters by means of pressure transducers connected to a software. In Table 26 the pressure values measured inside of the slit during the experiments are reported.

Table 26. *Pressure values measured by means of pressure transducers for PLA 2002D foamed by Nitrogen.*

Injection Flow Rate [ccm/s]	Without gas		0.40 g N$_2$		0.67 g N$_2$	
	P_1 [bar]	P_2 [bar]	P_1 [bar]	P_2 [bar]	P_1 [bar]	P_2 [bar]
4	206.6	182.9	183.1	158.5	98.0	85.1
7	343.01	286.2	272.0	219.3	147.5	124.8
14	452.4	372.9	357.4	290.6	232.9	191.2
30	645.2	530.1	417.6	342.0	313.3	252.1
61	-	-	526.9	422.2	430.7	348.7
75	-	-	595.2	484.7	426.7	333.3

The evolution of the differences between two subsequent transducers, *ΔP*, by changing the injection flow rate are reported in Figure 95.
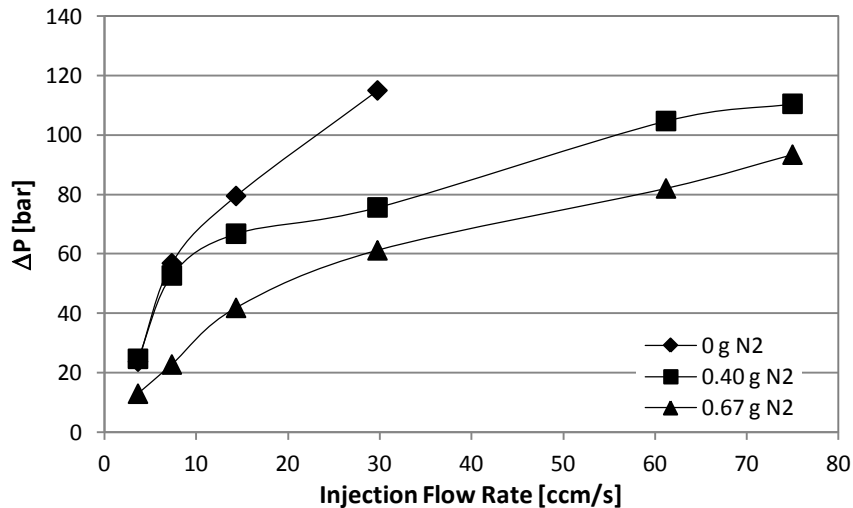
Figure 95. *Pressure drops at different values of injection flow rate for PLA 2002D with different amounts of nitrogen (second slit; T=220°C).*

With the increase of the amount of gas injected inside of the screw, there is a reduction of the pressure drops (Figure 95). The same behavior occurs in the case of viscosity, as it is shown in Figure 96.
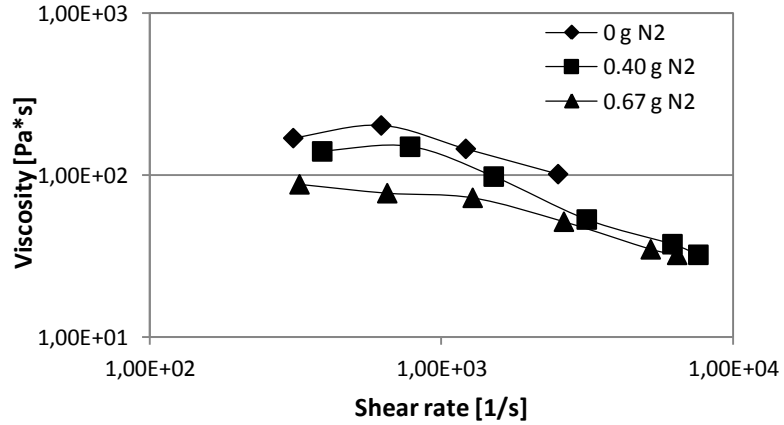
Figure 96. *PLA 2002D: evolution of viscosity at different values of shear rate (second slit;T=220°C)*

So, first experiments of injection molding of PLA with nitrogen as blowing agents showed that the solution gas/polymer with a greater amount of gas (0.67 g) at equal grams of polymer has values of viscosity lower than those of the unfoamed polymer.

6.3 Solubility

The solubility, amount of nitrogen on amount of polymers in grams, was evaluated in order to quantify the amount of gas dissolved in the polymer in the various phases of the injection process. So, the values obtained during the experiments were compared with experimental solubility data reported in literature [100].
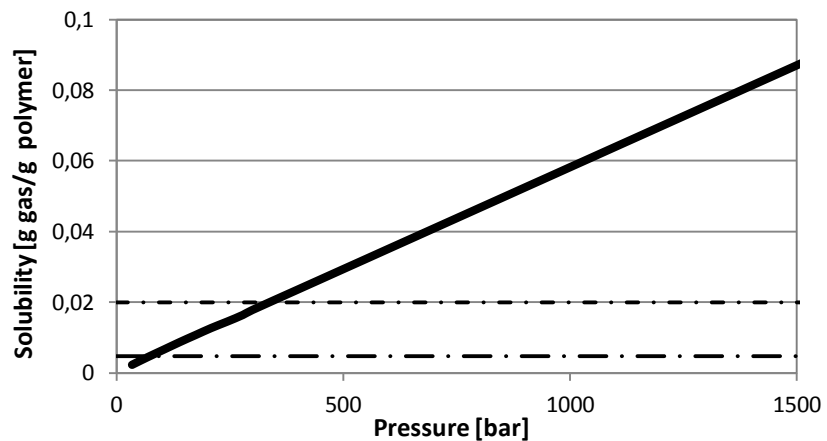
Figure **97** shows the curve of amount of nitrogen inside of PLA 2002D at different pressure of the system.
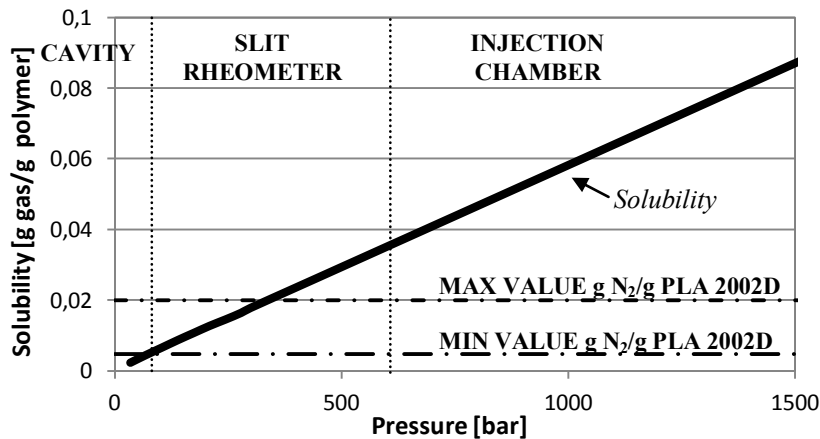
Figure 97. *Solubility of nitrogen inside of PLA 2002D.*

In this figure the maximum and minimum values of gas into the polymer, reached during all the experiments, are reported and the pressure ranges at every stage of the injection process (injection chamber, slit and cavity) are also indicated. The higher pressure is reached in the injection chamber, where the gas is completely dissolved in the polymer melt. When the gas/polymer mixture is injected into the cavity, there is a drastic reduction in pressure that allows the expansion of the polymer. In case of nitrogen and PLA 2002D, it can be seen that a partial demixing is possible already inside of the rheological slit, where very low pressures are established. So, for high amounts of gas at constant polymer loaded and high flow rates of injection, it has an amount of nitrogen which may exceed the limit of the saturation curve and induce a foaming already during the injection stage. This phenomenon affects negatively the final morphology of the part.

6.4 Density measurements

All foamed samples were weighed and measured in order to compare them with the ones molded without gas at the same experimental conditions. Figure 98 shows the length of the samples with increasing amount of gas at different injection flow rates.
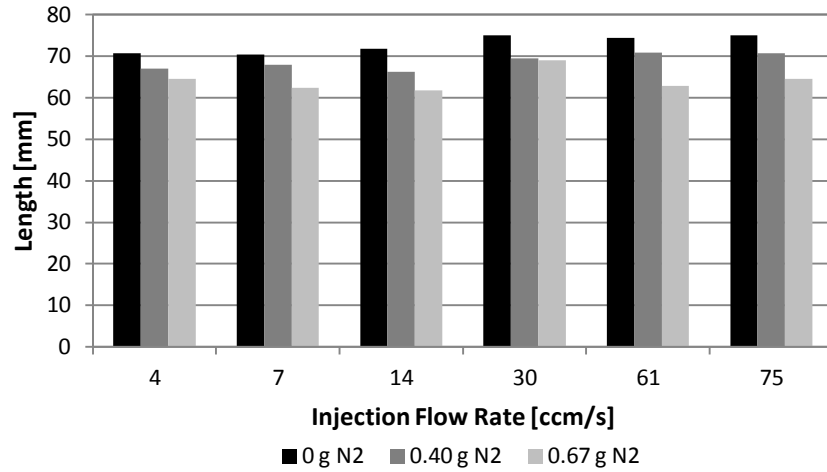
Figure 98. *Sample lengths at different values of injection flow rate for PLA 2002D with different amounts of nitrogen (T=220°C).*

The length of the samples decreases with the increasing of the grams of gas injected into the polymer. This abnormal behavior is probably due to the fact that the injection of gas causes the retreat of the screw, which, therefore, loads a smaller quantity of material. The lengths of the samples are almost costant with the injection flow rate.

Density measurements allow to calculate the reduction in density with respect to the unfoamed samples. As it is possible to observe in Figure 99, at low injection flow rate there is a small reduction in density, that increases slightly at higher flow rate (not more than 20.41%). Furthermore, another anomalous behavior is that a greater amount of gas causes a lower reduction in density.
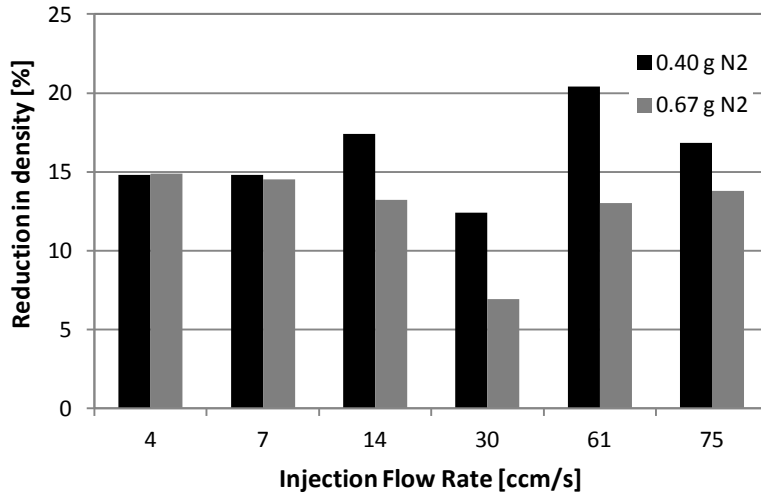
Figure 99. *Reduction in density with respect to the unfoamed samples at different values of injection flow rate for PLA 2002D with different amounts of nitrogen (T=220°C).*

The values of the reduction in density are reported in Table 27.

Table 27. *Values of reduction in density at different values of injection flow rate for different amount of gas.*

Injection Flow Rate [ccm/s]	0.40 g Nitrogen	0.67 g Nitrogen
	RIDUCTION IN DENSITY [%]	
4	14.79	14.88
7	14.80	14.52
14	17.41	13.22
30	12.40	6.94
61	20.41	13.03
75	16.84	13.77

All the abnormal behaviors found in pressure profiles, solubility, length and density and the problems of molding have led to the decision to change the grade of the PLA and to use a grade more suitable for injection molding.

Chapter 7
Poly(lactic) acid 4032D

After a series of experiments with the grade 2002D of the biodegradable polymer PLA foamed with nitrogen, which led to unstable behaviors and difficulties in moldability and foamability, it was decided to change with PLA 4032D, a commercial grade of poly(lactic) acid with a lower content of D-enantiomers. In fact, the amount of D-isomer present in the L-PLA polymer changes the properties significantly in terms of melting temperature, crystallization rate and therefore processibility and properties of foams. For example, the higher D-isomer content in the polymer then the lower the crystallization rate and lower the melting point [2].

7.1 Rheological part

7.1.1 Experimental conditions

Table 28 shows the experimental conditions utilized in this part of the work. Also in the case of PLA 4032D, preliminary tests at different injection temperatures were carried out before choosing the effective molding conditions. In particular, experiments at different temperatures showed that the ideal injection temperature for the foam injection molding of PLA with nitrogen is 200 °C. The other conditions (Rotation speed, volume of dosage back pressure and mold temperature) are the same as the case of the PLA 2002D. Also in this case, different flow rates were imposed to the injection molding machine. Differently to the case of polystyrene, with the PLA it was not possible to reach high injection flow rates because of the high values of pressure needed during the injection phase, values higher than the limit that the machine can guarantee.

Table 28. *Experimental conditions.*

Injection Temperature [°C]	**200**
Gas Pressure [bar]	0, 60, 80, 100
Injection Flow Rate [ccm/s]	3, 7, 13, 27, 34, 41
Rotation speed [rpm]	200
Shot volume [ccm]	32
Back pressure [bar]	2
Mold Temperature [°C]	30

The experiments were made with the thinner cavity (thickness 5 mm) as shown in Figure 100.
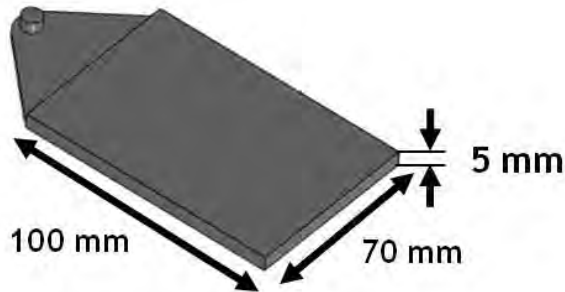
Figure 100. *Geometry of the mold cavity utilized for experiments with PLA 4032D (T=200°C).*

The volumetric pump allows to impose the injection pressure of nitrogen, whence it is possible to calculate the corresponding moles injected (Figure 101).
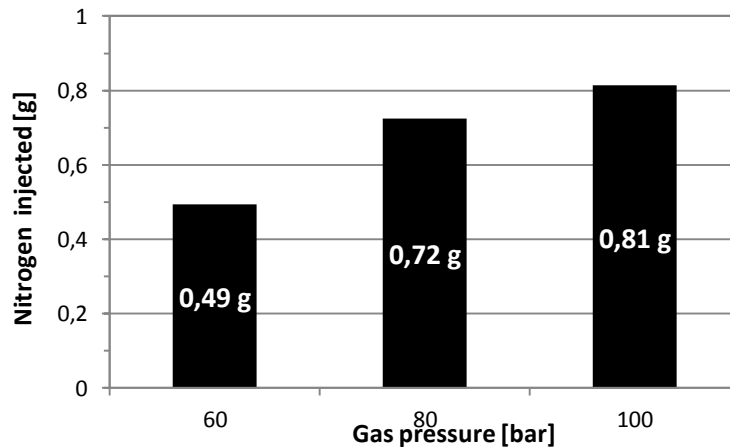
Figure 101. *Amount of nitrogen injected in PLA 4032D (T=200°C).*

7.1.2 Solubility

In the injection phase, very high pressures are established. As the material moves through the slit the pressure decrease. However, only within the cavity are established pressures so low as to allow the expansion of the gas and thus the foaming of the material. The minimum and maximum amount of nitrogen obtained in this case was compared with the solubility curve of nitrogen inside the PLA present in literature (black curve) at the different pressures established during the different phases of the process (Figure 102).
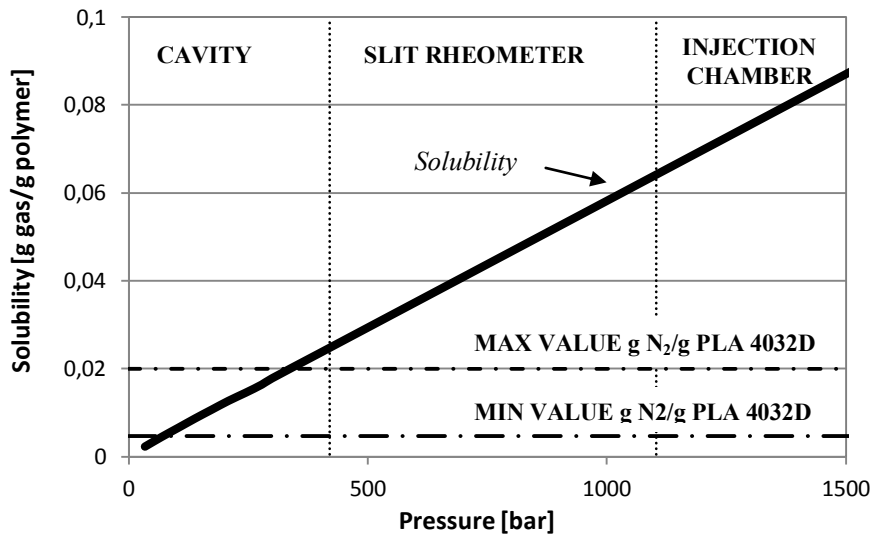
Figure 102. *Solubility of nitrogen inside of PLA 4032D (T=200°C).*

The graph shows that, just as expected, the amount of nitrogen is above the solubility curve only at low pressures established into the cavity. So, the foaming takes place only in the cavity and not before.

7.1.3 Analysis with Cross Model

One of the difficulties of the injection molding process of biodegradable polymers lies in the fact that they are easily subject to thermo-mechanical degradation during the process because of their chemical nature. The comparison between the experimental data obtained in absence of gas and the rheological measurements of the virgin material described by the Cross-Vogel Model, is not optimal, probably because of degradation induced by screw rotation and high temperature. This is confirmed by the fact that, if the same experimental data are compared with rheological data obtained with molded material, which then underwent the same degradation during the

117

Chapter 7

process, this comparison is good. Figure 103 and Figure 104 show the comparison of the experimental data with the Cross Model obtained from virgin material and the rheological data obtained from molded material respectively.
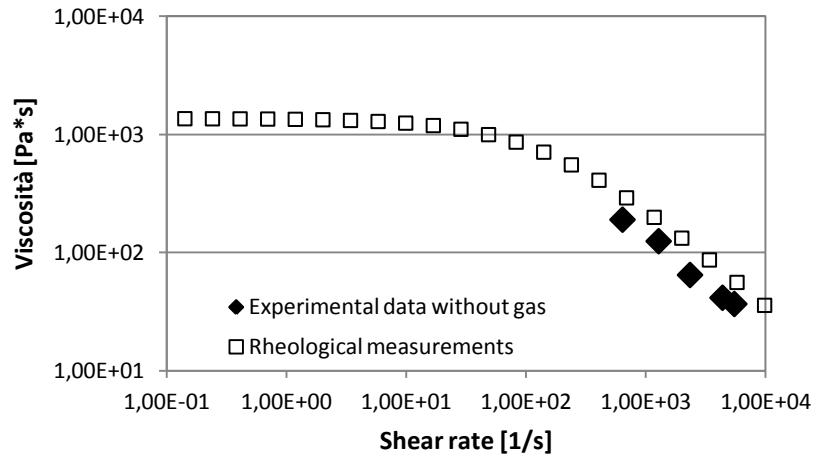
Figure 103. *Comparison of the experimental data of PLA 4032D without gas with the Model (second slit; T=200°C).*
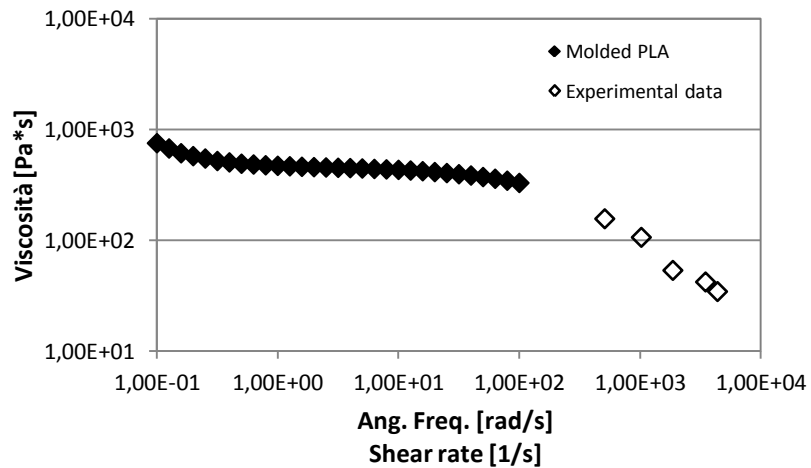
Figure 104. *Comparison of the experimental data of PLA 4032D without gas with the rheological data of the PLA 4032D molded (second slit; T=200°C).*

7.1.4 Rheological measurements

From the acquisitions of the pressure values in different positions into the rheological slit, it is possible to obtain the reduction of pressure both in the

118

case of pure PLA and in the presence of different amounts of gas. In Table 29 the pressure values measured inside of the slit can be observed.

Table 29. *Pressure values measured by means of pressure transducers for PLA 4032D foamed by Nitrogen (T=200°C).*

Injection Flow Rate [ccm/s]	Pure PLA		0.49 g N$_2$		0.72 g N$_2$		0.81 g N$_2$	
	P1 [bar]	*P2 [bar]*	*P1 [bar]*	*P2 [bar]*	*P1 [bar]*	*P2 [bar]*	*P1 [bar]*	*P2 [bar]*
3	492,3	456,4	560,4	527,5	511,5	482,7	461,1	438,4
7	583,9	534,8	918,7	887,9	805,1	772,8	620,8	586,9
13	900,2	855,1	895,7	858,8	851,2	810,7	790,2	754,6
27	926,4	860,2	1018,2	963,9	767,5	721,7	835,8	793,2
34	1100,3	1032,3	1091,7	1033,1	1079,0	1026,7	-	-
41	-	-	1080,2	1020,3	1114,5	1060,9	-	-

The pressure drops ΔP inside the slit at different injection flow rate are shown in Figure 105.
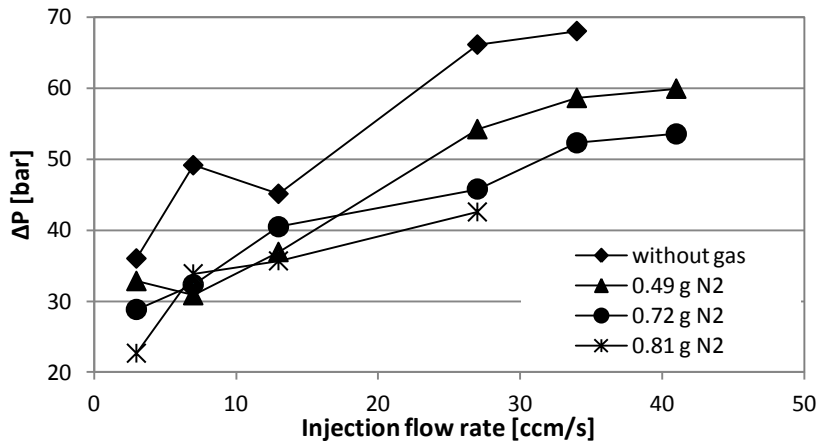
Figure 105. *Pressure drops at different values of injection flow rate for PLA 4032D with different amounts of nitrogen (second slit; T=200°C).*

The pressure drops increase with the injection flow rate. The curve of pure PLA shows values of ΔP higher than the curves of PLA with nitrogen, that has pressure drops always lower with increasing the amount of gas in solution.

Comparing the curve of viscosity versus shear rate obtained with pure PLA with the same curves obtained with gas/polymer solutions in different percentages, it can possible observe a great reduction in viscosity in the case of the solution (Figure 106).
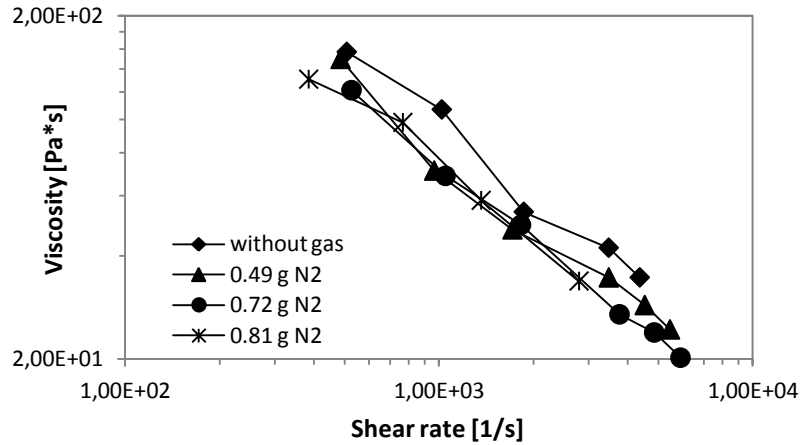
Figure 106. *Evolution of viscosity at different values of shear rate for PLA 4032D with different amounts of nitrogen (second slit; T=200°C).*

This reduction is due to the effect of the blowing agent in the polymer and allows to reach values of viscosity which, in the absence of gas, would be obtained by increasing considerably the injection temperature. It is worth underlining that the increase of the process temperature is very difficult in the case of biodegradable polymers due to their chemical nature which makes them easily prone to degradation thermo-mechanical and therefore difficult to be molded.

7.1.5 Density measurements

All the molded samples were analyzed in order to evaluate the effect of the blowing agent on weight and density. In fact, the expansion of the physical blowing agent within the polymer melt involves use of a smaller quantity of polymer for obtaining a part with the same sizes and lower density of the same part molded in absence of blowing agent.

Figure 107 shows the comparison between the lengths of the samples of pure PLA and the lengths of the samples with the minimum and maximum amount of gas within the PLA.
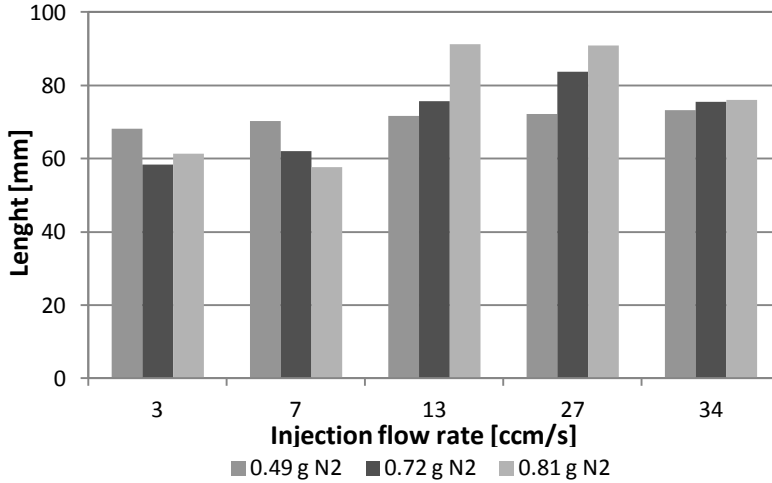
Figure 107. *Length of the samples of PLA 4032D molded with different amounts of gas (T=200°C).*

It is possible to observe that, at high injection flow rates, the length of the samples molded with gas is greater than that of the samples of pure PLA at equal amount of material injected and molding conditions. From the geometry and the weight of each samples it is possible to evaluate the average density of them, and therefore the reduction in density compared to the unfoamed samples.

In Figure 108 the values of reduction in density at different injection flow rates for the minimum and the maximum quantity of gas injected are reported.
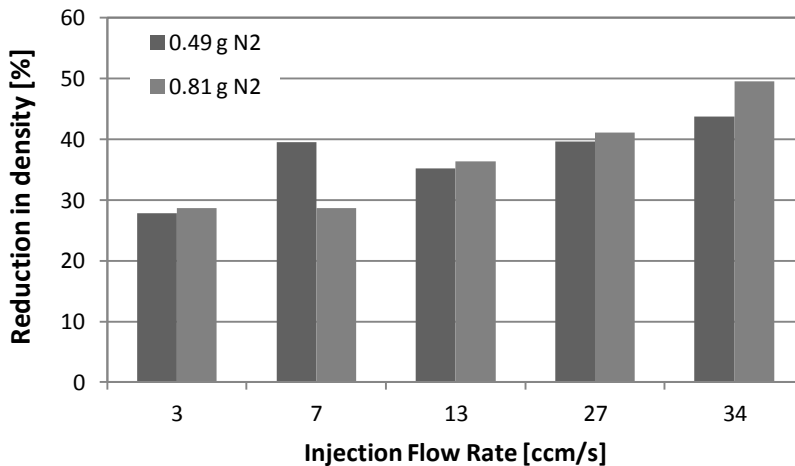
Figure 108. *Reduction in density with respect to the unfoamed samples of PLA 4032D at different values of injection flow rate and different amount of gas.*

121

Chapter 7

Table 30 shows the values of reduction in density corresponding to the graph in Figure 108.

Table 30. *Values of reduction in density at different values of injection flow rate for different amount of gas.*

Injection Flow Rate [ccm/s]	0.49 g N_2	0.72 g N_2	0.81 g N_2
	RIDUCTION IN DENSITY [%]		
3	27,81	23,30	28,63
7	39,54	30,10	28,64
13	35,21	35,71	36,39
27	39,66	24,04	41,09
34	43,80	40,31	49,57

In Figure 108 it is possible to observe that the reduction in density increases with the increasing of the injection flow rate, reaching a maximum reduction in density of 49.6%.

7.2 Mechanical properties

Currently, most studies on microcellular PLA are centered on understanding the mechanisms of bubble nucleation, growth, and stabilization. The relationships between morphological and mechanical properties of PLA foams are not well established because their mechanical properties have not been extensively characterized [101]. In the next paragraphs, mechanical properties of the PLA samples molded with and without gas are shown. The tests were carried out using a specimen cut in half of its length, as shown in Figure 109.
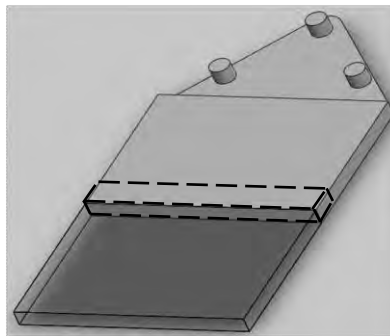
Figure 109. *Position of the specimen on which the mechanical tests were carried out.*

7.2.1 Flexural test

Flexural tests were made on samples of pure PLA, in order to compare them with the results obtained with the foamed ones. Figure 110 shows typical stress/strain curves obtained on a samples of pure PLA and a foamed sample molded in the same experimental conditions. It is possible to observe that the specimen undergo to yield before breaking.
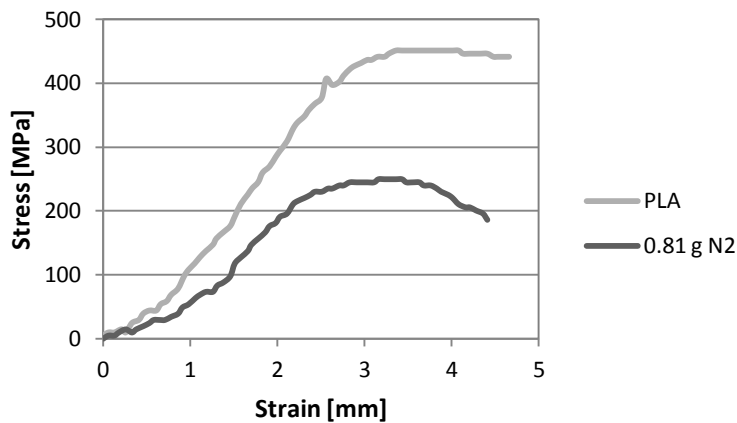
Figure 110. *Stress vs strain curve of an unfoamed sample of PLA 4032D and of a sample of PLA 4032D foamed with 0.81 grams of nitrogen in PLA with an injection flow rate of 13 ccm/s.*

The curve of pure PLA shows a larger slope with respect to the curve of the foamed PLA, and therefore a larger modulus of elasticity. In fact, foamed samples show a modulus of elasticity lower than that of the pure PLA and increasingly lower with increasing amount of gas in gas/polymer solution, as it is possible to observe in Figure 111, where the modulus is multiplied with the ratio between the density of the polymer without gas and the density of a foamed sample, in order to take into account the reduction in density of foamed samples respect to unfoamed ones in the evaluation of modulus.
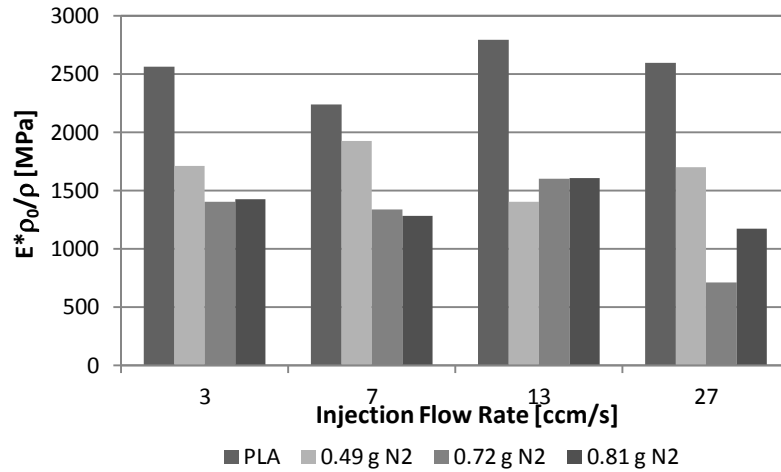
Figure 111. *Moduli of elasticity at different injection flow rates for PLA 4032D with different amounts of nitrogen injected (T=200°C).*

In Figure 112 the reduction in modulus (equation 58) of the foamed samples compared to that of pure PLA was quantified.

$$\frac{\Delta E}{E} = \frac{E_0 - E_f}{E_0} * 100 \tag{58}$$

It is possible to observe that, increasing the amount of gas in solution, there is a progressive increase of the reduction in modulus, which also increases slightly with the injection flow rate.
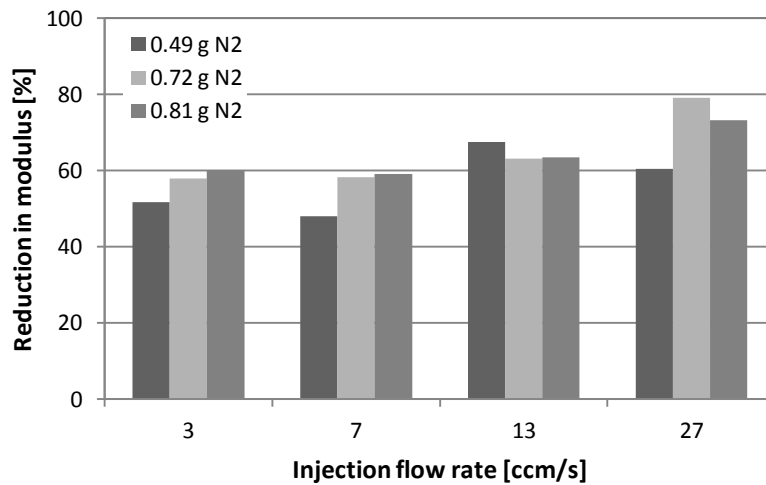
Figure 112. *Reduction in Modulus compared to the unfoamed samples of PLA 4032D at different injection flow rates (T=200°C).*

7.2.2 Impact Resistance

From the energy absorbed by breaking and the section of the test specimen it is possible to calculate the impact resistance of a foamed part.
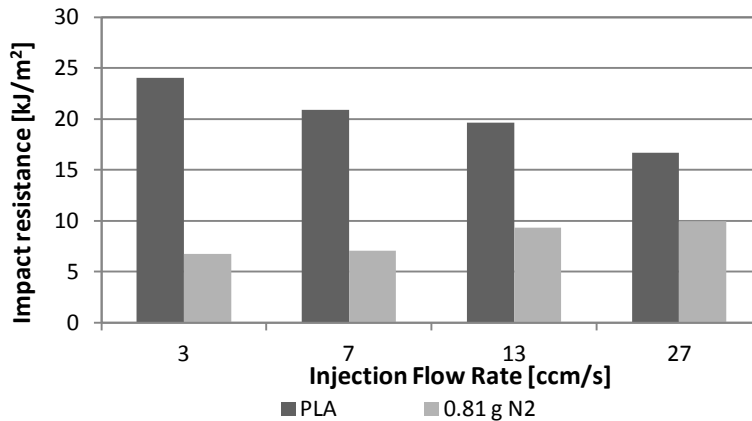
Figure 113. *Impact resistance of PLA 4032D at different injection flow rates (T=200°C).*

In Figure 113 it is observed that the impact resistance of the PLA foamed with the lowest amount of nitrogen is much lower than that of the sample of pure PLA. With the increase of the injection flow rate, this difference slightly decreases.

7.2.3 Tensile properties

Also in the case of the results of tensile tests, the modulus is multiplied times the ratio between the density of the polymer without gas and the density of a foamed sample, in order to take into account the reduction in density in the evaluation of modulus. In Figure 114 true modulus of the unfoamed samples and the foamed ones at different injection flow rate is reported. Modulus decrease on increasing injection flow rate.
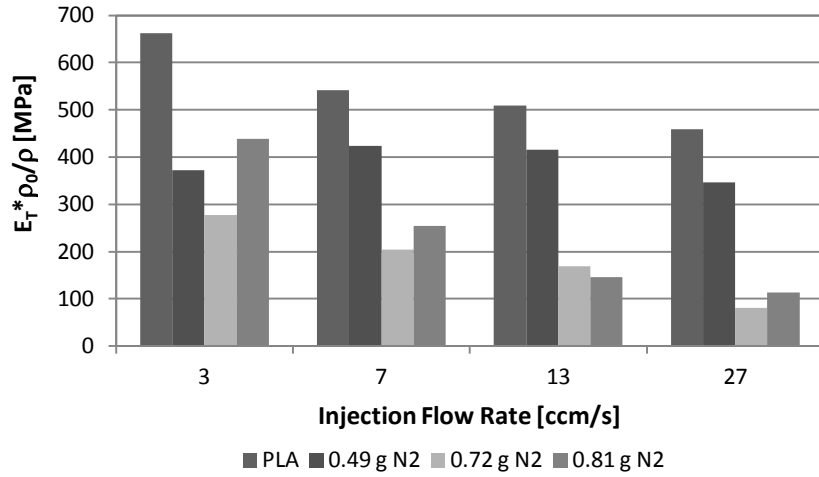
Figure 114. *True modulus of PLA 4032D with different amounts of nitrogen at different injection flow rates (T=200°C).*

The modulus of elasticity of samples molded with the lowest amount of gas in the PLA (0.49 grams of nitrogen) is slightly lower than modulus of the samples of pure PLA. Increasing the percentage of nitrogen in the gas/polymer solution, the reduction in modulus compared to the unfoamed samples strongly increases, as it is possible to observe in Figure 115.
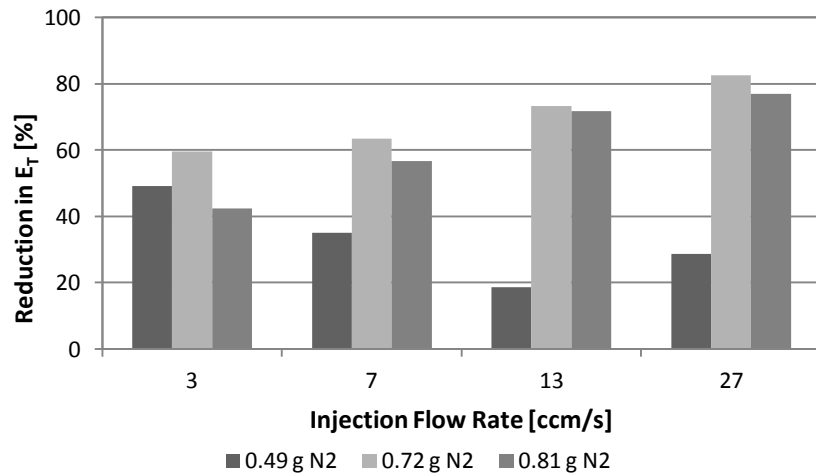
Figure 115. *Reduction in true modulus of PLA 4032D with different amounts of nitrogen at different injection flow rates (T=200°C).*
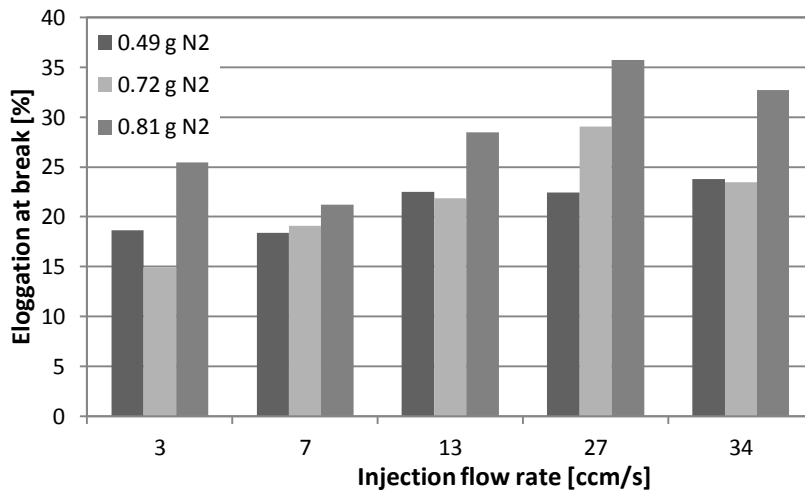
Figure 116. *Elongation at break of PLA 4032D with different amounts of nitrogen at different injection flow rates (T=200°C).*

The samples with 0.81 g N_2 presents always the highest values of elongation at break to each value of injection flow rate used. In addition, at all the percentage of gas injected, samples molded at higher injection flow rate (13 and 27 cm^3/s), which present the largest values of reduction in modulus compared to the unfoamed samples, have a greater elongation at break.

In conclusion, higher values of modulus were obtained from flexural tests. In all cases the modulus of elasticity decrease with the increase of the amount of gas in solution and with the increasing of the injection flow rate. However, at low injection flow rate there is greater elongation at break.

7.3 Morphology

Samples of foamed PLA obtained by foam injection molding were cut in order to evaluate the morphology in the different experimental conditions analyzed. Figure 117 and Figure 118 show micrographs of foamed samples molded at different injection flow rates and 0.49 and 0.81 grams of nitrogen into the PLA respectively. Micrographs show a better foaming on increasing the injection flow rate, but at 34 ccm/s, a change of this trend can be observed. Moreover, from the comparison between Figure 117 and Figure 118 it is possible to observe that, at the same injection flow rate, the samples molded with a greater amount of gas are more foamed than those molded with the lowest amount of gas.

3 ccm/s

7 ccm/s

13 ccm/s

27 ccm/s

34 ccm/s
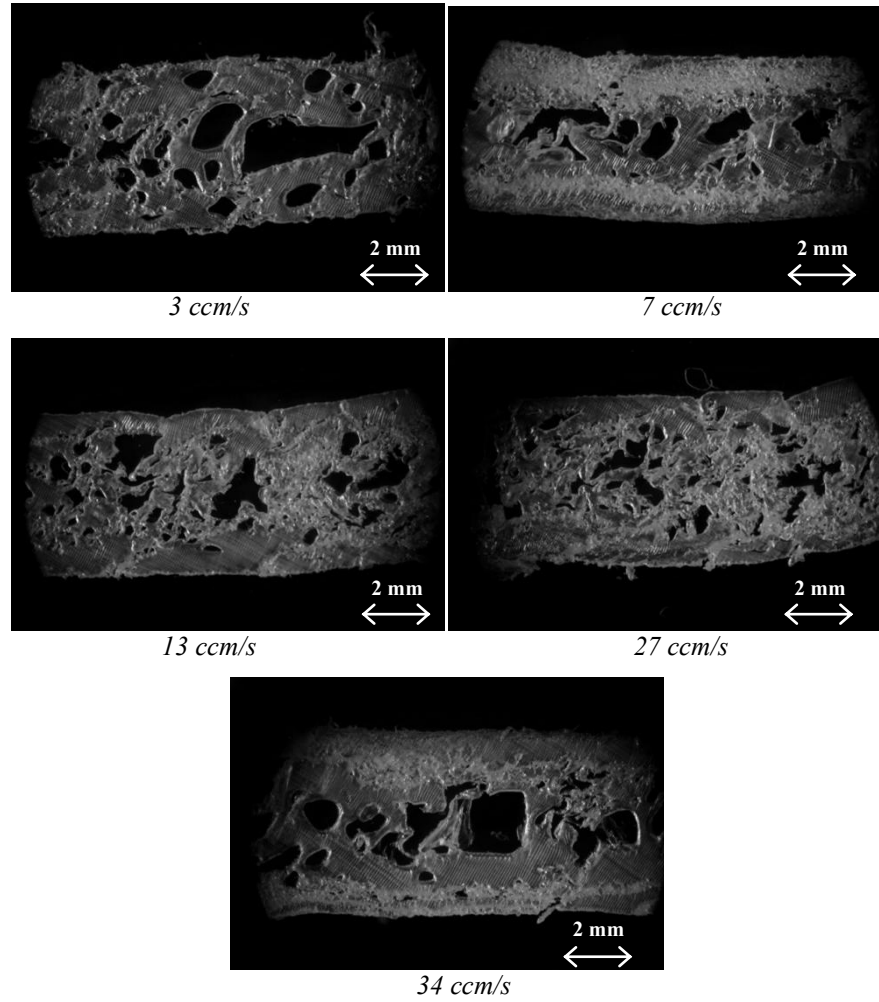
Figure 117. *Foamed samples of PLA 4032D molded at 200°C with 0.49 g of Nitrogen at different injection flow rates.*

3 ccm/s

7 ccm/s

13 ccm/s

27 ccm/s

34 ccm/s
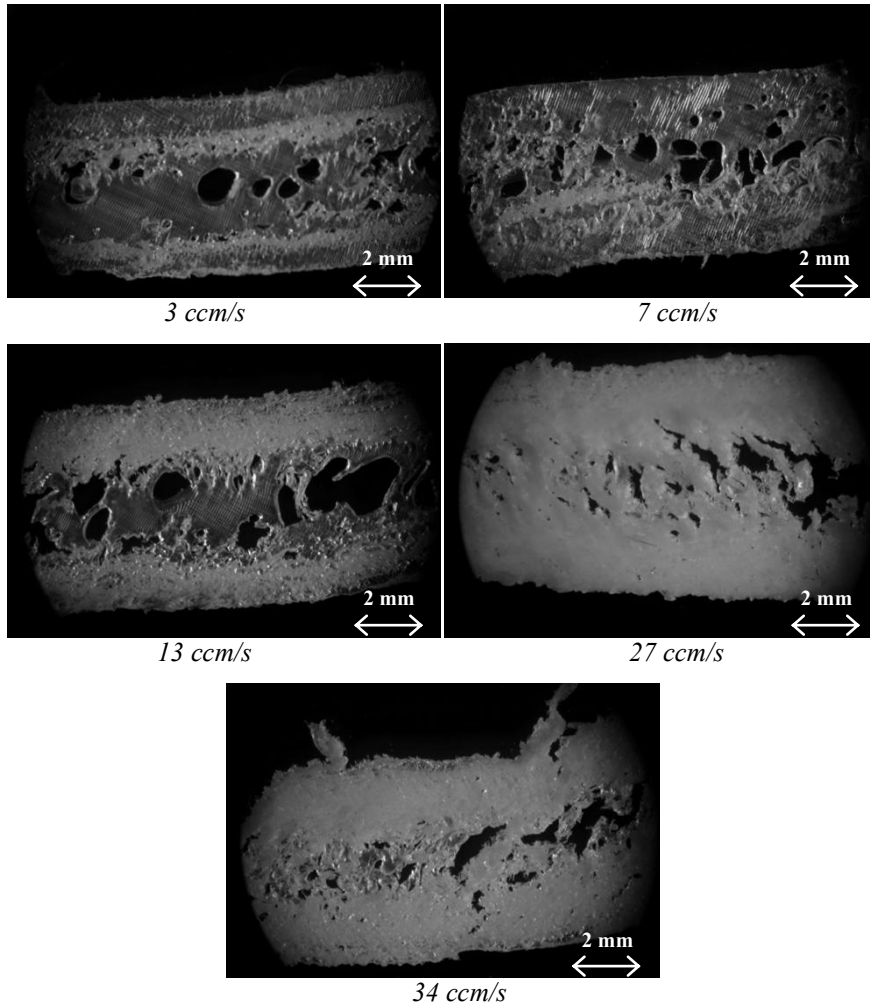
Figure 118. *Foamed samples of PLA 4032D molded at 200°C with 0.81 g of Nitrogen at different injection flow rates.*

Figure 119 and Figure 120 show the percentage of voids due to cells with radius included in defined ranges for samples of PLA 4032D at two different amounts of gas injected. It is possible to observe that, for low amount of nitrogen, the distribution of the cell sizes is wider than that of the samples molded with high amount of gas.
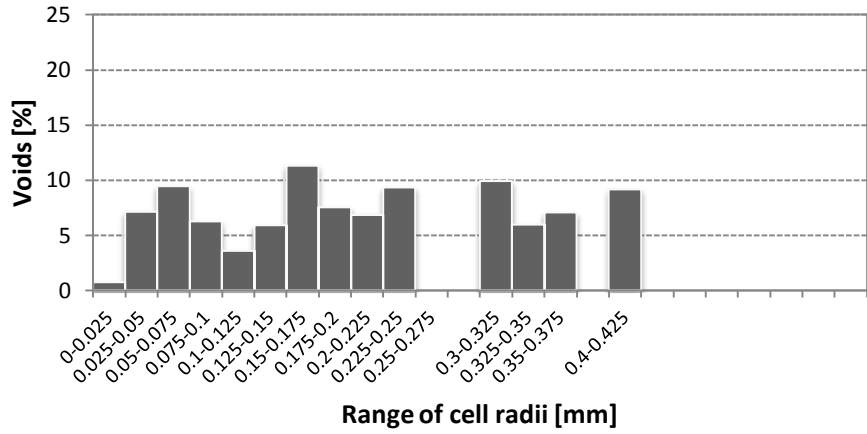
Figure 119. *Percentage of void due to cells with radius included in defined ranges for samples of PLA 4032D with 0.49 g of nitrogen into the PLA.*
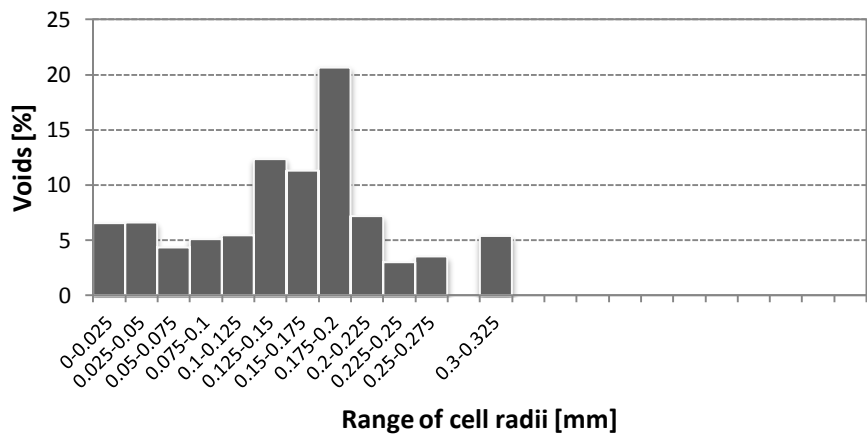
Figure 120. *Percentage of void due to cells with radius included in defined ranges for samples of PLA 4032D with 0.81g of nitrogen into the PLA.*

7.4 Cristallinity

Figure 121 and Figure 122 show the melting at 10 °C/min of skin (0-200 μm from the wall of the sample) and core of the samples obtained by foam injection molding without gas and with 0.81 grams of nitrogen respectively, by means of Differential Scanning Calorimetry.
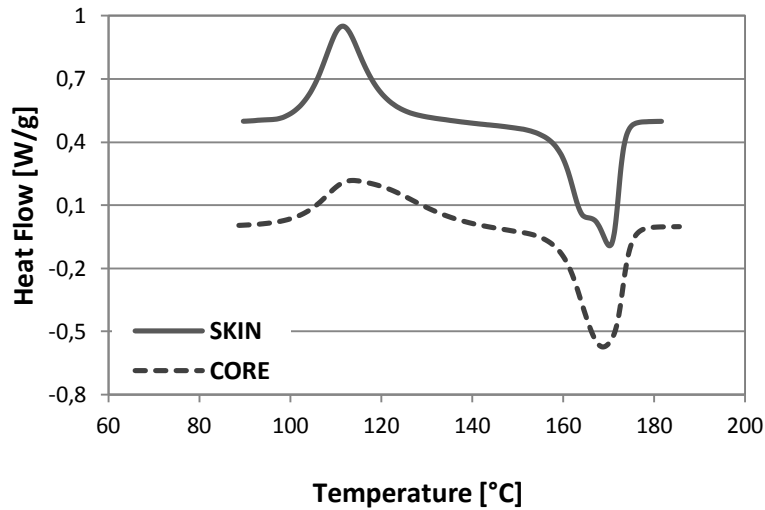
Figure 121. *Differential Scanning Calorimetry: melting at 10°C/min of skin and core of unfoamed samples of PLA 4032D (200°C).*
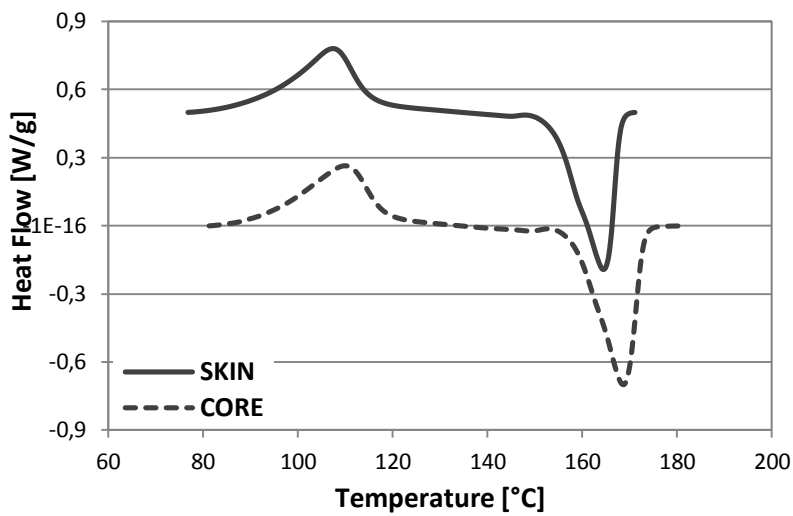
Figure 122. *Differential Scanning Calorimetry: melting at 10°C/min of skin and core of foamed samples with 0.81 g N_2 injected in PLA 4032D (200°C).*

Results of the study of the effect of gas on the crystallinity show a higher cristallinity of the foamed core (12%) with respect to the compact skin (9%) and the unfoamed part (9% core and 6% skin). It is very important to specify that the maximum cristallinity for this PLA grade is 35%. This is an aspect of considerable importance for biodegradable polymers, for which the crystallinity has a marked effect on properties.

Chapter 7

7.5 Effect of back pressure on the dosage phase

Back pressure means the pressure imposed inside of the cylinder when the screw is returning back to prepare a new amount of material to be injected. It was observed that, applying to the injection molding machine different values of back pressure, different amount of gas/polymer solution is injected inside the mold cavity. In this part of the work, the effect of the back pressure in the dosage was studied. Several experiments were carried out for each back pressure. In particular, once fixed the length of dosage and the amount of gas injected, the back pressure applied at the screw during the dosage phase was changed in order to measure the variation in weight of the quantity of PLA/N_2 solution to be injected into the mold cavity. The values reported correspond to the back pressure in the hydraulic system. On the melt, the pressure is about 20 times larger.

In the batching phase, polymer is loaded and the gas is simultaneously injected inside the cylinder. After the batching phase, the injection begins while maintaining the nozzle closed for 5 seconds, in order to allow a perfect solubilization of the gas within the polymer under pressure. After 5 seconds the nozzle is opened and the solution is injected. In Figure 123 it is possible to observe the amount of the solution PLA-N_2 injected at the different back pressures. Through this graph it can be observe that, at higher values of back pressure, a larger quantity of PLA/N_2 solution is injected. So, since the amount of gas injected and the length of dosage is constant, it can be deduced that the increase of the back pressure applied to the screw during the dosage phase allows the loading of a larger amount of polymer during that phase. Then, the ratio between grams of gas and grams of polymer in these solutions is high at low values of back pressure and decreases with the increasing of it, as shown in Figure 123.
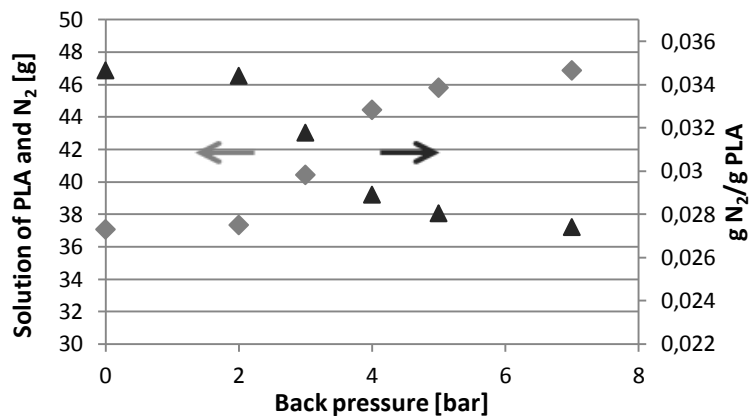
Figure 123. *Amount of N2/PLA 4032D solution injected at different back pressures (in hydraulic system) and variation of the respective ratio between the grams of gas and the grams of PLA.*

132

7.6 Results: monitoring of cavity pressure and temperature profiles

In the second part of the experimental work with the biodegradable polymer PLA 4032D, a different mold was utilized in order to monitor the pressure and temperature within the cavity during the filling phase.

This mold is equipped with four sensors, three in the cavity and one in the runner, to capture the real time temperature and pressure data during the filling and cooling stages.

The sprue tapered from a diameter of 7 mm (at mold side) to a diameter of 4,7 mm (at nozzle side) over a length of 80 mm. The runner had a diameter of 8 mm and was 68 mm long. The material was injected into a line gated rectangular cavity of 120 mm x 30 mm x 4 mm (cavity thickness). A gate with 0,5 mm of thickness and 6 mm of length was assembled in the mold, in order to have a maximum pressure drop in the cavity and to have only the foaming of the part (avoid the foaming of the sprue mold gate).

The molding machine and the mold were equipped with four piezoelectric transducers for pressure measurement, which were located along the flow course: one just before the gate, and three in the cavity at 15 mm, 60 mm and 105 mm from the gate. These positions will be referred to as P1, P2 P3 and P4, respectively. The transducers signals were acquired by a data acquisition system and stored in a desktop computer. A complete description of cavity geometry is expressed in the next Figure 124.
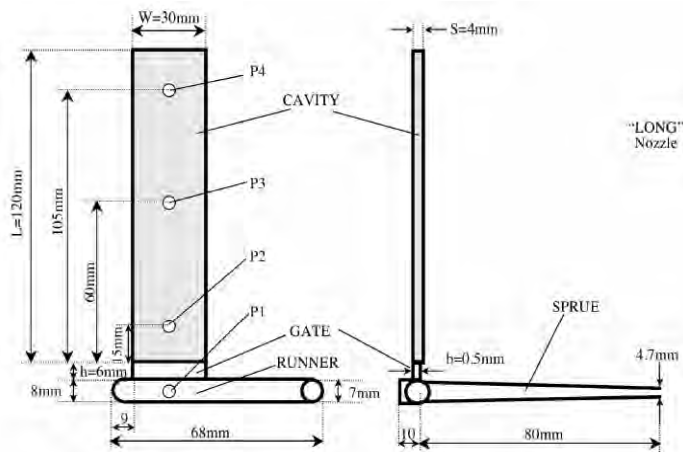
Figure 124. *Cavity geometry utilized for monitoring cavity pressure and temperature profiles with PLA 4032D.*

Chapter 7

7.6.1 Effect of back pressure

As it was stated previously, applying different values of back pressures to the screw during the batching phase, different amounts of material loaded in that phase are found. So, setting the gas pressure to the pump at 100 bar, that means setting the amount of gas to inject for each shot, values of back pressure in the range 2-5 bar (into the hydraulic system) were applied in order to observe the modifications in geometry and morphology of the final samples as well as pressure and temperature profiles into the cavity during the injection phase. Experimental conditions utilized for this set of tests are reported in Table 31.

Table 31. *Experimental conditions.*

Injection Temperature [°C]	**200**
Gas Pressure [bar]	0, 100
Injection Flow Rate [ccm/s]	15-25
Rotation speed [rpm]	200
Shot volume [ccm]	27
Back pressure [bar]	2-5
Mold Temperature [°C]	26

Once the amount of gas injected and the grams of polymer loaded are known, values of sorbed gas for each back pressure were calculated (Figure 125).
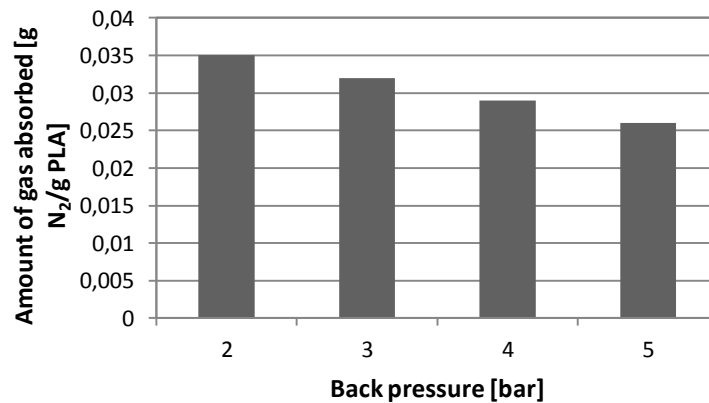
Figure 125. *Amount of gas absorbed corresponding to each back pressure applied during the dosage phase, with 1.2 g of nitrogen injected into molten PLA (T=200°C).*

These values were compared with the solubility curve in the literature and with the values of pressure that are established into the cavity in the four positions of the pressure transducers.

134

From the comparison between the amount of gas inside the gas/polymer solution at all the other back pressures and the solubility curve of literature, it was observed that at all the pressure values established in the cavity, our solution is above the solubility curve. So, in each position of the cavity, foaming of the solution should be obtained.

All samples were cut vertically in the middle and horizontally at three positions (1 cm from the gate, at half length and 1 cm from the end of the samples) in order to observe their morphology. In Figure 126, the images of the sample sections in the different position, the pressure and temperature profiles in the cavity and a table with the physical features of the samples at each back pressure are shown.

Back pressure 2 bar

Table 32. *Features of the sample of PLA 4032D molded at back pressure of 2 bar in the hydraulic system (T=200°C).*

Back pressure [bar]	Weight [g]	Length [mm]	Apparent density [g/ccm]	Reduction in density [%]
2	2.235	31.76	0.586	51.535

Figure 126. *Micrographs of the foamed samples of PLA 4032D molded with back pressure 2 bar (T=200°C).*

135

Chapter 7

The micrographs of the samples molded with a back pressure of 2 bar show a large layer of compact skin and an irregular foaming, with some unfoamed zones and other zones with large cavities and bubbles with different dimensions. Horizontally, it was possible to cut only at one centimeter from the gate, because of the size of the sample. In fact, during the experiments with a back pressures of 2 bar, the shot volume injected was just sufficient to fill one half of the cavity. Pressure and temperature profiles represented in Figure 127 and Figure 128 shown that during the injection phase, the flow of material reached only the first two sensors.
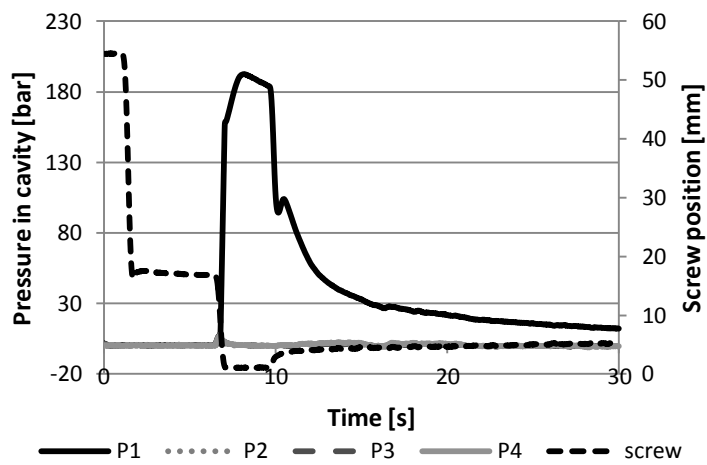
Figure 127. *Pressure profiles and screw position of a foamed sample of PLA 4032D molded at back pressure 2 bar (T=200°C).*
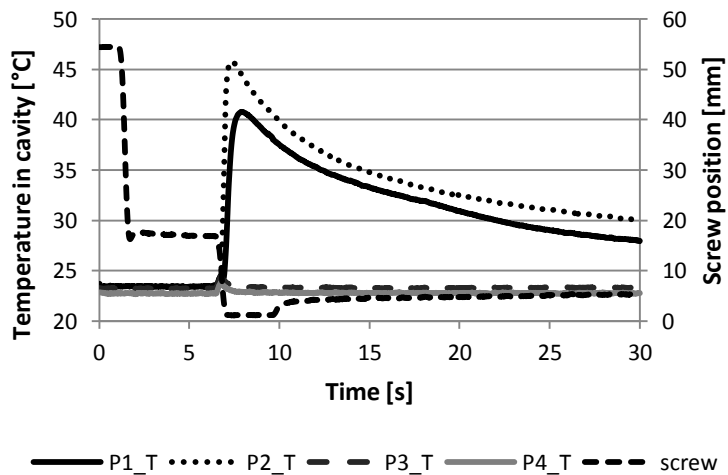
Figure 128. *Temperature profiles and screw position of a foamed sample of PLA 4032D molded at back pressure 2 bar (T=200°C).*

136

The line of the screw position shows a first phase of injection, a stage of compression of 5 seconds, in which there is the injection while the nozzle is closed, and a second phase of injection, when the nozzle is opened and the solution is injected into the cavity. During this phase, the pressure of the first sensor, positioned on the runner, raises and then drops when the cooling phase starts. The runner is connected to the gate, that separates it from the cavity. The very low thickness of the gate in comparison with the thickness of the cavity causes a sudden reduction in pressure that allows the expansion of the gas in solution and then the foaming. For this reason the pressure sensors in positions 2, 3 and 4 show pressure values much lower than those of the sensor inside the runner. The temperature detected by transducers in position 1 and 2 show an increment during the injection phase and a progressive decrease during the cooling phase. The temperature is lower as it moves away from the runner. In position 3 and 4 the values of temperature is about 23 °C, which means that the flow of solution has not reached these positions.

Chapter 7

Back pressure 3 bar

Table 33. *Features of the sample of PLA 4032D molded at back pressure of 3 bar in the hydraulic system (T=200°C).*

Back pressure [bar]	Weight [g]	Length [mm]	Apparent density [g/ccm]	Reduction in density [%]
3	5.617	76.34	0.613	49.326

Figure 129. *Micrographs of the foamed samples of PLA 4032D molded with back pressure 3 bar (T=200°C).*

Samples molded with a back pressure of 3 bar show the best morphology found in this series of experimental tests. The micrographs acquired on the vertical section shown a thin layer of skin, a good foaming with almost homogeneous distribution of the bubbles, that are slightly bigger in the middle of the section. In this cutting direction the bubbles seem oriented along the direction of the flow, while horizontally the bubbles don't show this orientation. The pressure profiles during the injection in cavity of the solution loaded at 3 bar of back pressure shows a trend very similar to that of the previous situation. In this case, the measures of temperature (Figure 130) show that the flow of solution during the injection stage has reached the transducer close to the tip of the cavity.

Figure 130. *Temperature profiles and screw position of a foamed sample of PLA 4032D molded at back pressure 3 bar (T=200°C).*

Back pressure 4 bar

**Table 34.** *Features of the sample of PLA 4032D molded at back pressure of 4 bar in the hydraulic system (T=200°C).*

Back pressure [bar]	Weight [g]	Length [mm]	Apparent density [g/ccm]	Reduction in density [%]
4	13.664	119.44	0.953	21.212

In the micrographs in Figure 131, corresponding to the samples obtained with a back pressure of 4 bar, it is possible to observe that, soon after the gate, the sample has few bubbles with large size and the most part of the section is compact.
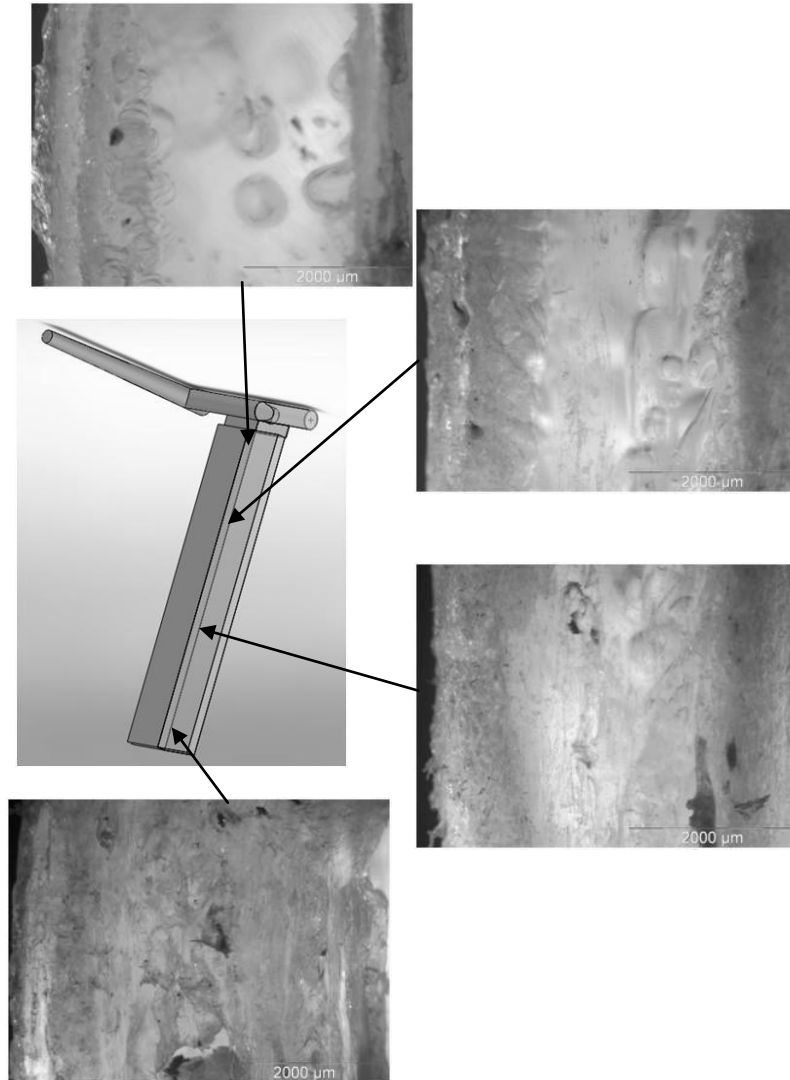
Figure 131. *Micrographs of the foamed samples of PLA 4032D molded with back pressure 4 bar (T=200°C).*

At longer distances to the gate, the number of bubbles slightly increases, but there is a large distribution of their size. Also from the pressure profiles it is possible to deduce that in position 2 and 3 there are a little number of bubbles in the section of the sample. In fact, the pressure in those position reaches values of about 30 bar and 20 bar respectively in phase of injection. From the temperature profiles it is possible to observe that the temperature decrease with the distance from the gate. Furthermore, also in the fourth

position there is a temperature higher than that of the mold. So, it is possible to deduce that the material has filled completely the mold cavity.
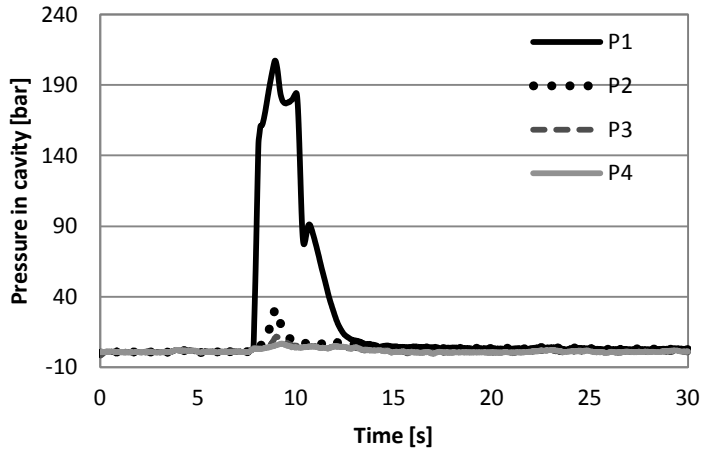
Figure 132. *Pressure profiles of a foamed sample of PLA 4032D molded at back pressure 4 bar (T=200°C).*
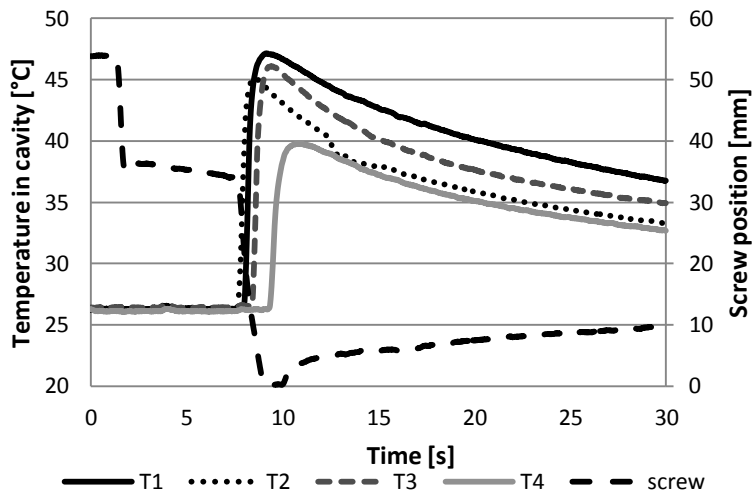
Figure 133. *Temperature profiles and screw position of a foamed sample of PLA 4032D molded at back pressure 4 bar (T=200°C).*

Chapter 7

Back pressure 5 bar

Table 35. *Features of the sample of PLA 4032D molded at back pressure of 5 bar in the hydraulic system (T=200°C).*

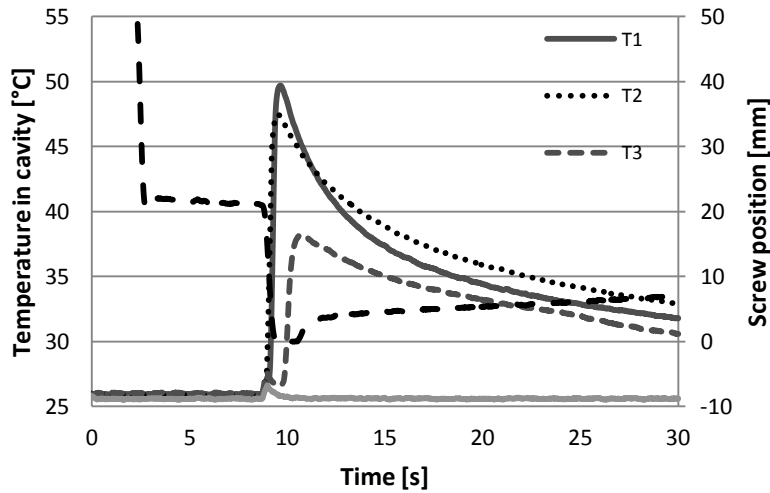| Back pressure [bar]	Weight [g]	Length [mm]	Apparent density [g/ccm]	Reduction in density [%]
5	13.348	113.7	0.978	19.148
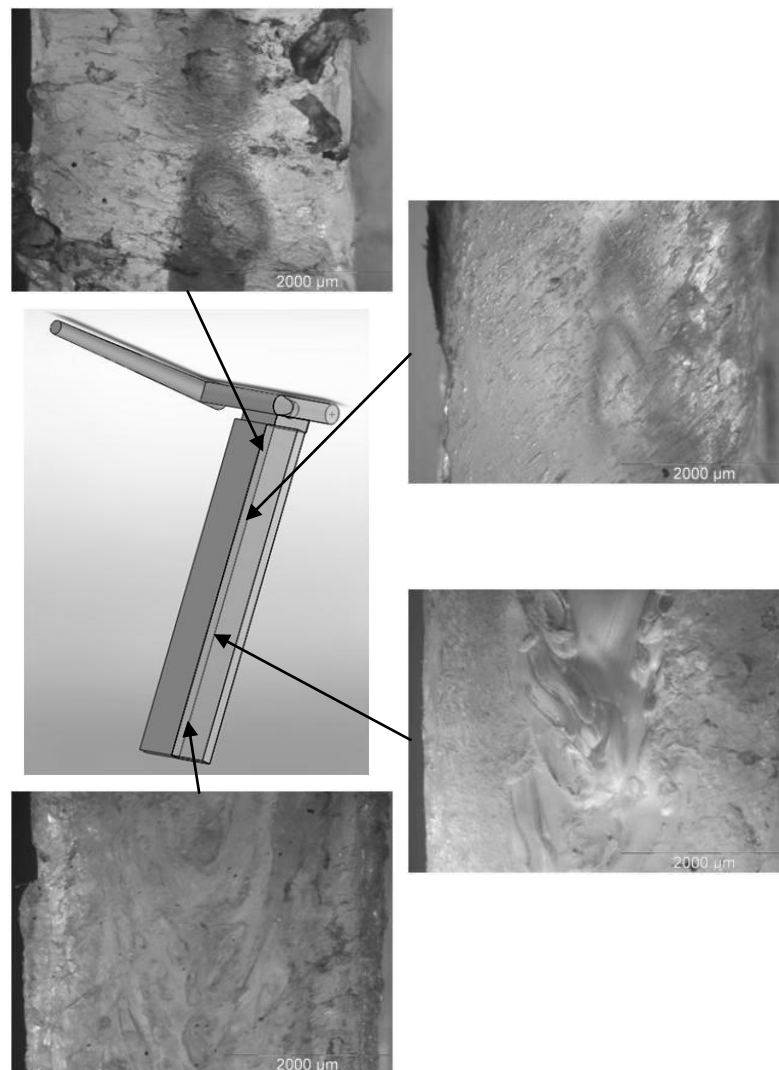
Figure 134. *Micrographs of the foamed samples of PLA 4032D molded with back pressure 5 bar (T=200°C).*

Also in this case, as in case of back pressure equal to 4 bar, the material has completely filled the cavity. However, the sample has a few large bubbles near the gate and a lot of compact material. At longer distances from the gate, the number of bubbles increase sligthly. In this part of the samples, the bubbles seems oriented in direction of the flow. The pressure and temperature profiles are very similar to those at backpressure 4 bar.

All the pressure profiles on the rummer (P1) related to the samples analized in this paragraph show a peak during the decrease of the pressure due to the cooling phase.

The pressure profiles obtained in P1 were plotted versus the screw position, in order to evaluate the compressibility of the solution in the different experimental conditions. Figure 135 shows the evolution of pressure with the screw position during the injection phase.
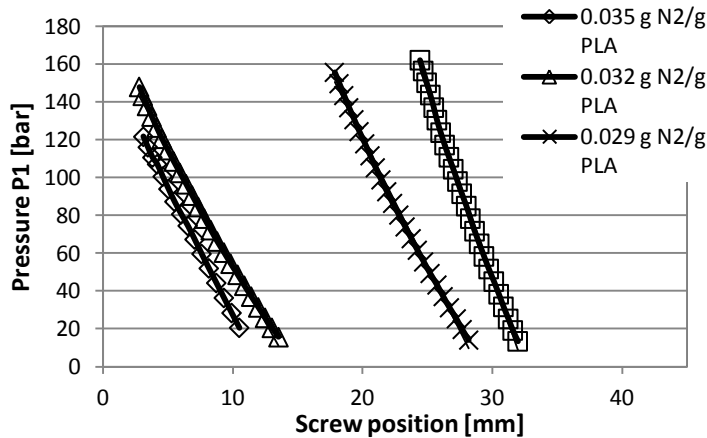
Figure 135. *Pressure versus screw position during the injection phase for PLA 4032D (T=200°C).*

From the slope of the lines at the different back pressures in Figure 135 the compressibility of the polymer/gas solution during the injection phase.

Figure 136 shows the values of compressibility of the polymer/gas solutions obtained from loading at different values of back pressures of the hydraulic system. It is possible to observe that, at higher values of back pressure, there are lower values of compressibility.
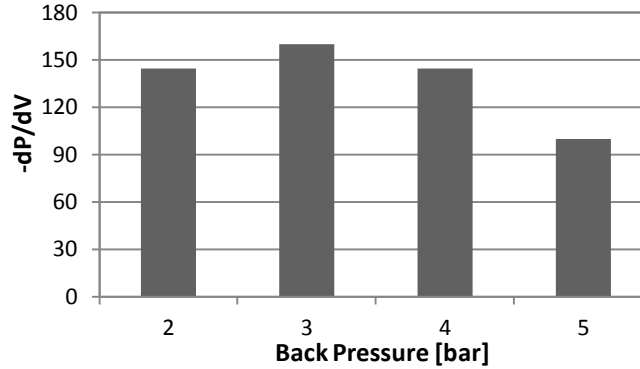
Figure 136. *Compressibility of the solution at different values of back pressures for PLA 4032D (T=200°C).*

The obtained samples were analyzed in terms of geometry and physical properties; results of that analysis are reported in Table 36.

Table 36. *Geometrical and physical features of the foamed samples of PLA 4032D at different back pressures in the hydraulic system.*

Back pressure [bar]	Amount of N_2 in PLA [g N_2/g PLA]	Weight [g]	Length [mm]	Apparent density [g/ccm]	Reduction in density [%]
2	0.035	2.235	31.76	0.586	51.535
3	0.032	5.617	76.34	0.613	49.326
4	0.029	13.664	119.44	0.953	21.212
5	0.026	13.348	113.7	0.978	19.148

From Figure 137, which shows the length of the samples obtained imposing different values of back pressure during the batching phase of the injection molding process, it is possible to observe that at higher values of back pressure, corresponding to lower solubility of nitrogen into molten PLA, the samples obtained are longer and less foamed (smaller reduction in density) than those molded with low back pressure.
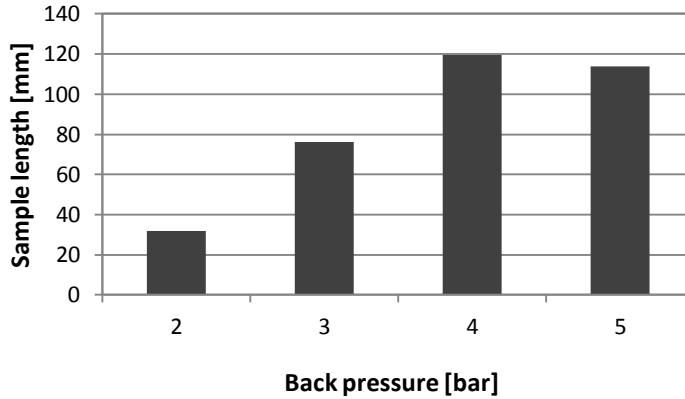
Figure 137. *Length of the samples of PLA 4032D at different back pressures in the hydraulic system (T=200°C).*

This trend is explained by the fact that, as previously reported in Figure 123, keeping constant the amount of gas injected and the length of dosage, the increase of the back pressure applied to the screw during the dosage phase allows the loading of a greater amount of polymer during that phase. So, with a length of dosage of 54 mm, at low values of back pressures an amount of nitrogen of almost 1.2 grams per shot dissolves in a small quantity of material, producing a good foaming. At higher values of back pressures, instead, the same amount of gas dissolves in a greater quantity of PLA, producing a poor foaming and longer samples. For this reason, the reduction in density with respect to the samples of pure PLA decreases with the increasing of the back pressure of the hydraulic system, as shown in Figure 138.
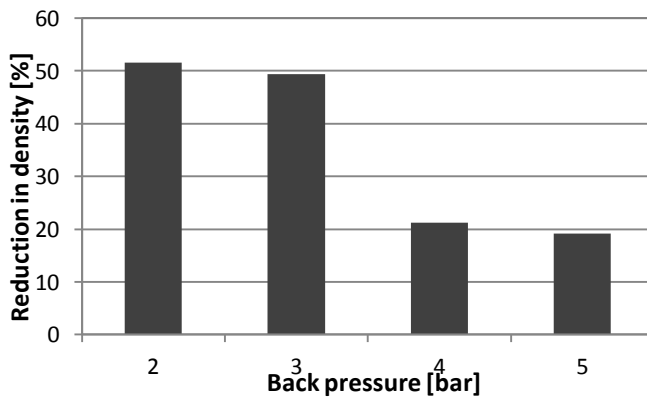
Figure 138. *Reduction in density of samples of PLA 4032D at different back pressure (T=200°C).*

Chapter 7

Mechanical properties

The mechanical properties of this set of samples were also carried out. Figure 139 shows the specimen utilized for mechanical tests.
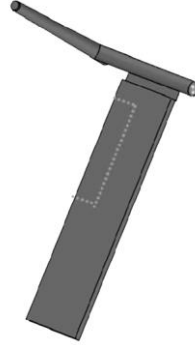
Figure 139. *Specimen utilized for mechanical tests with second set of samples of PLA 4032D.*

Flexural test

Flexural tests were carried out on these specimens at two different speeds, 2 mm/min and 5 mm/min. The distance between the two supports is 42 mm and the load is 10 kN. Figure 140 shows a comparison between the moduli of elasticity obtained at 2 mm/min and 5 mm/min. As reported in the figure, ther is no difference between the two speeds. So, subsequent tests have been conducted at 5 mm/min.
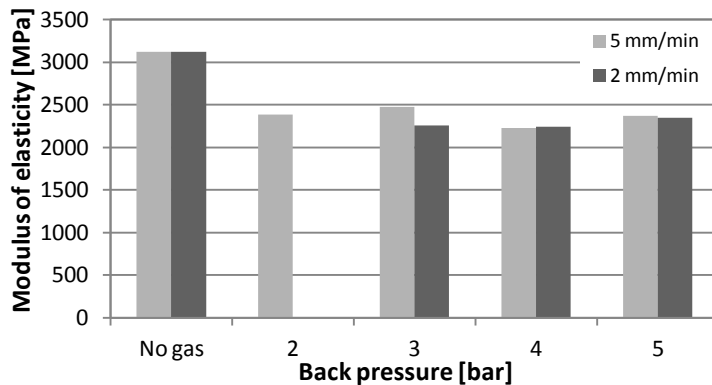
Figure 140. *Comparison between modules of elasticity obtained at 2 and 5 mm/min for PLA 4032D (T=200°C).*

Figure 140 does not show substantial differences between the moduli of the foams obtained at different back pressures. The reduction in modulus of

146

these on respect to the modulus obtained from pure PLA in standard conditions is about of 25%.

Impact resistance

Other tests were carried out to observe the impact resistance of the these set of samples. In Figure 141 it can be noticed that the impact resistance of foamed samples increases with the increasing of the back pressure, namely on increasing the density. At back pressures equal to 3, 4 and 5 the impact resistance appears higher than that of the unfoamed samples.
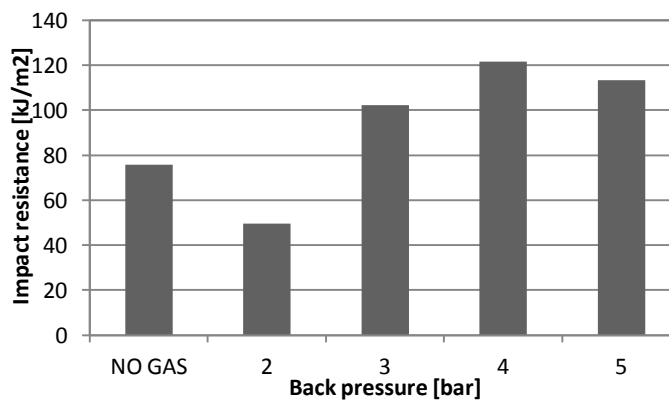
Figure 141. *Impact resistance of samples of PLA 4032D foamed at different values of back pressure in the hydraulic system (T=200°C).*

Tensile properties

The moduli of elasticity obtained from tensile tests were multiplied by the ratio between the density of the pure PLA and the density of the foamed PLA in each condition. In Figure 142 it is possible to observe that, for foamed samples, the modulus is lower than that of the unfoamed sample. Reduction in modulus compared to samples of pure PLA reaches values higher than 50%.
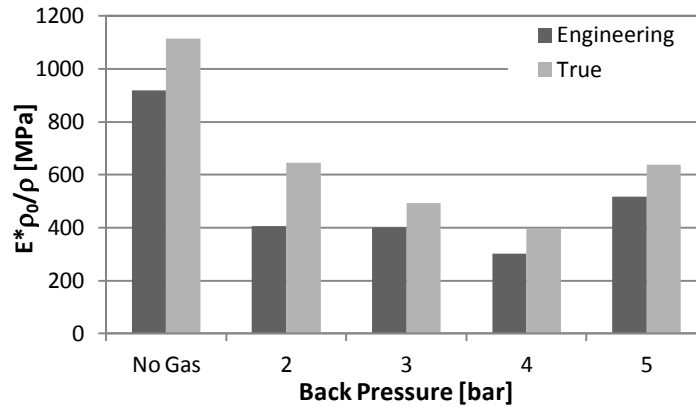
Figure 142. *Modulus of elasticity obtained from traction tests on samples of PLA 4032D at different back pressures in the hydraulic system (T=200°C).*

From this set of mechanical tests it is possible to observe that in flexural tests higher values of modulus of elasticity were obtained, the reduction in modulus compared to that of pure PLA is of about 25% and there are not considerable differences between the samples at the different back pressures.

7.6.2 Morphological analysis

The morphology of the foamed samples of PLA is very complex. For this reason, it was very difficult to analyze the morphology of the molded parts. So, only the samples molded with a back pressure of 3 bar, that from the analysis shown in section 7.4 seem to have the best properties, and 5 bar were analyzed by means of an algorithm created on a software for numerical calculation and statistical analysis. This algorithm allows to isolate the cell by a series of filters, as shown in Figure 143. The analyzed images were acquired in the same position on the length of the samples molded with back pressure of 3 and 5 bar.
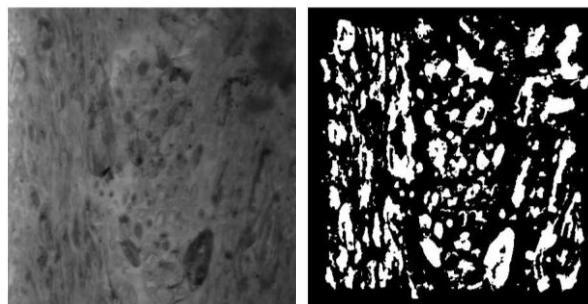
Figure 143. *Image of a sample molded with back pressure 3 bar and the same image modified with the software.*

The output of the software were analyzed in order to obtain the percentage of space occupied by cells with radius included at a given interval x (see paragraph 5.2.6). In Figure 144 and Figure 145, in which the void percentages for each range of radii in samples molded with a back pressure of 3 bar and 5 bar respectively (0.032 g N_2/g PLA and 0.026 g N_2/g PLA) are shown, it is possible to see that the sample at 3 bar presents cells with radii lower than 200 micron, while the sample at 5 bar presents a lower percentage of cells with sizes in the range 0-200 micron, and a high percentage of cells with higher radius.
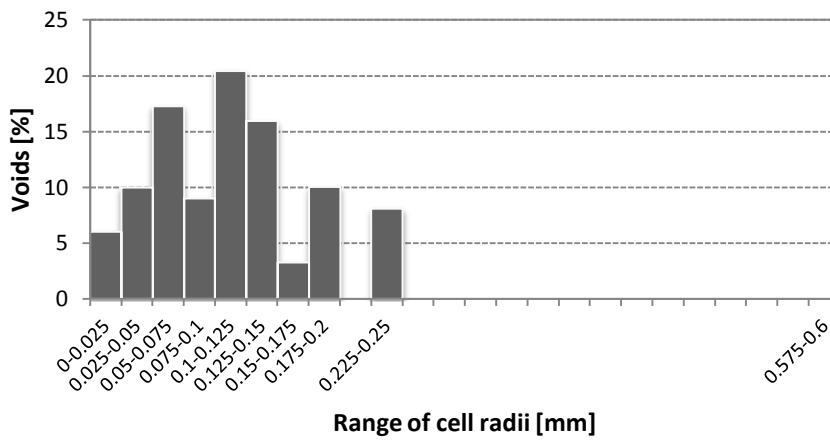
Figure 144. *Percentage of void due to cells with radius included in defined ranges for samples of foamed PLA 4032D molded with back pressure of 3 bar (T=200°C).*
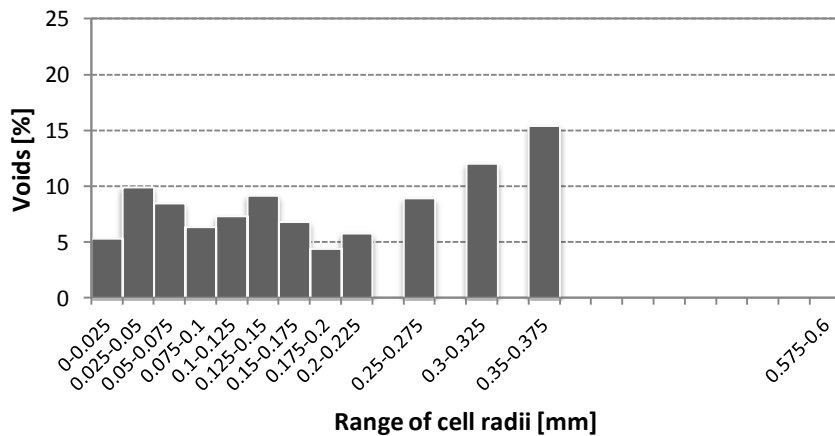
Figure 145. *Percentage of void due to cells with radius included in defined ranges for samples of foamed PLA 4032D molded with back pressure of 5 bar (T=200°C).*

149

Total voids percentage in the sample molded at 3 bar is higher than that of the sample molded at 5 bar, with a significantly larger number of cells.

Then, foam injection molding of PLA carried out by imposing a back pressure of 3 bar during the dosage phase allows to obtain a foam with a low density and good mechanical and morphological properties.

Chapter 8
Relationships between foam structure and properties

The principal aim of the foam injection molding is to reduce the density of the materials in order to get lightweight parts. Foam injection molding offers also many advantages compared to conventional injection molding, but to improve the properties of the material, it is necessary to understand the interrelationship between the morphology and the mechanical properties as well as to know how the processing parameters influence the morphology and the properties of the produced part.

Gibson and Ashby [97] suggested that mechanical properties could be related to the relative foam density, ratio between density of the foamed sample ρ and density of the unfoamed sample ρ_0, in the following equations:

$$\frac{E}{E_0} = \phi^2 \left(\frac{\rho}{\rho_0}\right)^2 + (1 - \phi)\frac{\rho}{\rho_0} \tag{59}$$

Where E is the Young's modulus of the foamed sample, E_0 the Young's modulus of the unfoamed sample and ϕ denotes the strut volume fraction. The first member on the RHS of eq. 59 is due to cell wall buckling and second member is due to cell wall stretch accountable to deformation. Figure 146 shows a cubic model for a cell foam.
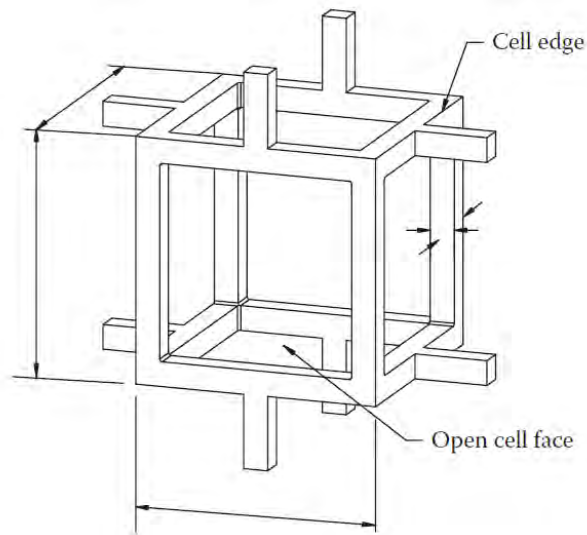
Figure 146. *Strut-Face cubic model.*

When the second member of the equation 59, typical of the closed-cells, dominates, the above equation becomes:

$$\frac{E}{E_0} = (1 - \phi)\frac{\rho}{\rho_0} \qquad (60)$$

Since Equation 60 is simply a linear density reduction function, as opposed to a square of density reduction valid for open-cell foams, it can be inferred that open cell foams demonstrate a lower modulus than that of corresponding closed cell foams by the expansion ratio [2].

Equation 60 was used to calculate the parameter ϕ from results obtained in physical and mechanical analysis made on the samples of polystyrene and poly(lactic) acid obtained during this work.

8.1 Polystyrene

Figure 147 shows the variation of the relative Young's modulus, namely the ratio between Young's modulus of the foamed samples and that of the unfoamed samples, with the relative foam density. It is possible to observe that all data sets, corresponding to the different amounts of gas injected in PS, are positioned very close to the bisector, demonstrating that the reduction in Young's modulus of the foamed parts compared to the Young's modulus of the unfoamed ones is almost entirely offset by the reduction in density.
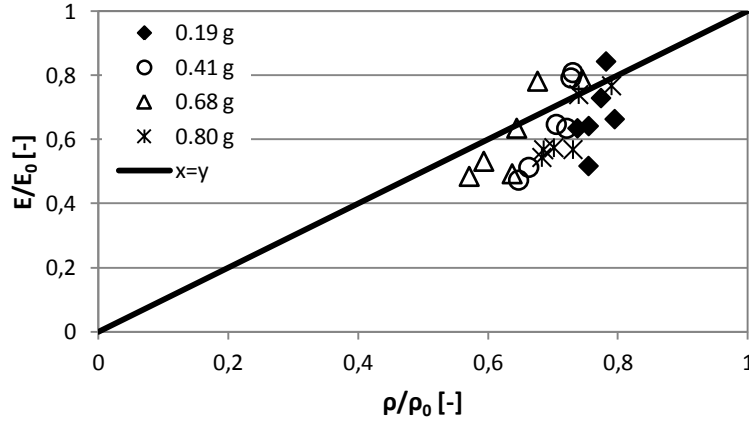
Figure 147. *Relative Young's modulus versus relative foam density for PS 678E (T=220°C).*

From equation 60 it is possible to deduce that, since the reduction in modulus is compensated by the reduction in density of the foamed samples compared to that of the samples not foamed, the parameter ϕ (strut volume fraction) should assume values close to zero.

Values of density and the Young's modulus obtained from analysis on samples of polystyrene were utilized to evaluate the parameter ϕ, in order to estimate the dependence of the mechanical properties on morphological and physical parameters. In Table 37 it is possible to observe that, at low injection flow rates, the values of ϕ are close to zero. With the increase of the flow rate, the parameter ϕ assumes values slightly above zero and settles around the value 0.2.

Table 37. *Strut volume fraction φ at different injection flow rates for PS 678E with different amounts of gas injected (T=220°C).*

Injection flow rate [ccm/s]	Strut volume fraction φ			
	0.19 g N_2	0.41 g N_2	0.68 g N_2	0.80 g N_2
4	0,06	-0,11	-0,06	0,03
7	-0,08	-0,09	-0,16	0,00
15	0,16	0,12	0,01	0,22
30	0,15	0,08	0,23	0,20
60	0,14	0,23	0,10	0,17
74	0,31	0,27	0,15	0,18

Relative Young's modulus was plotted versus the parameter ϕ, as shown in Figure 148.
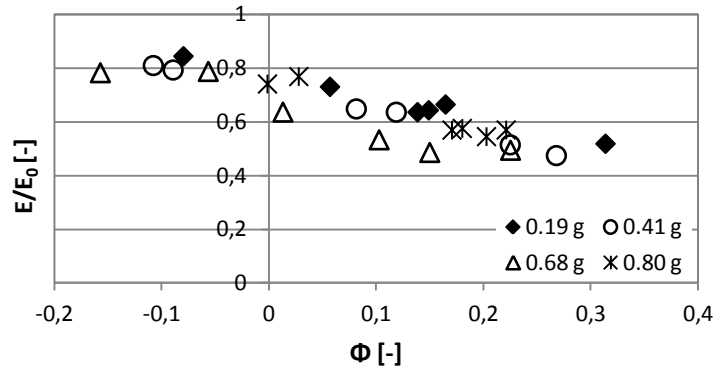
Figure 148. *Relative Young 's modulus versus strut volume fraction φ for PS 678E (T=220°C).*

For values of ϕ close to zero, the relative Young's modulus takes values close to 0.8, while with the increasing of the strut volume fraction, the relative modulus decreases at 0.5.

The mechanical properties of a foamed part are closely related to the morphology of the foam itself. In order to obtain a foamed part with good mechanical properties, it is necessary to study the correlation of these properties with morphological and physical parameters. From the analysis of cells distribution showed in paragraph 5.2.6, the percentage of voids for each polymer/gas solution was evaluated. In Figure 149 and Figure 150, the void percentage was plotted versus the average Young's modulus, namely the average of the Young's modulus values at different flow rates for each solution, and versus the foam density respectively.
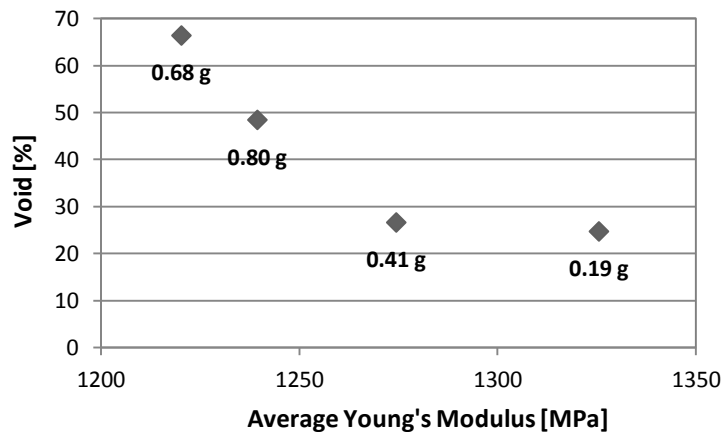
Figure 149. *Variation of the void percentage with the average Young's modulus for PS 678E (T=220°C).*
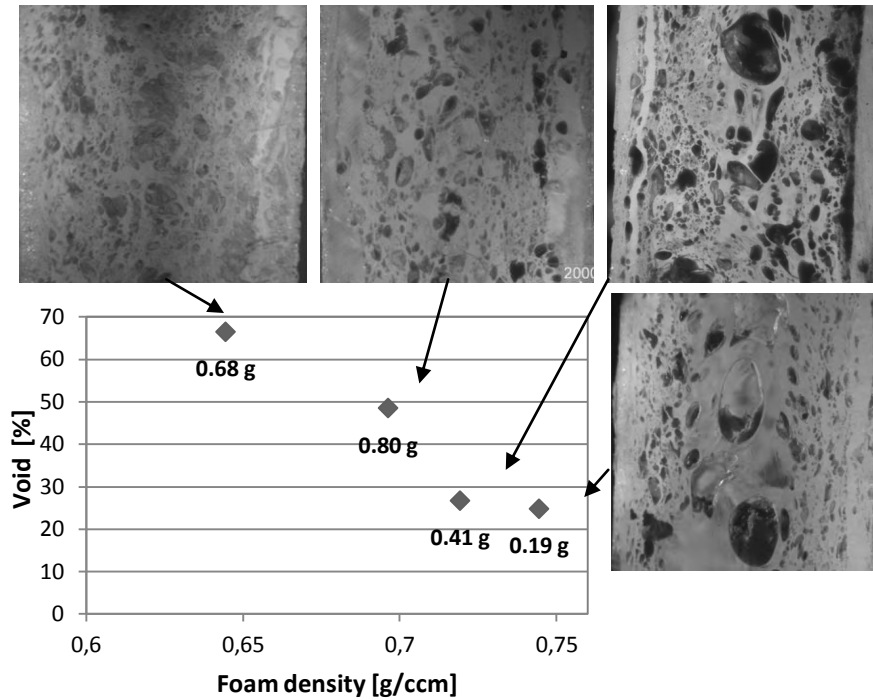
Figure 150. *Voids percentage inside of the foamed samples of PS 678E versus the foam density (T=220°C).*

As expected, samples with a lower percentage of void have higher average modulus and foam density. From both the graphs it can be observed that the polystyrene samples with 0.68 g of nitrogen have higher void percentage and lower foam density than the samples with 0.80 g of nitrogen, and a very small reduction in average Young's modulus (almost 19 MPa).

8.2 Poly(lactic) acid

As done for polystyrene, also the samples of PLA were analyzed in order to evaluate a parameter that correlates the mechanical properties to those physical. Values of density and the Young's modulus obtained from analysis on samples of poli(lactic) acid were utilized to evaluate the strut volume fraction ϕ through the equation 60. The results obtained from the analysis on the first set of samples of PLA (geometry in Figure 151) are reported below.
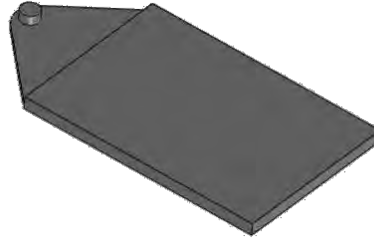
Figure 151. *Sample geometry of the first set of tests on PLA 4032D.*

Errore. L'origine riferimento non è stata trovata. shows the evolution f the parameter ϕ with the injection flow rate for the three PLA/N$_2$ solutions.
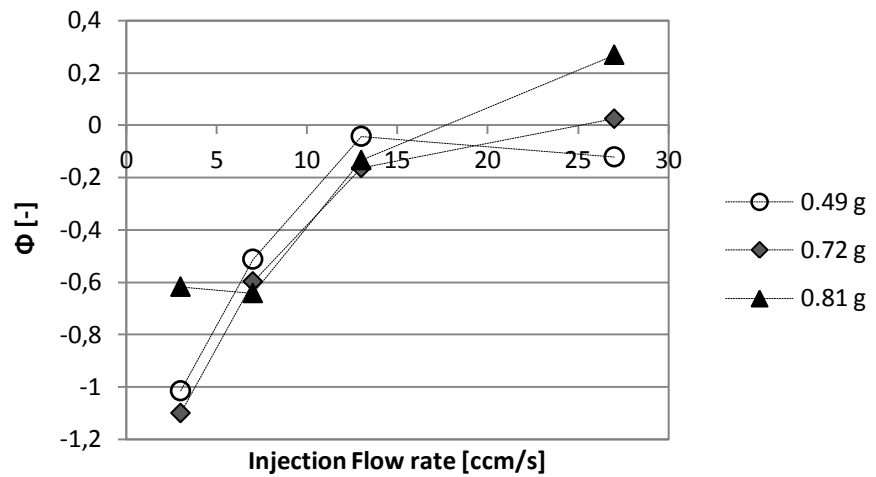
Figure 152. *Strut volume fraction at different injection flow rates for all the solution of PLA 4032D (T=200°C).*

It is possible to observe that the parameter φ takes values higher than 0.3 and increases on increasing the flow rate. However, during the flexural tests, a dependence of the mechanical properties from the direction in which the sample was positioned was observed. In particular, mechanical properties were obtained positioning the sample in two different ways: deformation parallel and perpendicular to flow direction during the injection phase (Figure 153).

(a)

(b)
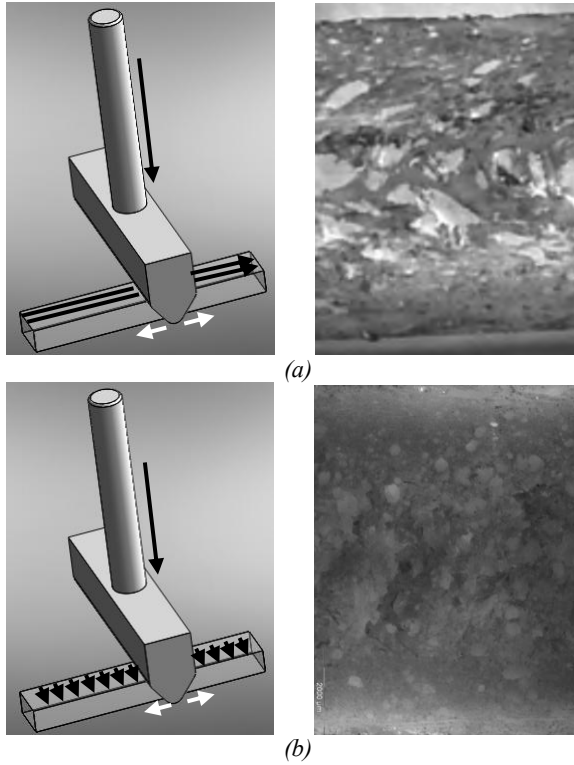
Figure 153. *Deformation parallel* (a) *and perpendicular* (b) *to flow direction.*

As shown in Figure 154, on positioning the samples with flow direction parallel to the direction of deformation, the values of Young's Modulus were lower than those obtained from flexural tests carried out on samples positioned with flow direction perpendicular to the direction of deformation.
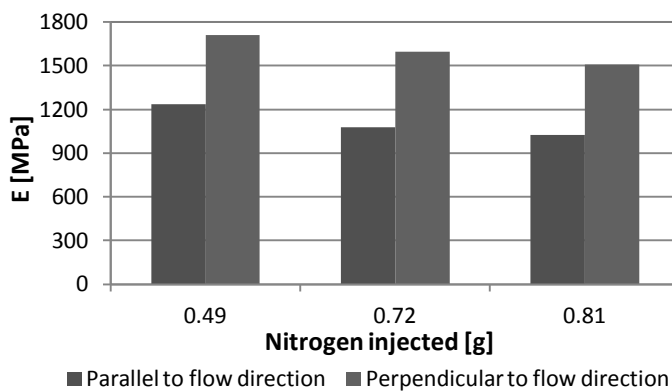
Figure 154. *Strut volume fraction for PLA 4032D with different amounts of gas in the two direction of positioning.*

This trend can be due to the fact that, in the samples with flow direction parallel to the direction of deformation, the cells were oriented along the flow direction.

Also in this case, the reduction in Young modulus is almost entirely compensated by the reduction in density, as it is possible to observe in Figure 155.
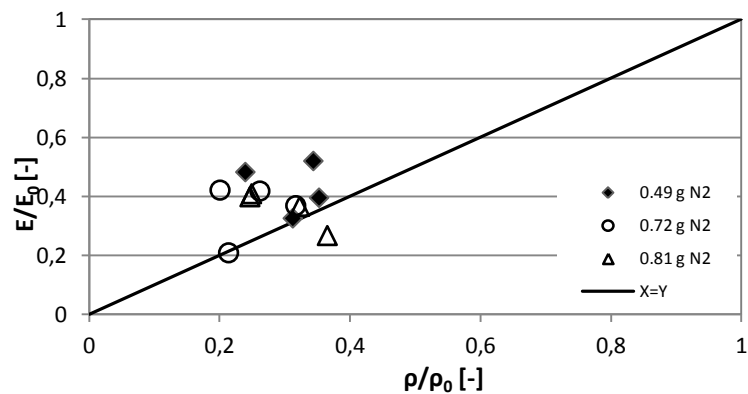
Figure 155. *Relative Young's modulus versus relative foam density for PLA 4032D (T=200°C).*

Also the samples obtained with cavity provided with pressure and temperature sensors (Figure 156) were analyzed in order to evaluate the dependence of the mechanical properties from the foam density.

Figure 156. *Sample geometry of the second set of tests on PLA 4032D.*

In this set of experiments, the effect of back pressure imposed during the batching phase was analyzed.

Figure 157 shows the variation of the relative Young's modulus, ratio between Young's modulus of the foamed samples and that of the unfoamed samples, with the relative foam density of the PLA samples.
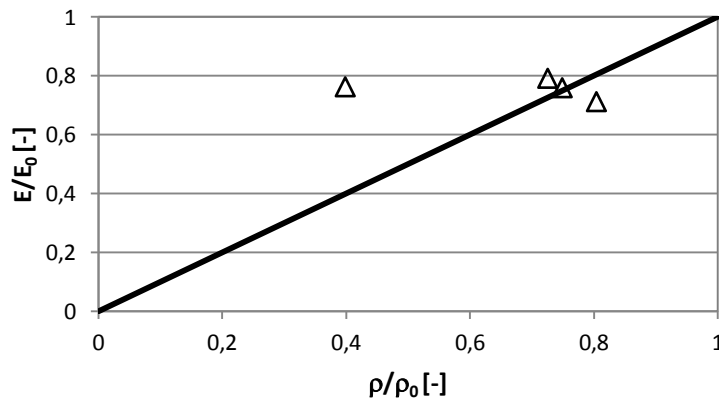
Figure 157. *Variation of the relative Young's modulus with the relative foam density for PLA 4032D (T=200°C).*

Figure 157 clearly shows that the points, corresponding to the different back pressures applied during the dosage phase of the foam injection molding process, are positioned very close to the bisector. In particular, points corresponding to low values of back pressure (2 and 3 bar in the hydraulic system) are above the bisector. This means that the reduction in density compensates the reduction in modulus of the foamed samples compared to the unfoamed ones.

Also in this case the parameter ϕ, evaluated through the equation 60, is very close to the value zero, with the exception of samples molded with back pressure equal to 2 bar, where the ϕ is lower than zero. This confirms that the reduction in modulus is completely compensated by the reduction in density of the foamed samples compared to the unfoamed ones. On plotting the reduction in density versus ϕ, it is possible to observe a linear dependence of the two parameters. In fact, increasing the reduction in density, the strut volume fraction ϕ decreases linearly, approaching to the case in which there is no foaming.
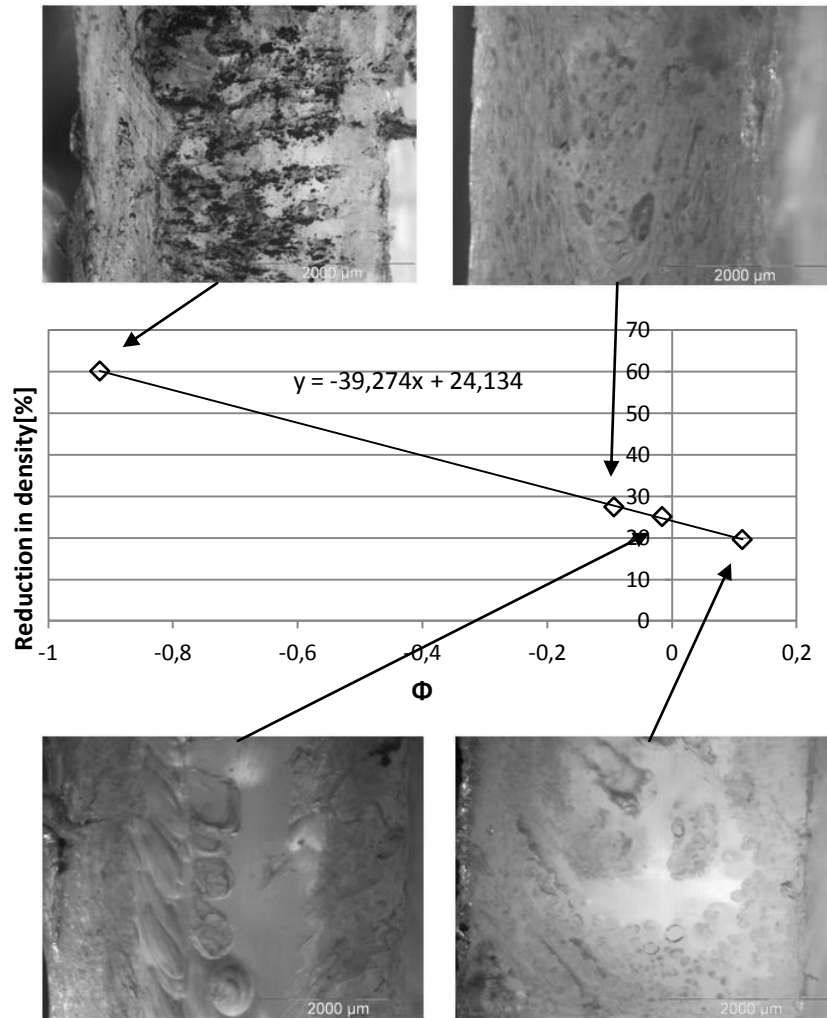
Figure 158. *Reduction in density versus φ for PLA 4032D (T=200°C).*

Chapter 9
Conclusions

The effect of a physical blowing agent (nitrogen) on the viscosity of polymer melt and on the physical and mechanical properties of a part obtained by foam injection molding was analyzed.

Design and implementation of modifications to a conventional injection molding machine were made in order to obtain a foam injection molding machine. In particular, a slit rheometer was mounted in-line to observe the effect of the amount of gas on rheology.

In this work four materials were adopted: two conventional polymer, polypropylene and polystyrene, and two different grades of a biodegradable polymer, poly (lactic) acid. For each of these materials similar conclusions were reached.

✓ Rheological measurements showed a significant reduction in viscosity due to the injection of gas (this is particularly useful for biodegradable polymers).

✓ High values of reduction in density, that increases with increasing of injection flow rate, were reached. At high flow rates, in fact, the material inside the cavity presents a more homogeneous initial temperature profile.

✓ Density decreases with increasing amount of gas. At too high amount of gas, the density begins to increase again. This trend is also followed by the morphology of the sample: on increasing the amount of gas, samples with a more homogeneous morphology are obtained. At too high amount of gas the morphology worsens, probably due to a premature foaming already in adduction channels

✓ Reduction in Young's modulus of the foamed parts compared to the Young's modulus of the unfoamed ones is almost entirely compensated by the reduction in density.

Therefore, there seems to be an optimal physical blowing agent content that leads to the best microcellular structure and the maximum density reduction and mechanical properties.

Development of a batch foaming system allowed to analyze the effect of foaming temperature, solubilization time and cooling rate on the morphology of the PLA samples and on their density.

Melting at 10 °C/min of skin and core of unfoamed sample and foamed samples of PLA by means of Differential Scanning Calorimetry was made in order to evaluate the effect of gas on the crystallinity of the molded samples. Results show a higher cristallinity of the foamed core (12%) with respect to the compact skin (9%) and to the unfoamed part (9% core and 6% skin). It is very important to specify that the maximum cristallinity for this PLA grade is 35%.

Bibliography

[1] Cellular materials in Encyclopedia of Polymer Science and Technology 1st ed., Vol. 5

[2] S.T. Lee, C. B. Park, and N.S. Ramesh, "Polymeric Foams: Technology and Science", Taylor and Francis Group, LLC Published, 2007

[3] Klempner D., Sendijarevic V., Polymeric foams and foam technology, Hanser Gardner Publications, Munich (2004)

[4] Blander, M. and Katz, J. L., "Bubble Nucleation in Liquids," AIChE J., 21, 5, 833–848, 1975

[5] Kagan Y., "The Kinetics of Boiling of a Pure Liquid," Russ. J. Phys. Chem., 34, 42–46, 1960

[6] Uhlmann, D. R., Chalmers, B., "Nucleation phenomena", ACS Symposium, June 1965

[7] Y. Moon, K. Lee and S. W. Cha, "Bubble growth in mold cavities during microcellular injection molding processes", Journal of Mechanical Science and Technology 23 (2009) 3349-3356

[8] E. Bociaga, P. Palutkiewicz, J. Wawrzyniak, Investigations of sink marks of foam polypropylene injection moulded parts, PPS-2009

[9] J. A. Bridson, Plastics Materials, Seventh edition

[10] J. Lee, L.-S. Turng, E. Dougherty, P. Gorton, "Novel foam injection molding technology using carbon dioxide-laden pellets", Polymer Engineering And Science-2011

[11] Martini, JE. PhD Thesis, Massachusetts Institute of Technology, USA; 1981.

[12] Nam PH, Okamoto M, Maiti P, Kotaka T, Nakayama T, Takada M, et al. Polym Eng Sci 2002;42(9):1907

[13] Ray SS, Okamoto M. New polylactide/layered silicate nanocomposites, 6a melt rheology and foam processing. Macromol Mater Eng 2003;288:936–44.

[14] Ema Y, Ikeya M, OkamotoM. Foam processing and cellular structure of polylactide-based nanocomposites. Polymer 2006;47:5350–9.

[15] Corre Y.M. Maazouz A. Duchet J, Reignier J. Batch foaming of chain extended PLA with supercritical CO2: Influence of the rheological properties and the process parameters on the cellular structure. Journal of Supercritical Fluids 58 (2011) 177– 188

[16] Da-chao Li, Tao Liu, Ling Zhao, Xiao-song Lian, and Wei-kang Yuan. Foaming of Poly(lactic acid) Based on Its Nonisothermal Crystallization Behavior under Compressed Carbon Dioxide. Ind. Eng. Chem. Res. (2011), 50, 1997–2007.

Bibliography

[17] Nalawade S, Picchioni F, Janssen LPBM. Supercritical carbon dioxide as a green solvent for processing polymer melts: processing aspects and applications. Prog Polym Sci 2006;31:19–43.

[18] E. Di Maio, G. Mensitieri, S. Iannace,, L. Nicolais, W. Li, R.W. Flumerfelt. Structure optimization of polycaprolactone foams by using mixtures of CO_2 and N_2 as blowing agents. Polymer. Engineering. Science., 45:432–441, (2005).

[19] Di, Y.W., Iannace, S. and Di, M.E., Poly(lactic acid)/organoclay nanocomposites: Thermal, rheological properties and foam processing, Journal of. Polymeric. Science., PartB-Polym. Phys., 43 (6), 689–698, (2005).

[20] K.T .Okamoto, Microcellular Processing, Hanser Gardner Publications (2003)

[21] J.Xu and D.Pierick, J. Inj. Molding Tech. 5, 152 (2001)

[22] S.Gong, M.Y uan, A.Chandra, H.Kharbas, A.Osorio, and L.S. Turng, Int. Polym. Processing 2, 202 (2005)

[23] E. Gulari and C. W. Manke, Paper presented at the 219th ACS Nation al Meeting, I&EC–106, San Francisco, CA, March 26–30 (2000)

[24] J. R. Royer, Y. J. Gay, J. M. Desimone, and S. A. Khan, J. Polym. Sci., Part B: Polym. Physics, 38, 3168 (2000)

[25] A. Kramschuster, R. Cavitt, D. Ermer, Z.B. Chen, L.-S. Turng, "Effect of processing conditions on shrinkage and warpage and morphology of injection moulded parts using microcellular injection moulding", Plast. Rubber Compos. 35 (2006) 198

[26] Shyh-Shin Hwang, Peming P. Hsu, Chi-wei Chiang, "Shrinkage study of textile roller molded by conventional/microcellular injection-molding process" - International Communications in Heat and Mass Transfer 35 (2008) 735–743

[27] S.-S. Hwang , Z.-S. Ke, "The dimensional stability of a microcellular injection molded gear shaft" - International Communications in Heat and Mass Transfer 35 (2008) 263–275

[28] H.-L. Chen, R.-D. Chien, S.-C. Chen, "Using thermally insulated polymer film for mold temperature control to improve surface quality of microcellular injection molded parts" - International Communications in Heat and Mass Transfer 35 (2008) 991–994

[29] S.-C. Chen, P.-S. Hsu, S.-S. Hwang, "The effects of gas counter pressure and mold temperature variation on the surface quality and morphology of the microcellular polystyrene foams", J. APPL. POLYM. SCI. 2012

[30] J. Lee, L.-S. Turng, E. Dougherty, P. Gorton, "A novel method for improving the surface quality of microcellular injection molded parts" - Polymer 52 (2011) 1436e1446

[31] A. N.J. Spörrer; V. Altstädt, "Controlling the morphology of injection molded structural foams by the mold design and processing

parameters" - Journal of Cellular Plastics, vol. 43, pp. 313-330, July/September 2007.

[32] Handbook of Plastic Foams pp. 325-326

[33] L. S. Turng, "Special and Emerging Injection Molding Processes", Journal of injection molding technology, september 2001, Vol. 5, No. 3

[34] N. P. Suh, In Innovation in Polymer Processing—Molding, J. F. Stevenson, (Ed.), Hanser, Munich, 93 (1996)

[35] Klempner D, Frisch KC, editors. Handbook of polymeric foams and foam technology. New York: Oxford University Press; 1991

[36] Chen L, Straff R, Wang X. Effect of filler size on cell nucleation during foaming process. SPE-ANTEC 2001;59:1732

[37] Zeng C, Han X, Lee LJ, Koelling KW, Tomasko DL. Polymer–clay nanocomposite foams prepared using carbon dioxide. Adv Mater (Weinheim, Germany) 2003;15(20):1743

[38] Di Y, Iannace S, Di Maio E, Nicolais L. Poly(lactic acid)/ organoclay nanocomposites: thermal, rheological properties and foam processing. J Polym Sci, Part B: Polym Phys 2005;43(6):689

[39] Nam PH, Maiti P, Okamoto M, Kotaka T, Nakayama T, Takada M, et al. Foam processing and cellular structure of polypropylene/ clay nanocomposites. Polym Eng Sci 2002;42(9):1907

[40] L.J. Lee et al., Composites Science and Technology 65 (2005) 2344–2363

[41] N.S. Ramesh, S.T. Lee, Cellular Polymers 24, 269 (2005)

[42] M. Okamoto, P.H. Nam, P. Maiti, T. Kotaka, T. Nakayama, M. Takada, M. Ohshima, A. Usuki, N. Hasegawa, H. Okamoto, Nano Letters 1, 503 (2001)

[43] P.H. Nam, P. Maiti, M. Okamoto, T. Kotaka, T. Nakayama, M. Takada, M. Ohshima, A. Usuki, N. Hasegawa, H. Okamoto, Polymer Engineering and Science 42, 1907 (2002)

[44] M. Mitsunaga, Y. Ito, S.S. Ray, M. Okamoto, K. Hironaka, Macromolecular Materials and Engineering, 288, 543 (2003).

[45] Y. Fujimoto, S.S. Ray, M. Okamoto, A. Ogami, K. Yamada, K. Ueda, Macromolecular Rapid Communications, 24, 457 (2003)

[46] S.-s. Hwang, P. P. Hsu, J. Yeh, J. Yang, K. Chang, Y Lai, "Effect of clay and compatibilizer on the mechanical/thermal properties of microcellular injection molded low density polyethylene nanocomposites", International Communications in Heat and Mass Transfer 36 (2009) 471–479

[47] Rizvi, S.J.A., Bhatnagar, N., "Microcellular PP vs. microcellular PP/MMT nanocomposites: A comparative study of their mechanical behavior", International Polymer Processing, Volume 26, Issue 4, 2011, Pages 375-382

Bibliography

[48] R. Pantani and G. Titomanlio, "The Simulation Of Post-Filling Steps In Injection Molding" in "Injection Molding - Fundamentals and Applications" – M. R. Kamal, A. I. Isayev and S.-J. Liu eds. – Hanser Munchen – 2009

[49] V. L. Bravo and A. N. Hrymak: Nozzle Injection of Physical Blowing Agents, Intern. Polymer Processing XX (2005)

[50] "Cellular Materials" in EPST 1st ed., Vol. 3, pp. 80–130, by R. E. Skochdopole, The Dow Chemical Co

[51] "Cellular Materials" in EPSE 2nd ed., Vol. 3, pp. 1–59, by K. W. Suh and D. D. Webb, The Dow Chemical Co

[52] M. Mahmoodi, A. H. Behravesh, S. A. M. Rezavand, A. Pashaei, "Visualization of Bubble Dynamics in Foam Injection Molding", Journal ofAppliedPolymer Science,Vol. 116, 3346–3355 (2010)

[53] Bledzki AK, Rohleder M, Kirschling H, Chate A, Cellular Polymers, 27-6, 2008, 327-345

[54] A. K. Bledzki, H. Kirschling, M. Rohleder, A. Chate, "Correlation between injection moulding processing parameters and mechanical properties of microcellular polycarbonate", Journal of Cellular Plastics 48(4) 301–340 – (2012)

[55] L. J. Hyde and L. A. Kishbaugh, How Microcellular Foam Molding Changes the Cost Structure of Injection Molded Automotive Components: A Review of the Process and Automotive Applications, 2002-01-0717

[56] Gomes ME, Ribeiro AS, Malafaya PB, Reis RL, Cunha AM. A new approach based on injection moulding to produce biodegradable starch-based polymeric scaffolds: morphology, mechanical and degradation behaviour. Biomaterials 2001;22: 883–9

[57] L. Wu, D. Jing, J. Ding, A ''room-temperature'' injection molding/particulate leaching approach for fabrication of biodegradable three-dimensional porous scaffolds, Biomaterials 27 (2006) 185–191

[58] Z. Cui, B. Nelson, Y. Peng, K. Li, S. Pilla, W.-J. Li, L.-S. Turng, C. Shen, "Fabrication and characterization of injection molded poly (ε-caprolactone) and poly (ε-caprolactone)/hydroxyapatite scaffolds for tissue engineering", Materials Science and Engineering C 32 (2012) 1674–1681

[59] J., Peng, L.-S. Turng, X.-F. Peng, "A new microcellular injection molding process for polycarbonate using water as the physical blowing agent", Polymer Engineering And Science-2012

[60] ASTM D-5488-94d, 1994

[61] Lloyd AW., "Interfacial bioengineering to enhance surface biocompatibility". Med Device Technol 2002;13:18–21

[62] Rogers Me, Long Te, Synthetic Methods in Step-Growth Polymers – chapter 2– Polyesters. John Wiley & Sons, 2003

166

[63] L.-T. Lim, R. Auras, M. Rubino, Processing technologies for poly(lactic acid), Progress in Polymer Science 33 (2008) 820–852

[64] De Maio, F. Effect of processing on properties, crystallinity and biodegradation rate of PolyLactic Acid – PhD Thesis. University of Salerno, 2010

[65] Donald Garlotta, (2002), Literature Review of Poly(Lactic Acid). Journal of Polymers and the Environment, Vol. 9, No. 2

[66] Kunimune, N., Kunimune, T., Nagasawd, T., Tamada, S., Yamada, K., Leong, Y.W., Hamada, H., "Effectiveness of supercritical fluid for foaming of poly(lactic acid) during injection molding", Annual Technical Conference - ANTEC, Conference Proceedings, Volume 1, 2010, Pages 683-686

[67] H. Zhao, Z. Cui, X. Sun, L.-S. Turng, X. Peng, "Effects of gas and d-lactic acid contents on the structure and properties of microcellular injection molded poly (lactic acid)", ANTEC 2011

[68] Byler JR LL, K. T. (s.f.). "Flow behavior of polyethylene melts containing dissolved gases", Amer Chem Soc, Div Org Coatings Plast Chem Volume 31, Issue 1, 1971, Pages 47-53

[69] C. Gornik, Determining rheological data directly at the machine, Kunststoffe Plast Europe 4 (2005) 1.

[70] P.F. Bariani, M. Salvador, G. Lucchetta, Development of a test method for the rheological characterization of polymers under the injection molding process conditions, Journal of Materials Processing Technology 191 (2007) 119.

[71] A.L. Kelly, T. Gough, B.R. Whiteside, P.D. Coates, High shear strain rate rheometry of polymer melts, Journal of Applied Polymer Science 114 (2009) 864.

[72] C. Mobuchon, P.J. Carreau, M.C. Heuzey, M. Sepehr, Shear and extensional properties of short glass fiber reinforced polypropylene, Polymer Composites 26 (3) (2005) 247.

[73] J. Aho, S. Syrjälä ,"Shear viscosity measurements of polymer melts using injection moldingcmachine with adjustable slit die", Polymer Testing 30 (2011) 595–601

[74] Hsu C.-L., Turng L.-S., Osswald T. A., Rudolph N., Dougherty E., Gorton P., Effect of pressure and supercritical fluid on viscosity of LDPE in conventional and microcellular injection molding, Intern. Polymer Processing XXVII (2012) 1.

[75] Rawabdeh, I. A., and P. F. Petersen. "In-line Monitoring of Injection Molding Operations: A Literature Review." The Journal of Injection Molding Technology 3, no. 2 (1999): 47-53.

[76] Vietri.U. Intelligent monitoring of the injection moulding process, Ph.D thesis. University of Salerno, 2006

Bibliography

[77] U. Vietri, A. Sorrentino, V. Speranza, R. Pantani Improving the predictions of injection molding simulation software. POLYMER ENGINEERING AND SCIENCE. Vol. 51. Pag.2542-2551, (2011).

[78] Pontes, A. Shrinkage and Ejection Forces in injection Moulded Product- Ph.D Thesis,. University do Minho, Portugal, 2002.

[79] Berry, M., Kishbaugh, L., "Process monitoring and control for microcellular injection molding" Annual Technical Conference - ANTEC, Conference Proceedings, Volume 2, 2010, Pages 1434-1438

[80] Montell Polyolefins. "Development Data." (1998).

[81] De Santis, F., R. Pantani, V. Speranza, and G. Titomanlio. "Analysis of shrinkage development of a semi crystalline polymer during injection moulding." Industrial Chemical Engineering Research 49 (2010): 2469–2476.

[82] Pantani, R., V. Speranza, and G. Titomanlio. "Relevance of Crystallization Kinetics in the Simulation of the Injection Molding Process". Munich: Hanser Publishers, 2001.

[83] MoldFlow Plastic Insight . "database ver.6.1." 2006.

[84] Flaman, A. A.M. Build-up and relaxation of molecular orientation in injection molding- PhD. Thesis . TU Eindhoven, Netherland, 1990.

[85] Laven, J. Nonisothermal Capdby Flow of Plastics, Ph.D thesis. Delft University, Netherlands , 1985.

[86] Pantani, R. Analysis of Shrinkage Development" Ph.D Thesis¬. University of Salerno , Italy, 1999.

[87] Pantani, R., V. Speranza, and G. Titomanlio. "Relevance of mold-induced thermal boundary conditions and cavity deformation in the simulation of injection molding." Polymer Engineering & Science 41, no. 11 (2001a): 2022-2035.

[88] www.materialdatacenter.com.

[89] www.natureworksllc.com.

[90] Sungsanit et al. Physical and rheological properties of plasticized linear and branched PLA. Korea-Aust Rheol J (2010) vol. 22 (3) pp. 187-195

[91] David Kazmer (s.f.). Injection mold design engineering

[92] Tim A. Osswald,Lih-Sheng Turng,Paul J. Gramann (s.f.). Injection Molding Handbook

[93] www.skyscan.be

[94] G. Li, H. Lia, L.S. Turng, S. Gongc, C. Zhang, Measurement of gas solubility and diffusivity in polylactide Fluid Phase Equilibria 246 (2006) 158–166.

[95] Q. F. Shi, H. Y. Mou, L. Gao, J. Yang, W. H. Guo, Double-Melting Behavior of Bamboo Fiber/Talc/Poly (Lactic Acid) Composites J Polym Environ (2010) 18:567–575

168

[96] Matuana, L.M., Solid state microcellular foamed poly(lactic acid): Morphology and property characterization, Bioresource Technology 99 (2008) 3643–3650

[97] Matuana, L.M., Park, C.B., Balatinecz, J.J., 1997. Processing and cell morphology relationships for microcellular foamed PVC/cellulosicfiber composites. Polym. Eng. Sci. 37, 1137–1147

[98] Yves-Marie Correa, Abderrahim Maazouza, Jannick Ducheta, Joël Reigniera, Batch foaming of chain extended PLA with supercritical CO2: Influence of the rheological properties and the process parameters on the cellular structure, Journal of Supercritical Fluids 58 (2011) 177– 188.

[99] L. J. Gibson, M. F. Ashby, ''Cellular Solids: Structure and Properties'', Cambridge University Press, Cambridge 1999

[100]   G. Li, H. Lia, L.S. Turng, S. Gongc, C. Zhang, Measurement of gas solubility and diffusivity in polylactide Fluid Phase Equilibria 246 (2006) 158–166.

[101]   Matuana, L. M., "Foaming" in "Poly(lactic acid)", Wiley (2010).